A KINETIC AND EQUILIBRIUM STUDY OF ROOIBOS TEA INFUSIONS

by

PETER JOHN WHEELER B.Sc. (HONS), (NATAL)

A thesis submitted in partial fulfillment of the requirements for the degree of Master of Science in the Faculty of Science, University of Natal, Pietermaritzburg.

Department of Chemistry and Chemical Technology
University of Natal
Pietermaritzburg

November 1998

Dedicated

to

HERBERT RUSSELL WHEELER

DECLARATION

I hereby certify that this research is the result of my own investigation which has not already been accepted in substance for any degree and is not being submitted in candidature for any degree.

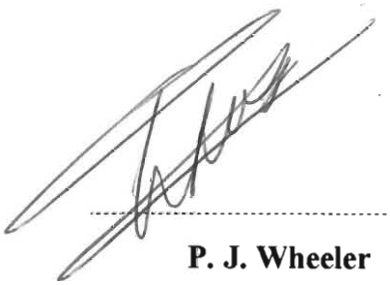

P. J. Wheeler

I hereby certify that this statement is correct.

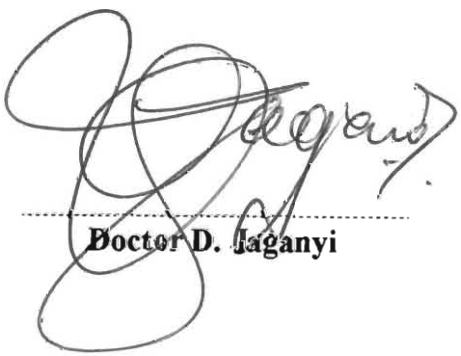

Doctor D. Jaganyi

Department of Chemistry and Chemical Technology
University of Natal
Pietermaritzburg

November 1998

ABSTRACT

The total mineral ion concentration of Rooibos Tea was determined using ICP-OES. Significant concentrations of Na, K, Mg, Ca, P were found, and trace levels of Al, Fe, Mn, Sr, Zn, Ba, Cu and Pb detected. Protocatechuic acid, aspalathin and rutin were identified in Rooibos Tea infusions analysed with HPLC. Analysis of tea samples by Ion Chromatography showed the presence of Cl^- and SO_4^{2-} ions. Rooibos Tea liquor had a pH of 4.6 once equilibrium had been reached.

Partition coefficients (1.0 – 1.4 mm sieving fraction) for Na^+, K^+, Mg^{2+}, protocatechuic acid, aspalathin, rutin, SO_4^{2-} and Cl^- were determined for infusions at 80 °C using a graphical and a successive extraction method. A total mineral content method was also used to determine the partition coefficients for the mineral ions.

The Na^+, K^+, Mg^{2+}, SO_4^{2-}, $H_2PO_4^-$ (as P) and Cl^- ions as well as protocatechuic acid, aspalathin and rutin all displayed first order behavior, allowing the determination of infusion rate constants. The particle size effect was investigated at 80 °C. All the mineral ions showed an increase in infusion rate constant with decreasing particle size, protocatechuic acid and aspalathin showed no trend, while the rutin infusion rate constant was independent of particle size. Calcium uptake by the leaf was observed, this was more pronounced with the smaller particle sizes.

Infusion rate constants and hence diffusion coefficients were determined for the nine species for temperatures ranging from 45 to 90 °C. These diffusion coefficients for the mineral ions were compared with those for the respective species in aqueous media to give hindrance factors, which were of the order of 10^2. Except for Cl^-, all hindrance factors increased with an increase in temperature. The infusion rate constants for all the species at the various temperatures were fitted to an Arrhenius equation and activation energies of infusion determined. The values were lower than those predicted theoretically.

ACKNOWLEDGEMENTS

I wish to express my sincere appreciation to my supervisor, Doctor Deogratius Jaganyi, for the guidance, constructive advice and encouragement offered throughout my experimental work and during the writing of this thesis.

A special word of thanks is extended to Doctor Colin Southway for his advice and assistance with the ICP-OES and HPLC.

I also gratefully acknowledge:

Professor Daniel Ferreira from the University of the Orange Free State, Bloemfontein, for his generous donation of the aspalathin used in the investigations.

Professor Sigfried Drewes for his advice regarding flavonoids.

Mrs. Janet "Flash" Poulter for her assistance in the physical chemistry laboratory.

Mr. Ron Berry and Mr. Ian Peirson for the many helpful discussions shared with me.

The Foundation for Research and Development and the University of Natal for their generous financial assistance.

Most of all I am thankful to my father, Russell Wheeler, my mother, Georgina Wheeler, and my brother, Gerald Wheeler for supporting me during my years as a student. To my sister Gwen thank you for being there for me and finally Kathy – for your loving support and encouragement.

TABLE OF CONTENTS

CHAPTER 1

1 INTRODUCTION

1.1 Rooibos Tea

The leaves and fine stems of the leguminous shrub *Aspalathus Linearis*, known as Rooibos, are used to produce Rooibos tea. A beverage that is becoming more and more popular due to it's unique taste, versatility and most importantly the it's reputation as a health drink. This reputation stems from claims of antioxidant activity and it's therapeutic and physiological properties[1]. Normal consumption involves brewing the leaves and then consuming the liquor hot or cold, or it is used as an ingredient in various recipes.

1.2 Growth and Production

1.2.1 Location and Cultivation

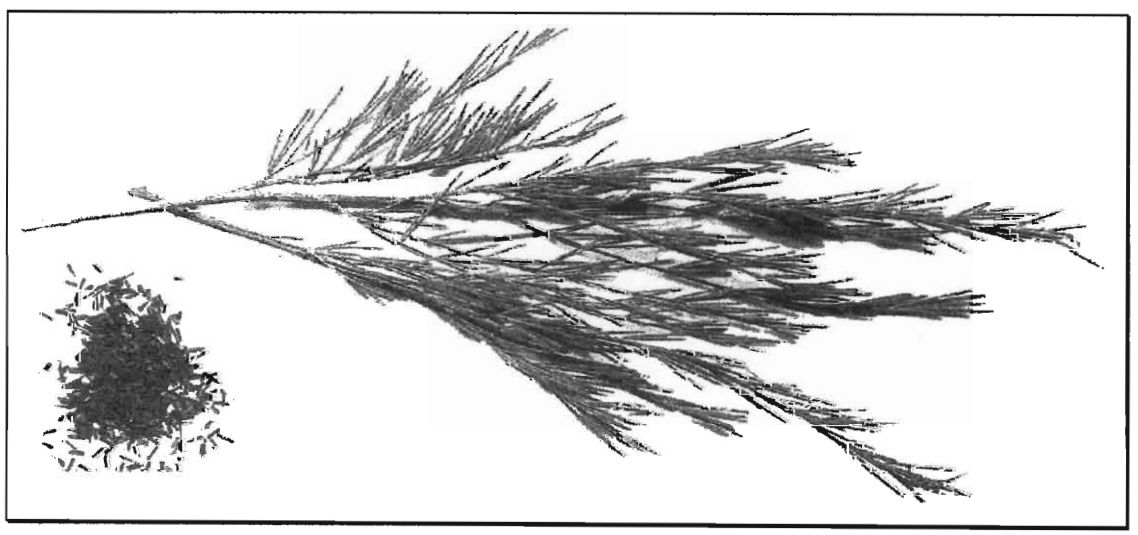

Figure 1.1a A scanned picture of *Aspalathus Linearis* (Rooibos) in both the natural and processed forms.

Aspalathus Linearis, as illustrated above in Figure 1.1a is indigenous to the Cedarberg mountains near Clanwilliam in the Cape Province of South Africa [2,3,4]. Scanning Electron Microscope (SEM) photographs were taken of the processed tea. These are presented in

Figures 1.1b – 1.1e. Figures 1.1b and 1.1c illustrate the laminar nature of most of the leaves, while figure 1.1d depicts a cylindrical shape associated with a minor fraction of the processed leaves. Randomly selected leaves were photographed.

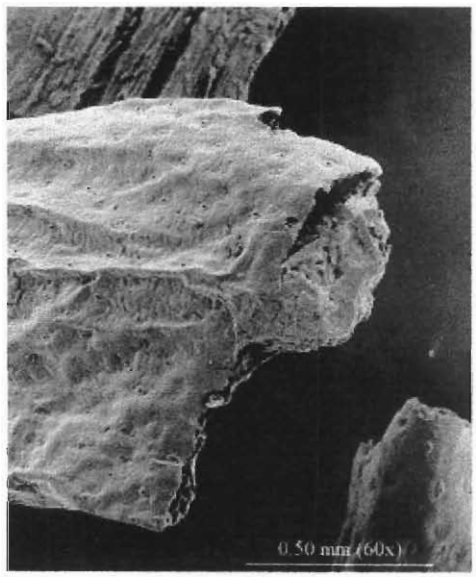

Figure 1.1b SEM photograph of leaf at 60 x magnification.

Figure 1.1c SEM photograph of leaf at 50 x magnification.

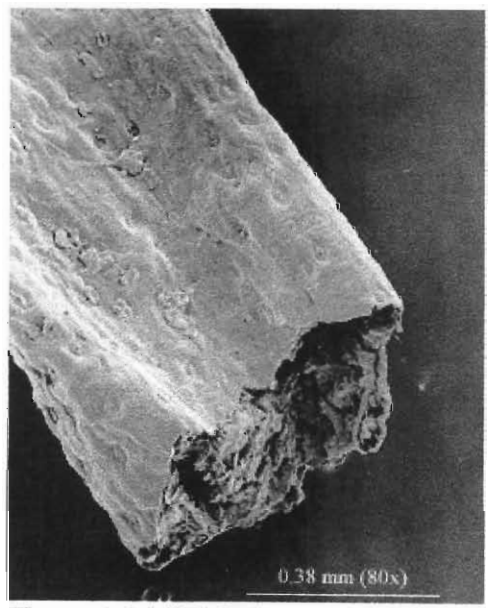

Figure 1.1d SEM photograph of leaf at 80 x magnification.

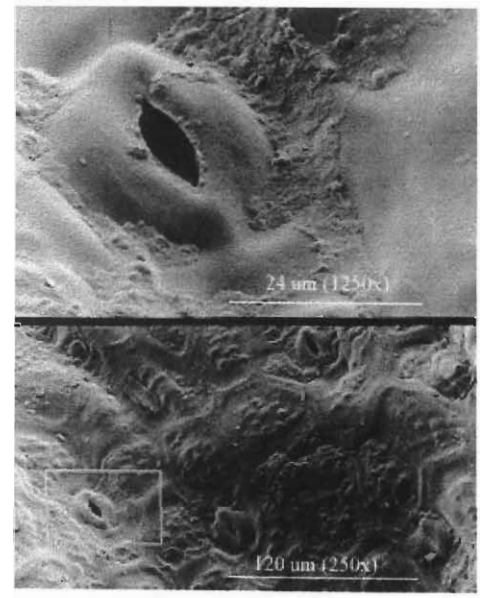

Figure 1.1e SEM photograph of leaf at both 250 and 1250 x magnification

Figure 1.1e captures stomata at different magnifications. Stomata are small openings on a leaf surface that allow the distinction between leaf and stalk material.

The tea flourishes in this region due to the unique climatic conditions prevailing in the area. The combination includes winter rainfall and coarse sandy soil. The shrub is hard seeded by nature and hence the seeds are sacrificed to increase their germinating potential prior to planting. During February and March the seeds are sown in prepared seedbeds. By June and July the plants have reached a height of 10-15 cm and are then planted out into plantations in spaced rows. In some cases the seeds are planted directly into the latter plantations. After one and a half years the first crop can be harvested by cutting the branches from the plant 35 cm above the ground. These are bound into sheaves and transported to the processing grounds. Thereafter harvesting can occur every year.

1.2.2 Processing

The sheaves are taken through a cutting machine which produces fines of a uniform length of 5 mm, this facilitates efficient packaging in the loose form or in tea bags. These cuttings are transported *via* conveyor belt to the bruiser. This consists of two rollers which bruise the tea, damaging cells and exposing them to oxygen, ensuring the occurrence of important chemical reactions that enhance the characteristic colour and flavour of the tea. These reactions include the enzymatic and chemical oxidation of polyphenols. The nature of these reactions is still unknown but involvement of enzymes such as polyphenol oxidase and peroxidase is suspected [5]. A major component of the polyphenols is composed of dihydrochalcones such as Aspalathin and Nothofagin. Investigation of the degradation of these dihydrochalcones was first investigated by Koeppen and Roux[6] and subsequently by Joubert [5]. After this the tea is watered and aired, and left to "sweat" in heaps allowing the "fermentation" process to take place, imparting to the tea the typical amber-red colour and sweet flavour.

Once the sweating process is complete, the tea is spread out in large drying yards to undergo solar drying. This is an inexpensive drying method that ensures temperatures remain below 60°C so as to preserve tea flavours[7]. When the tea has been adequately dried (*c.a.* 10 % moisture[7]), it is sucked up by huge vacuum machines specially fitted to tractors. At this stage the dried product is delivered to Rooibos Ltd where the Rooibos Tea Board ensures it's correct packaging. The packaging involves the sorting and grading into various quality grades

according to cutting length, colour, flavour and taste. These grades are then sifted and sterilised by steam pasteurisation and again dried over an exclusive hot air bed drier. Strict quality and bacteriological control is maintained throughout the process *via* laboratory testing. The dried tea is weighed (35 kg) into polypropylene bags. Packers purchase these and then further package the tea to be sold in tea bags or as leaf tea[1]. Some of the brand names that Rooibos Tea is sold under include: Laager, Cedro, Freshpak, Lipton, Ouhuis and Vital.

1.3 Rooibos Tea as a Health Food Supplement

Rooibos Tea is claimed to be a beverage which has no deleterious effects on human health[3], hence it's reputation as a health food supplement. It contains many mineral ions which are a part of a healthy diet. The tea also contains ascorbic acid, is low in tannin content (as gallic acid) and is caffeine free[3,8]. Rooibos Tea also contains a range of polyphenolics and other organic substances which bring with them an assortment of therapeutic and physiological properties that are beneficial to man. These will be discussed in section 1.3.1.

Much of the attention that Rooibos Tea has received in the world of research is due to it's antioxidant properties. These have been found to be comparable with that of green, oolong and black tea[9]. The antioxidant activity of the tea is associated with a number of it's constituents which have the ene-diol functionality, often in an electron rich B-ring system. It has also been established that Rooibos Tea contains substances that mimic superoxide dismutase (SOD) in it's antioxidant activity[10,11]. The tea as a whole is often prescribed for nervous tension, allergies and various stomach and indigestive problems. It has also had positive effects on dermatological diseases such as Behcet's disease, Sweet disease and photosensitive dermatitis[12].

1.3.1 Rooibos Tea chemical constituents and their health contributions.

Ferreira *et al*[8] have investigated and identified polyphenols, flavonoids and other chemical constituents in Rooibos Tea from an aqueous extract. They also conducted a comprehensive literature survey on the physiological effects of these constituents. Some of their findings are discussed in the following sections.

1.3.1.1 Phenolic Carboxylic Acids

Seven different phenolic carboxylic acids have been identified from the aqueous extract and one, **(8)**, from an ethyl acetate extract[8]. The structures of these acids are shown in Figure 1.2(a) and (b) while Table 1 lists the claimed therapeutic and physiological properties[12,13,14,15] of the respective compounds.

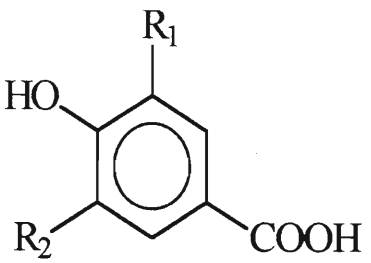

(1) 4-hydroxybenzoic acid, $R_1 = H$, $R_2 = H$
(2) 3,4-dyhydroxybenzoic acid (protocatechuic acid), $R_1 = OH$, $R_2 = H$
(3) 4-hydroxy-3-methoxybenzoic acid (vanillic acid), $R_1 = OCH_3$, $R_2 = H$
(4) 4-hydroxy-3,5-dimethoxybenzoic acid (syringic acid), $R_1 = OCH_3$, $R_2 = OCH_3$

Figure 1.2 (a) The structures of the Phenolic Carboxylic acids

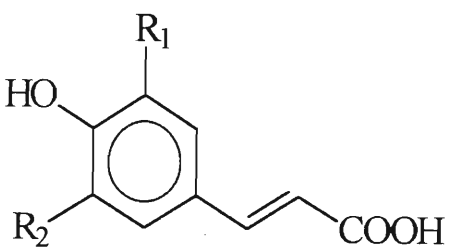

(5) 4-hydroxycinnamic acid (p-coumaric acid), $R_1 = R_2 = H$
(6) 3,4-dihydroxycinnamic acid (caffeic acid), $R_1 = OH$, $R_2 = H$
(7) 4-hydroxy-3-methoxycinnamic acid (ferulic acid), $R_1 = OCH_3$, $R_2 = H$
(8) 4-hydroxy 3,5-dimethoxycinnamic acid, $R_1 = R_2 = OCH_3$

Figure 1.2(b) The structures of the Phenolic Carboxylic acids

Table 1 Physiological and therapeutic properties of phenolic carboxylic acids in Rooibos Tea.

Activity	**Active compounds**							
	(1)	**(2)**	**(3)**	**(4)**	**(5)**	**(6)**	**(7)**	**(8)**
Antibacterial		•				•	•	•
Antifungal		•			•	•	•	•
Anti-yeast							•	•
Antiviral		•				•		
Athelmintic			•					
Antiarrhythmic							•	
Reduce myocardial O_2 consumption		•						
Antihepatoxic		•			•	•	•	•
Antimitotic							•	
Antitumor							•	
Antimutagenic	•							
DNA-binding effect						•		
Gene conversion						•		
Anti-oestrogenic							•	
Antioxidant		•		•		•	•	
Antithiamine						•		
Phagocytosis stimulant							•	
Platelet aggregation inhibition						•	•	
Prolactin stimulant							•	
Spasmolytic	•							
Clastogenic						•		
Anti-ulcer						•		

The anti-microbial properties [12,16,17] of hydroxybenzoic acids have been well documented, consequently (**1**)-(**4**) may function as natural preservatives in Rooibos Tea. From the table it is clear that a number of these acids function as antioxidants, the common denominator being the *o*-dihydroxy functionality. The antioxidant activity of the acids can be ranked in decreasing order of protocatechuic acid (**2**) > caffeic acid (**6**) > 4-hydroxybenzoic acid (**1**) > ferulic acid (**7**) > vanillic acid (**3**) > syringic acid (**4**) > *p*-coumaric acid (**5**)[15].

1.3.1.2 Flavones, Flavonols and C-O-glycosides

A number of flavones, flavonols and C-O-glycosides have been isolated from Rooibos Tea by Ferreira *et al* [8,18], these are depicted in Figure 1.3 (a) and (b) with the common name given in parenthesis. Also documented are the physiological and therapeutic properties which are tabulated in Table 1.2.

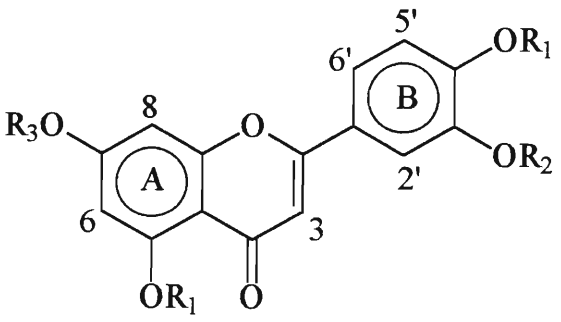

(**9**) $R_1 = R_2 = R_3$ = H3',4',5,7-tetrahydroxyflavone (luteolin) *

(**10**) $R_1 = R_3$ =H, $R_2 = CH_3$, 4',5,7-trihydroxy-3'-methoxyflavone (chrysoeriol) *

(**11**) $R_1 = R_2$ = H, R_3 =β-D-glucopyranosyl luteolin-7-O-β-D-glucopyranoside *

* = flavone

Figure 1.3 (a) The structures of the Flavones of Rooibos Tea

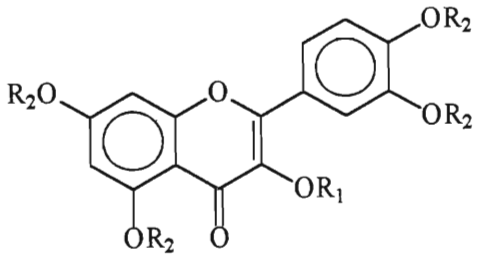

(12) $R_1 = R_2$ = H3',4',5,7-tetrahydroxyflavonol (quercetin) #

(13) R_1 = β-D-glucopyranosyl, R_2 = H quercetin 3-O-β-D-glucopyranoside derivative (isoquercitrin) #

(14) R_1 = rutinosyl, R_2 = H quercetin-3-O-rutinoside (rutin)+

= flavanol

\+ = C-O-glycosides

Figure 1.3 (b) The structures of the Flavonols and C-O-glycosides of Rooibos Tea

Table 1.2 Physiological and therapeutic properties of (9) and (12) - (14).

Activity	**Active Compounds**			
	(9)	**(12)**	**(13)**	**(14)**
Antioxidant	•	•	•	•
Antispasmodic	•	•		
Antineoplastic		•		•
Antiviral		•		
Inhibition of Calcium Transport Systems		•		
Aldose Reductase Inhibition	•	•	•	•
Vitamin P Activity				•

Luteolin (**9**) and quercetin (**12**) are reported to have anti-spasmodic qualities[19,20]. In terms of antioxidant activity the glycosides isoquercitrin (**13**) and rutin (**14**) are equally significant. Rutin (**14**) is also beneficial in terms of it's pharmacodynamic properties, and it's established vitamin P (Permeability) activity enhances the permeability and stability of capillary arteries. Due to this and the natural abundance of rutin, it is included in a range of medical formulations[21]. Furthermore all but chrysoeriol (**10**) mentioned compounds exhibit aldose reductase inhibition which is of significance for diabetics. Aldose reductase is considered a target enzyme in the pharmacological control of diabetic complications[22]. The oxidation of low density lipoproteins is also inhibited by quercetin (**12**) which implies possible anti-atherosclerotic activity[8].

1.3.1.3 C-C-linked Flavone Glycosides

The aqueous extract has been shown to contain C-C-linked Flavone glycosides[8,23]. These are illustrated in Figure 1.4. The compounds show a wide taxonomic distribution[24], but little is known about their physiological and therapeutic properties. The coexistence of these species in the same plant, namely Rooibos Tea, has only been demonstrated recently by Ferreira *et al*[18].

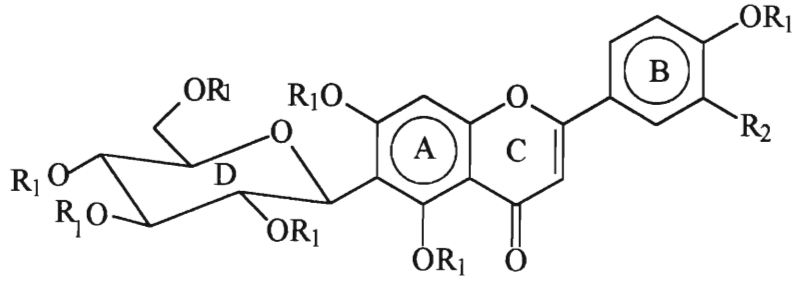

(15) R_1 =H, R_2 =OH, 3',4',5,7-tetrahydroxy-6-C-β-D-glucopyranosylflavone (iso-orientin)

(16) R_1 = R_2 = H, 4',5,7-trihydroxy-6-C-β-D-glucopyranosylflavone (iso-vitexin)

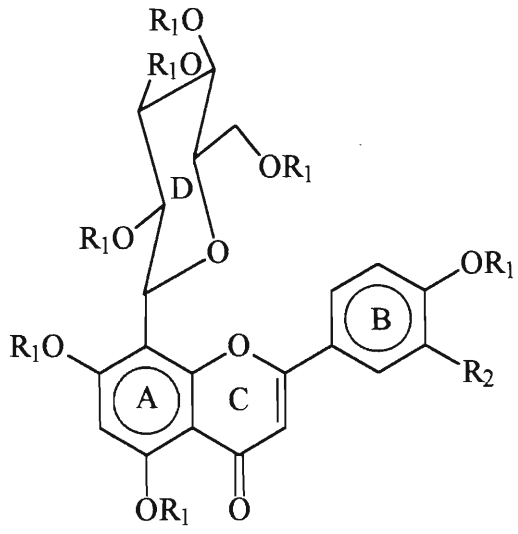

(**17**) R_1 =H, R_2 = OH, 3',4',5,7-tetrahydroxy-8-C-β-D-glucopyranosylflavone (orientin)

(**18**) R_1 = R_2 = H, 4',5,7-trihydroxy-8-C-β-D-glucopyranosylflavone (vitexin)

Figure 1.4 The structures of the C-C-linked Flavone Glycosides

1.3.1.4 C-C-linked Flavanone Glycosides

The two identified flavanones shown in Figure 1.5 represent natural products in this class that are unique to *Aspalathus Linearis*. Both of these compounds are claimed to possess the stereochemical features that are usually associated with non-nutritional sweeteners[8], however this is debatable according to the Shallenberger-Acree-Kier receptor model[25]. Thus the natural sweet taste of Rooibos Tea in contrast to the bitter taste of most Oriental teas, may in part be attributed to the presence of these and related compounds.

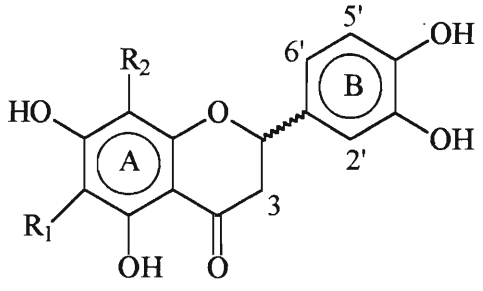

(**19**) R_1 = *C*-β-D-glucopyranosyl, R_2 = H,

3',4',5,7-tetrahydroxy-6-C-β-D-glucopyranosylflavanone (dihydro-iso-orientin)

(**20**) R_1 = H, R_2 = *C*-β-D-glucopyranosyl

3',4',5,7-tetrahydroxy-8-C-β-D-glucopyranosylflavanone (dihydro-orientin)

Figure 1.5 The structures of the C-C-linked Flavanone Glycosides

1.3.1.5 C-C-linked Dihydrochalcone Glycosides

The unique composition of *Aspalathus Linearis* is also in part due to the fact that it is the only known natural source of aspalathin (**21**)[23]. Present also in the shrub is the related compound nothofagin (**22**)[8], previously only isolated[26] from *Nothofagus fusca.* These two compounds, shown in Figure 1.6, constitute *c.a.*0.55 % and 0.9 % of the soluble solids[8] respectively.

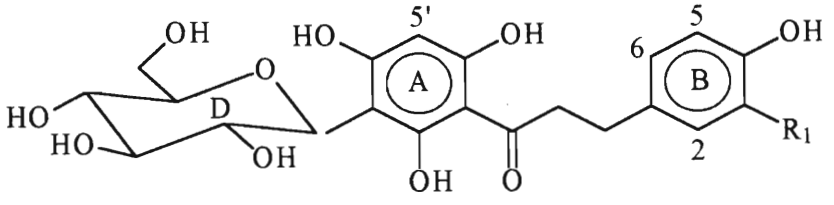

(**21**) R_1 = OH, 2',3,4,4',6'-pentahydroxy-3'-C-β-D-glucopyranosylhydrochalcone (aspalathin)

(**22**) R_1 = H, 2',4,4',6'-tetrahydroxy-3'-C-β-D-glucopyranosylhydrochalcone (nothofagin)

Figure 1.6 C-C-linked Dihydrochalcone Glycosides

It has been shown that the aspalathin in the shrub is oxidised to flavanone glycosides (2R)- and (2S)-2,3-dihydro-iso-orientin (**19**)[27]. The reaction is reportedly the first enzyme catalysed cyclization of compounds of this type. This process also occurs during the production process of the tea decreasing the aspalathin (**21**) content significantly. It is also postulated by Ferreira *et al*[8] that these dihydrochalcones contribute to the naturally sweet taste of Rooibos Tea, although this is also debatable according to the aforementioned Shallenberger-Acree-Kier receptor model [25].

1.3.1.6 Condensed Tannin and C-C-linked Chromone Glycoside Type Compounds

Rooibos Tea also gives rise to other compounds such as the C-C-linked chromone glycoside labelled (**23**). This is formed as a result of *post mortem* processes *via* phenol oxidation of 4'-hydroxyflavanones [8], possibly the product of an oxidative conversion of dihydro-iso-orientin (**19**) during the fermentation stage of the manufacturing process. The other compounds found at very low concentrations[3, 8,28] are the condensed tannin type compounds (**24**)-(**26**) shown in Figure 1.7.

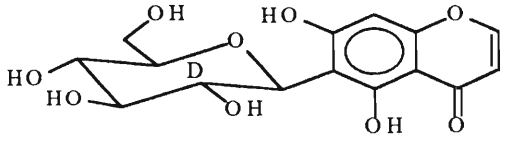

(**23**) 5,7-dihydroxy-6-C-β-D-glucopyranosylchromone

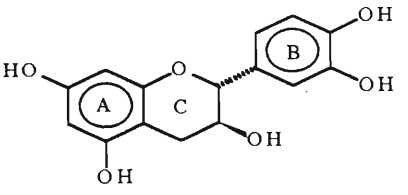

(**24**) Catechin

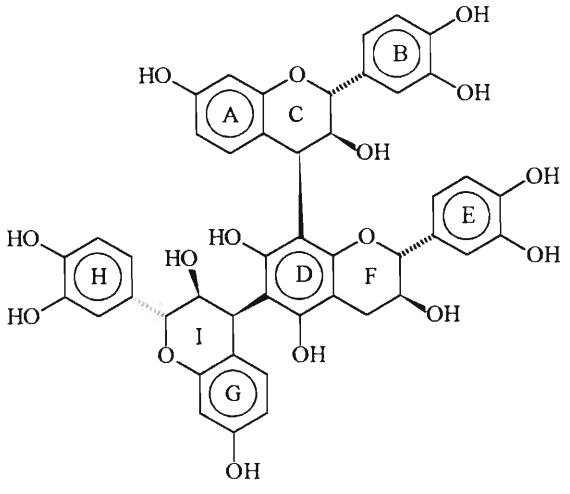

(**25**) procyanidin B3

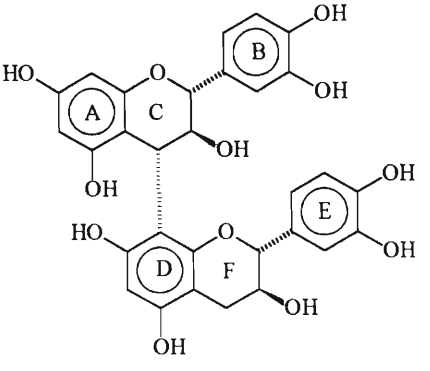

(**26**) bis-fisetinidol-(4β,6:4βB,8)-catechin

Figure 1.7 The structures of the condensed tannin and C-C-linked chromone glycoside type compounds described above.

An interesting contradiction is found in the literature as to the effects of condensed-type tannins on human health. There is evidence that the tannins are detrimental to animals and humans[29], as well as evidence to the contrary for low concentrations of these compounds[30,31].

1.3.1.7 Non- phenolic Metabolites

There are three principle non-phenolic metabolites in Rooibos Tea as seen in Figure 1.8. The inositols and their phosphates are important in cellular communication and valued for their antiglycosidic and antiviral properties[32]. They are also known for their contribution to hypoglycemic and antidiabetic concerns[33], and (+)-pinitol is also used as an expectorant. Uridine (**28**) has successfully been applied in the treatment of symptoms of hereditary orotic aciduria[34] which is a disease caused by deficient pyrimidine metabolism. Another unique compound in the Rooibos Tea metabolic pool is compound (**29**). α-Hydroxy- and α-ketoacids including phenylpyruvic acid are often used in the therapeutic preparations for, and in the prevention of dermatological diseases[35].

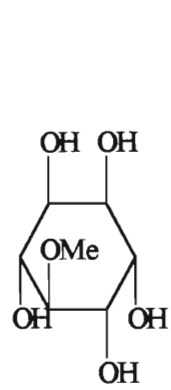

(27) (+)-pinitol

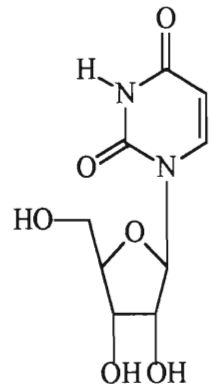

(28) uridine

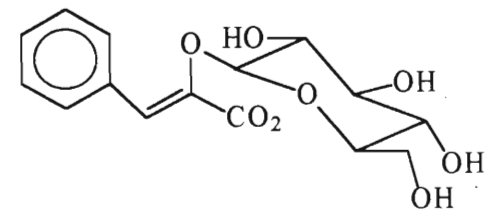

(29) phenylpyruvic acid-O-β-D-glucopyranosyl derivative

Figure 1.8 The structures of some of the Non-phenolic metabolites.

1.3.1.8 Mineral Constituents of Rooibos Tea and their Health Implications

A range of mineral ions is found in Rooibos Tea, these include iron, potassium, calcium, copper, zinc, magnesium, fluoride, manganese and sodium[1]. The presence of all except fluoride was confirmed in this work. The analysis undertaken by this work included the detection of the chloride ion, the sulphate ion and phosphorus, possibly existing as the othophosphate ion H_2PO4^- since the pH of the tea liquor ranged between 4.5 and 4.6 .The therapeutic and physiological attributes of these minerals are given below[1,36]. Included in parenthesis, where available, are the Recommended Daily Allowances (RDA) in milligrams.

- **Sodium (500), Potassium (2000) and Chloride:** These represent the major ions of the body fluids, with sodium and chloride found mainly in the extracellular fluids, and potassium within the cells. Sodium is essential for fluid and acid-base balances. Potassium is essential for many enzymatic and metabolic processes, nerve impulse transmission, and for muscle function [36].
- **Calcium (1200) and Phosphorus (1200):** Calcium phosphate in the form of hydroxyapatite is the principal component in the hard structures of teeth and bones. Deficiency can result in osteoporosis, osteomalacia, rickets, tetany and hypertension. Higher dietary calcium is protective against hypercholesteremia, non-insulin dependant

diabetes, and colon and rectal cancer[37]. Calcium is involved in nerve and muscle excitability, blood coagulation, mediation of hormonal responses and some enzyme activities. Phosphate in the form of organic esters plays an important role as various intermediary metabolites. It also has an important role in the storage of chemical energy in the form of adenosine 5'-triphosphate (ATP). Deficiencies result in neuromuscular, skeletal, hematological and renal abnormalities[37].

- **Magnesium (400):** This is largely bound as phosphates in the skeleton. Magnesium is essential for metabolism particularly in those reactions involving ATP. Mg^{2+} is a depressant of the central nervous system and also elicits hypotension, in high concentrations it will reduce the heart rate and ultimately result in cardiac arrest. Deficiency is manifested clinically through tremor, muscle spasm, personality changes, anorexia, nausea and vomiting [37], and is linked to osteoporosis[38] and "vitamin D resistance"[39].
- **Sulphur:** Forms part of some amino acids e.g. cystein and methionine, the coenzyme CoASH, and the vitamins thiamine and biotin [36]. All of which are of value to humans.
- **Iron (12):** This is essential for a range of critical processes in the human body. Most significantly, iron is required for the synthesis of the haeme portion of haemoglobin and myoglobin essential for the transport of oxygen in the blood. Deficiency causes anaemia [36].
- **Fluoride (2.75):** There is evidence to show that fluoride consumption inhibits the formation of dental cavities, and the proper fluoride intake[36] is in line with normal skeletal maintenance.
- **Copper (2.0):** Necessary for various metabolic processes and enzyme systems. It is also linked to the absorption of iron and hence lack of it can cause anaemia [37].
- **Zinc (15):** Plays an important role in some enzyme systems, is necessary for normal growth and development, and for a healthy skin. Lack of zinc in early years has resulted in "Nutritionally dwarfed" children, especially boys[37].
- **Manganese (3.5):** Also plays an important role in some enzyme systems and is necessary for various metabolic processes and for bone growth and development. Manganese deficiencies are also related to osteoporosis and poorly healing bone fractures, these problems are often rectified with manganese supplements[40].

- **Strontium:** Pharmacologic supplements of strontium have lessened bone pain in sufferers of osteoporosis and high levels of the mineral in drinking water has been shown to reduce the incidence of dental cavities[40].

1.3.2 Antioxidant Constituents of Rooibos Tea

As insight is gained into the diseases of today, scientists are becoming more aware of the toll that oxidative stress is taking on the human body. It is primarily for this reason that Rooibos Tea is gaining such popularity as a health beverage [1] with its contribution to combating this oxidation.

1.3.2.1 The Adverse Effects of "Active Oxygen Species" on Human Health

Molecular oxygen (O_2) plays an integral part in sustaining life. At the same time during normal metabolism, oxygen results in the formation of free radicals e.g. superoxides and peroxides as depicted in Equation A.

$$O_2 \xrightarrow[+H^+]{+e'} HO_2\bullet \xrightarrow[+H^+]{+e'} H_2O_2 \xrightarrow[+H^+\text{-}H_2O]{+e'} HO\bullet \xrightarrow[+H^+]{+e'} H_2O \qquad \text{(A)}$$

These free radicals are detrimental to human health[41]. The superoxide and hydrogen peroxide toxicity arises from their *in vivo* transformation into the highly active hydroxyl radical [8]. This occurs in the presence of suitable transition metals such as Fe [33]. It is well known that this radical indiscriminately attacks proteins, lipids and DNA[42], causing lipid peroxidation, protein denaturation and DNA mutation[43]. Another reactive oxygen species is singlet oxygen, formed both in the lens and the retina of the mammalian eye, which attacks some lipids resulting in lipid peroxidation[8].

Usually the body can cope with these oxidative onslaughts with defence mechanisms that include antioxidant defence enzymes and antioxidant nutrients such as the vitamins A, C and F[44]. Ageing[45] and malnutrition [46] weaken these defence mechanisms and the result is serious oxidative stress on the mammalian body. An imbalance in oxidative levels is believed to be a contributing factor in a spectrum of diseases including atherosclerosis, arthritis, heart disease, Alzheimer's disease, various cancers and even AIDS. Free radicals also attack food products.

This results in the formation of off-flavours, odours, pigment discoloration, texture alteration, and potentially dangerous by-products which are contributing factors to the limiting of the shelf life of a variety of foods[47].

1.3.2.2 The Deactivation of "Active Oxygen Species"

Superoxide dismutase (SOD) is one of the human body's natural defence mechanisms in dealing with active oxygen species[8]. It is an enzyme that quenches excess superoxides as described in Equation B.

$$2\ O_2^{-\bullet} \xrightarrow{SOD} H_2O_2 + O_2 \qquad (B)$$

However when abnormally high amounts of superoxides are produced, the SOD present in the body is not sufficient to quench this active oxygen species and oxidative damage is likely to occur. Often as man passes about 40 years of age SOD production in the body decreases and this also results in more free radical attack, especially from superoxides. This may well be related to the fact that victims of the three major adult diseases apoplexy, myocardial infarction and cancer, are found amongst people that are over the age of 40 and whose SOD production has decreased.

With the concept of preventative medicine booming, the consumption of beverages and foods that contain antioxidants (Bio-antioxidants), is receiving growing support. Not only are these generally less expensive but they are administered orally as opposed to SOD itself and liposome-SOD, which need to be administered intravenously to effect the same defence against free radicals.

1.3.2.3 Phytochemicals as Antioxidants

In the past antioxidant research was mainly focused on the activity of vitamin C, vitamin E and β- carotene. Recent times have shown the discovery of a much wider range of antioxidants, many of which are stored in Nature's Pantry, protecting Man and his food from free radical attack[48,49]. With the discovery of these natural antioxidants, there has been a

move from using synthetic antioxidants as food stabilisers, to the use of these phytochemicals instead.

A range of flavonoids forms a group of phytochemical antioxidants. Within this group there exists a selection that is of specific interest to the tea drinker, namely the theaflavins and the thearubigins. These are polyphenolic flavan-3-ol oligomers and play an important part in the quality of black tea[50]. These flavonoids are efficient primary antioxidants[51], scavenging for amongst others the superoxide-[52], hydroxyl-[53] and peroxyl-radicals[54]. Flavonoids are also known for their secondary antioxidant activity owing to their metal-chelating ability[55] and their ability to quench singlet oxygen[56].

With flavonoids occurring widely in nature, it is to be expected that they constitute an integral part of the human diet. The daily intake of flavonoids through plant food consumption is estimated at 1 g, black tea contributing about 48% with quercetin being a major contributor[57]. While this information gives one an indication of flavonoid consumption by humans, no recommendations regarding daily antioxidant intake exist. Human antioxidant requirements are dictated by oxidative stress levels which are related to fat intake, alcohol intake, smoking, life-style, occupation, infections and age[8].

1.3.2.4 Antioxidant Properties of of Rooibos Tea Constituents

The ene-diol functionality present in the twelve main flavonoid type constituents in Rooibos Tea is similar to the ene-diol configuration in vitamin C (**30**), also found in Rooibos Tea. Vitamin C (**30**) (ascorbic acid) is well known for it's action as an antioxidant in which it can reduce two equivalents of superoxide ($O_2^{-\bullet}$), quench both the peroxyl ($HO_2\bullet$) and hydroxyl (•OH) radicals as well as singlet oxygen ($^1O_2$)[42]. The mechanism of the ene-diol functionality (boxed in structure (**30**) as a radical scavenger is illustrated below in Figure 1.9. The two electrons that are lost in the successive steps (**30**)-(**31**)-(**32**) are transferred to the "active oxygen" as described in Equation 1, reducing them to water. The carboxylic acids and flavonoids with the 3',4'-dihydroxy functionality[51] of their B-rings are claimed to be potential antioxidants, able to scavenge "active oxygen species".

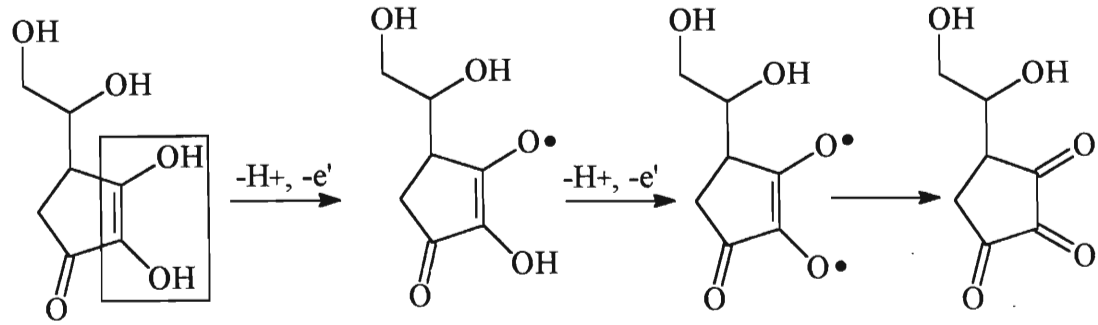

(30) **(31)** **(32)** **(33)**

Figure 1.9 The proposed mechanism of ene-diol radical scavenging.

The ene-diol functionality (**34**), shown in Figure 1.10, is present in two of the carboxylic acids; protocatechuic acid (**2**) and caffeic acid (**6**). It is also present in the flavonoids luteolin (**9**), quercetin (**12**), isoquercitrin (**13**), rutin (**14**), iso-orientin (**15**), orientin (**17**), and the related flavanones dihydro-iso-orientin (**19**) and dihydro-orientin (**20**), aspalathin (**21**), catechin (**24**), procyanidin B_3 (**25**) and the profisetinidin triflavanoid (**26**) These constitute the twelve main flavanoid-type compounds in Rooibos Tea.

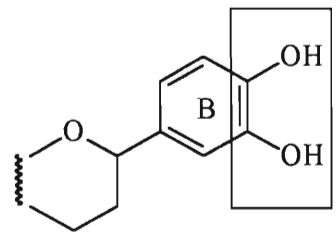

(34)

Figure 1.10 The ene-diol functionality.

It is clear that the electron-rich aromatic B-ring system should be more susceptible to oxidation than the relatively electron deficient vitamin C system. As a result the compounds discussed should theoretically be excellent suppliers of the electrons needed in Equation 1 for the reduction of the active oxygen species to water.

Findings from recent work[58] has shown that flavonols such as quercetin (**12**), are oxidised by superoxide ($O_2^{-\bullet}$) to the carboxylic acids (**36**) and (**2**) *via* the peroxy intermediate (**35**) in

aprotic media as shown in Figure 1.11. The enol functionality of the C-ring (boxed in (**12**)) is essential for the reaction.

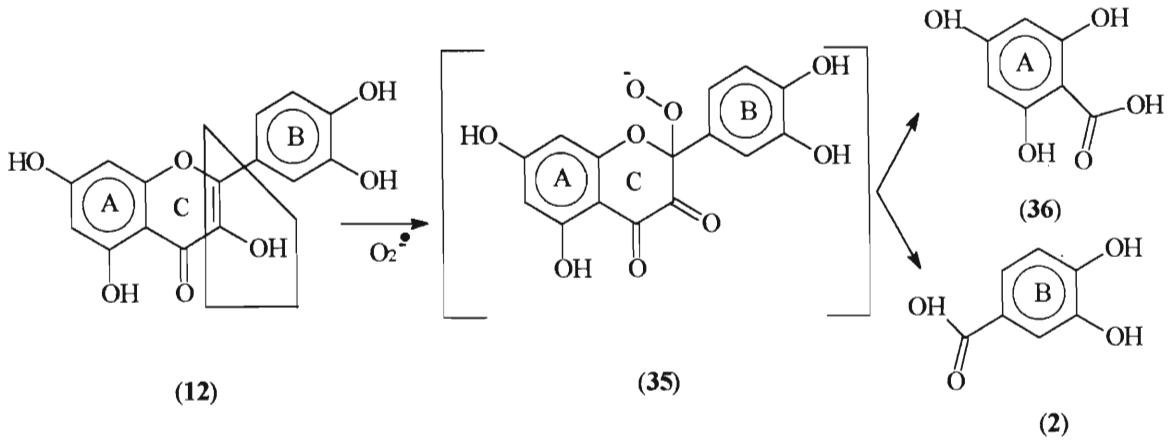

Figure 1.11 The oxidation of flavonols to carboxylic acids.

More significant are the findings by Tournaire *et al* [58] that other Rooibos Tea flavonoids (flavones and flavanones) only *induce* the disproportionation of the superoxide anion without undergoing further oxidation as seen in Equation C.

$$O_2^{-\bullet} + H^+ \longrightarrow HO_2^{\bullet}$$

$$HO_2\bullet + O_2^{-\bullet} \rightarrow HOO^- + O_2 \qquad (C)$$

Compounds displaying this activity include luteolin (**9**), chrysoeriol (**10**), luteolin-7-O-β-D-alucopyranoside (**11**), the orientins (**15**) and (**17**), the vitexins (**16**) and (**18**), the dihydro-orientins (**19**) and (**20**), and presumably aspalathin (**21**)[8]. In terms of aspalathin's contribution to the Rooibos Tea health aspect, research has been done comparing the antioxidant activity of aspalathin with other phenolics within the tea, and known antioxidants such as BHT (Butylated hydroxytoluene), BHA (Butylated hydroxyanisole), Alpha Tocopherol[59]. Aspalathin showed one of the highest degrees of DPPH (Alpha, alpha-diphenyl-beta-picrylhydrazyl) radical scavenging.

Rooibos Tea due to it's constituents, is thus a beverage of indisputable antioxidant potential as shown in it's comparison with other teas[9]. The presence of these antioxidants in Rooibos Tea along with it's considerable vitamin C content[3,28] make Rooibos Tea a significant contributor to the renewable range of bio-antioxidative foodstuffs. Scientific quantification of the antioxidant performance has given credence to the anti-ageing claims made about the tea and fortified the tea's therapeutic reputation. In the long term, claims of a healthier life are more realistic than those of an increased lifespan[8].

1.4 RESEARCH PROJECT AIMS

Research on the brewing of Rooibos Tea has been, and is still concerned with the kind of constituents extracted during the infusion process and their benefits to human health. A literature survey showed that no published information is available on the physico-chemical aspect of the dissolution process of the various species from the leaf. This type of information has proved useful in the manufacturing of instant black tea. The aim of this project was therefore to provide new experimental results by applying a simple two-phase model. Hence, determine the kinetic and equilibrium data for the extraction of individual constituents and calculate the appropriate thermodynamic properties of their infusion.

CHAPTER 2

2 THEORY

2.1 Kinetics

For a theoretical representation[60] of the kinetics of the extraction of soluble constituents from tea, consider an infusion experiment a tea leaf of mass W is immersed in a volume of water V at a constant temperature. The leaf absorbs water rapidly and it swells. This is almost immediately followed by the infusion of the soluble constituents into the water, assuming that the swelling is essentially complete before any significant solute extraction[61,62] occurs. The absorption of water by the leaf is assumed to have a negligible effect on the solution volume, since the ratio of water : leaf is large (100:1). The swollen leaf is conveniently regarded as a lamina of width $2d$, and of total surface area A. The area around the edges of the leaf is considered to be negligible. It therefore follows that the leaf volume V_{leaf} is equal to

$$2d\left(\frac{A}{2}\right) = Ad = V_{leaf} \qquad (1)$$

Figure 2.1 shows the change of concentration of extracted material with time. There is an initial rapid increase in concentration of the solute, which slows down as equilibrium is reached.

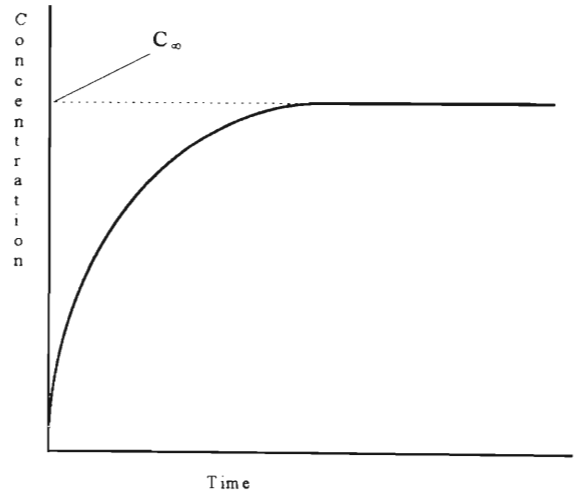

Figure 2.1 A plot showing the relationship between concentration and time.

A steady-state treatment of the system similar to the one applied for the kinetics at liquid/liquid interfaces[63] is used to derive a quantitative relationship between concentration and time and hence the infusion rate constant can be calculated. The concentration profiles in Figure 2.2 illustrate the physical model of the infusion process. Part (b) of the model shows that from the centre of the leaf lamina to the surface there is a linear decrease in solute concentration with distance d. This is followed by another linear drop through the Nernst diffusion layer of thickness δ surrounding the leaf.

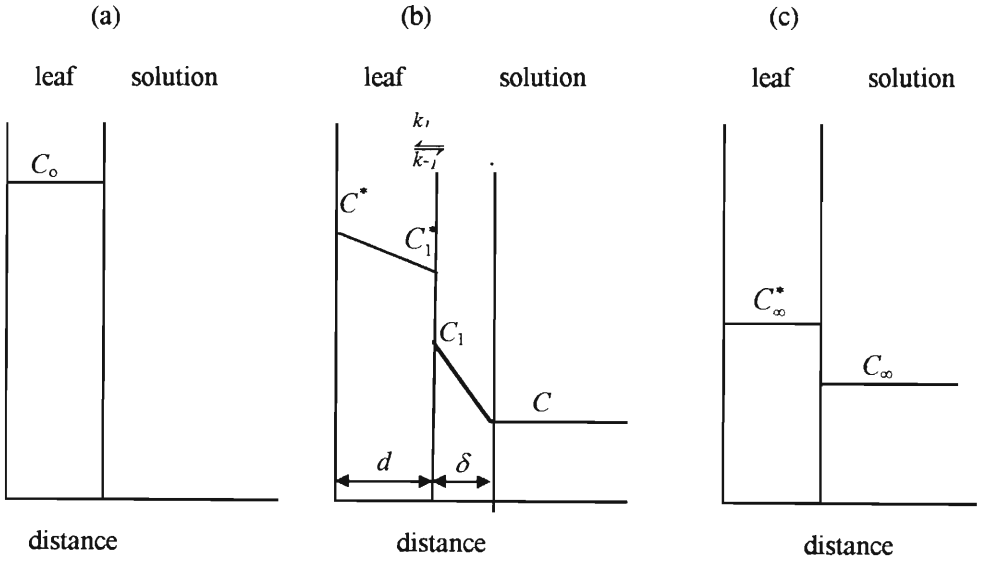

Figure 2.2 Concentration profiles during tea infusion at (a) t = 0; (b) t = t and (c) t = ∞

In this concentration profile, the concentration of the respective species (in g dm^{-3} or mol dm^{-3}) in the centre of the leaf lamina is represented by C^*. The concentration on the leaf and solution sides are denoted by C_1^* and C_1 respectively. The concentration of the solutes in the stirred bulk solution outside of the Nernst layer is C. The transfer of the constituent across the interface proceeds by a first order rate constant k_1 from the leaf to the solution and from the solution to the leaf at a rate constant of k_{-1} (both in ms^{-1}). The partition coefficient K of the constituent is thus given by :

$$K = \frac{k_1}{k_{-1}} = \frac{C_\infty}{C_\infty^*} \qquad (2)$$

In the assumed steady state, the flux J (g s^{-1} or mol dm^{-3}) of a soluble species, rutin for example, is given by the following equations:

$$J = \frac{d(CV)}{dt} \tag{3}$$

$$= AD_L\left(\frac{C^* - C_1^*}{d}\right) \tag{4}$$

$$= A\left(k_1 C_1^* - k_{-1} C_1\right) \tag{5}$$

$$= AD_S\left(\frac{C_1 - C}{\delta}\right) \tag{6}$$

Equations (4) and (5) are applications of Fick's first law of diffusion, with D_L and D_S denoting the diffusion coefficients of the soluble constituent in the leaf and solution respectively. Even though D_L is possibly dependant on either concentration or distance or both, the practice of substituting a Fickian diffusion system with a non Fickian one is well established [64]. The concentrations C_1^* and C_1 are both unknown and can be eliminated between equations (4) and (6) to give :

$$k_1 C^* - k_{-1} C = \frac{J}{A}\left(1 + \frac{k_1 d}{D_L} + \frac{k_{-1}\delta}{D_S}\right) \tag{7}$$

Substituting equation (2) into equation (7) gives :

$$k_1\left(C^* - C_\infty^*\right) + k_{-1}\left(C_\infty - C\right) = \frac{J}{A}\left(1 + \frac{k_1 d}{D_L} + \frac{k_{-1}\delta}{D_S}\right) \tag{8}$$

The term C^* can be eliminated by using the conservation of mass equations. If T is the total amount of the soluble component in the system, then at times t = 0, t = ∞ and t = t respectively :

$$T = AdC_0 \tag{9}$$

$$= AdC_\infty^* + VC_\infty \tag{10}$$

$$= Ad\left(\frac{C^* + C_1^*}{2}\right) + A\delta\left(\frac{C_1 + C}{2}\right) + (V - A\delta)C \tag{11}$$

Combining equations (10) and (11) and substituting for C_∞^* and C_1 with :

$$C_1^* = C^* - \frac{Jd}{AD_L} \quad \text{and} \quad C_1 = C + \frac{J\delta}{AD_S}$$

from equations (4) and (6) one obtains:

$$Ad\left(C^* - C_\infty^*\right) = V\left(C_\infty - C\right) + \frac{J}{2}\left(\frac{d^2}{D_L} - \frac{\delta^2}{Ds}\right) \tag{12}$$

Using equation (12) one can eliminate (C^*- C_∞^*) from equation (8) to give :

$$\left(C_\infty - C\right)\left(k_{-1} + \frac{k_1 V}{Ad}\right) = \frac{J}{A}\left(1 + \frac{k_1 d}{2D_L} + \frac{k_{-1}\delta}{Ds} + \frac{k_1 \delta^2}{2dDs}\right) \tag{13}$$

Equation (13) can be simplified further by dividing through by k_{-1} and incorporating equation (2):

$$\left(C_\infty - C\right)\left(1 + \frac{KV}{Ad}\right) = \frac{J}{A}\left(\frac{1}{k_{-1}} + \frac{Kd}{2D_L} + \frac{\delta}{Ds} + \frac{K\delta^2}{2dDs}\right)$$

$$\left(C_\infty - C\right)\left(1 + \frac{KV}{Ad}\right) = \frac{J}{Ak^*} \tag{14}$$

where k^* is short for bracketed terms.

Hence using equation (3) the following equation is obtained:

$$\left(C_\infty - C\right)\left(1 + \frac{KV}{Ad}\right) = \frac{V}{Ak^*}\left(\frac{dC}{dt}\right) \tag{15}$$

This equation can be rearranged and a new parameter k_{obs} introduced to give :

$$\frac{dC}{dt} = k_{obs}\left(C_\infty - C\right) \tag{16}$$

Integrating equation (16)

$$\int_{C=0}^{C=C} \frac{dC}{\left(C_\infty - C\right)} = \int_{t=0}^{t=t} k_{obs}\, dt$$

results in :

$$\ln\left(\frac{C_\infty}{C_\infty - C}\right) = k_{obs} t \tag{17}$$

Where k_{obs} is the observable overall first order rate constant.

A plot of $\ln\left(\frac{C_\infty}{C_\infty - C}\right)$ versus t should be linear, with a slope equal to k_{obs} and passing through the origin.

It follows then that the overall first order rate constant k_{obs} is equal to :

$$k_{obs} = k^*\left(\frac{A}{V} + \frac{K}{d}\right) \tag{18}$$

Combining equations (14) and (18) gives :

$$\frac{1}{k_{obs}}\left(\frac{A}{V} + \frac{K}{d}\right) = \frac{1}{k^*} = \left(\frac{1}{k_{-1}} + \frac{Kd}{2D_L} + \frac{\delta}{Ds} + \frac{K\delta^2}{2dDs}\right) \tag{19}$$

Multiplying throughout by d/K affords :

$$\frac{1}{k_{obs}}\left(\frac{Ad}{VK} + 1\right) = \frac{d}{k^*K} = \left(\frac{d}{k_1} + \frac{d^2}{2D_L} + \frac{\delta d}{KDs} + \frac{\delta^2}{2KDs}\right)$$

From equation (1)

$$Ad = V_{leaf}, \text{ but } V_{leaf} << V$$

this makes the first bracketed term approximately equal to 1 giving equation (20):

$$\frac{1}{k_{obs}} = \frac{d}{k^*K} = \left(\frac{d}{k_1} + \frac{d^2}{2D_L} + \frac{\delta d}{KDs} + \frac{\delta^2}{2Ds}\right) \tag{20}$$

The $K\delta^2 / (2dD_S)$ term in equation (19) can be ignored because it will almost always be smaller than the δ/D_S term. This leaves us with three special cases according to the relative sizes of the other three terms on the right-hand side of equation (19):

(i) If d/k_1 is the largest term the infusion is transfer-controlled, implying that

$$k_{obs} \approx \frac{k_1}{d} \tag{21}$$

(ii) If the second term is the largest, the rate-limiting step is diffusion of the constituent through the swollen leaf and :

$$k_{obs} \approx \frac{2D_L}{d^2} \tag{22}$$

(iii) If the third term is the largest, the rate-limiting step is diffusion of the constituent across the Nernst layer and as a result :

$$k_{obs} \approx \frac{KDs}{d\delta} \qquad (23)$$

2.2 The Rate Limiting Step for Tea Infusion

To understand the mechanism of the infusion process one needs to ascertain which of the three steps (i)-(iii) described above is the rate-limiting step. It has been established by Spiro and Jago[60], using a horizontal rotating disc with black tea glued onto it, that diffusion through the Nernst layer is not the rate-determining step. They found that the rate of caffeine infusion, was independent of the disc rotation speed and therefore independent of the thickness of the Nernst layer (δ) described by the Levich equation to be:

$$\delta = 0.643\upsilon^{1/6} D^{1/3} f^{-1/2}$$

where υ = Kinematic viscosity, D = Diffusion coefficient and f = Disc rotation speed (Hz). This is assumed to be true for all constituents other than caffeine and suggests that the last term in equation (20) is not the most significant contributor to k_{obs} and therefore equation (23) does not apply.

Since for the remaining two terms of interest, k_{obs} depends inversely on d^2 and d, one could determine whether intra-leaf or interfacial transfer is the rate-limiting step by conducting extraction experiments on tea leaves of varying thickness. This is not practical as the thickness of the leaf cannot be varied by the experimenter. Price[65] has compared the rate constants of a variety of species infusing from tea leaves. He noticed that the observed rates were not very different even though the size, shape and character of the leaves were markedly different. Also noted was that diffusion coefficient (D) for a wide range of species did not vary enormously. This can be explained with the help of the Stokes-Einstein relationship:

$$D = kT / 6\pi\eta r$$

where k is the Boltzmann constant, T is absolute temperature, η is the viscosity of the medium and r is the radius of the diffusing species regarded to be a sphere whose volume is given by $V = {}^4/_3\pi r^3$

It is clear that D depends inversely on r, whereas the volume (V) of the supposedly spherical species depends on r^3. Hence the diffusion coefficient will be much less sensitive to size variation than the volume. From this investigation and the work done by Spiro and Selwood[66] on infusions of ground coffee of different particle size, as well as the extraction of solutes from tobacco leaves[67], all indicate that the rate-determining step is diffusion of the soluble constituent through the leaf.

2.3 Correction for Water Loss

Corrections for variations in analyte concentrations from sampling and evaporation during experiments need to be performed[60]. In order to do this, firstly equation (24) is obtained from equations (1), (2), (9) and (10):

$$T = V_{leaf} C_0$$

$$T = V_{leaf} C_\infty^* + V C_\infty$$

$$T = V_{leaf} \frac{C_\infty}{K} + V C_\infty$$

$$T = C_\infty \left(V + \frac{V_{leaf}}{K} \right) \qquad (24)$$

During the course of the experiment, ΔT (mol or g) of a particular component will have been removed from the reaction vessel through the sampling process. Also a small volume of water ΔV will be lost through evaporation and sampling. The measured concentration of the soluble constituent at equilibrium C_∞ is therefore given by :

$$V_{leaf} C_0 - \Delta T = C_{obs}^\infty \left(V - \Delta V + \frac{V_{leaf}}{K} \right) \qquad (25)$$

where

$$\Delta T = \sum C_i \Delta V_i \qquad (26)$$

Substituting equation (24) into (25) and rearranging affords :

$$C_\infty = C_{obs}^\infty - \frac{C_{obs}^\infty \Delta V - \Delta T}{V + V_{leaf} K} \qquad (27)$$

The partition coefficient at 80° C have been determined in section 4.3 to be small for various soluble species. Assuming that this is true at all other temperatures, the term $V_{leaf}K$ in equation (27) will be much smaller than the V term, thus reducing the equation to :

$$C_{\infty} = C_{obs}^{\infty} - \frac{C_{obs}^{\infty}\Delta V - \Delta T}{V} \qquad (28)$$

This is similar to what has been determined by Spiro and Siddique [68] and Price's[65] work on various teas. Even though ΔT is included, it represents a very small value as only a small volume (3 ml out of 400 ml) of tea solution was sampled each time. Correction for the individual concentrations obtained from the experiment requires another equation. When a sample is drawn from the reaction vessel, ΔT moles of the respective component are removed and ΔV ml of the solvent is lost by this act and by the evaporation process. The volume of solvent remaining in the vessel will then be V-ΔV. Assuming that c is the true concentration after each sampling, then the amount of the component after each sampling will be equal to cV-ΔT.

The concentration measured experimentally will be given by :

$$C = \frac{cV - \Delta T}{V - \Delta V} \qquad (29)$$

Manipulating this relationship gives :

$$c = C - \left(\frac{C\Delta V - \Delta T}{V}\right) \qquad (30)$$

This equation is similar to equation (27) without the $V_{leaf}K$ term which is only applicable to the equilibrium sample.

2.4 Equilibrium Theory

2.4.1 The Graphical Method

To determine the partition coefficients of the soluble constituents between the tea leaves and the aqueous medium, Spiro and Selwood[66] have derived the equilibrium theory. This was used to determine the partition coefficient of caffeine in coffee. This theory is adapted here for tea infusions.

From equation (1) the volume (V_{leaf}) of the swollen (wet) leaves can be equated to its mass (m) and density (ρ) to give :

$$Ad = \frac{m}{\rho} = V_{leaf} \tag{31}$$

Substituting equation (31) into equation (10) gives:

$$T = V_{leaf} C_{\infty}^{*} + VC_{\infty} \tag{32}$$

Multiplying equation (32) by $1/K$ from equation (2) gives :

$$T = C_{\infty}\left(\frac{V_{leaf}}{K} + V\right) \tag{33}$$

On substituting equation (9) into equation (33) :

$$V_{leaf} C_0 = C_{\infty}\left(\frac{V_{leaf}}{K} + V\right) \tag{34}$$

Rearranging equation (34) results in :

$$\frac{1}{C_{\infty}} = \frac{1}{KC_0} + \frac{V}{V_{leaf} C_0} \tag{35}$$

which on substitution of equation (31) produces:

$$\frac{1}{C_{\infty}} = \frac{1}{KC_0} + \frac{\rho V}{mC_0} \tag{36}$$

Plotting $1/C_{\infty}$ versus V/m will produce a straight line whose intercept and slope should yield values for C_0 and K.

2.4.2 The Successive Extraction Method

The value of K determined using the graphical method is dependent on the value of the intercept. These are often small and uncertain as found by Spiro and Selwood[66]. As a result they devised an alternative method for determining the partition coefficients. This involves successive equilibrium extractions of a given sample of tea leaves with fresh volumes of water V. Using equations (2) and (9) the following expression is obtained:

$$\frac{C_{\infty}^{*}}{C_0} = \frac{C_{\infty} V_{leaf}}{KT} \tag{37}$$

which on substitution of equation (33) gives :

$$\frac{C_{\infty}^{*}}{C_0} = \frac{V_{leaf}}{V_{leaf} + KV} \tag{38}$$

Thus after the first extraction the concentration of the soluble constituent remaining in the tea leaf is :

$$\frac{C_{\infty}^{*}}{C_0} = \frac{1}{1 + K\dfrac{V}{V_{leaf}}} \tag{39}$$

Using equation (31) to replace V_{leaf} one gets :

$$\frac{C_{\infty}^{*}}{C_0} = \frac{1}{1 + KV\dfrac{\rho}{m}} \tag{40}$$

Hence the concentration of the solution on the second extraction $C_{\infty 2}$ is related to $C_{\infty 1}$, the concentration after the first extraction by:

$$C_{\infty 2} = \frac{C_{\infty 1}}{1 + KV\dfrac{\rho}{m}} \tag{41}$$

Which gives the following relationship:

$$K = \frac{m}{\rho V}\left(\frac{C_{\infty 1}}{C_{\infty 2}} - 1\right) \tag{42}$$

Once K has been obtained by this method, C_0 can be calculated from $C_{\infty 1}$ and equation (36). It is important to note that in all these equilibrium equations V_{leaf}, m and ρ are the volume, mass and density of the wet swollen tea leaves respectively. In line with this C_0 is the initial concentration of the solubles in the tea leaf after penetration of water but before any solubles are extracted.

CHAPTER 3

3. EXPERIMENTAL

3.1 Experimental Procedures

3.1.1 Determination of Total Mineral Ions

Rooibos Tea leaves used in this investigation were obtained from the Rooibos Tea Board in Clanwilliam, South Africa. These leaves were first sieved into different fraction sizes using a set of stainless steel and brass coated Endecott sieves and a mechanical shaker. Seven fraction sizes were obtained with particle sizes ranging from 0.250-0.425 mm, 0.425-0.60 mm, 0.60-0.85 mm, 0.85-0.100 mm, 1.00-1.40 mm, 1.40-1.70 mm and 1.70-2.00 mm. The last three fraction sizes were found to contain a significant amount of stalk material. The fraction range selected for determination of total mineral ions was 0.85-0.60 mm. The procedure involved accurately weighing 1.000 g of the tea leaves using a Mettler AJ100 digital weighing balance. Nine pre-weighed crucibles were used in weighing the samples. Six of the crucibles were vitreous silica and the other three were platinum. Different crucibles were used to avoid inaccurate results since, with trace analysis, losses can occur with respect to certain analytes and particular crucible materials[69].

The tea leaf samples were dried overnight at 120 °C in an oven, and then cooled in a desiccator for one hour before re-weighing. This gave an average moisture content of 0.594% (m/m). In accordance with Bock[69], 0.8ml of H_2SO_4 (Merck) was used as an ashing aid. This produced a multitude of sulphates and thus inhibited losses due to volatilisation of the more volatile analytes. The samples were inserted into the oven at room temperature and allowed to heat and combust as the oven reached the target temperature of 450 °C. The ashing process took 22 hours. The crucibles were removed from the oven with the help of a pair of tongs and placed in a desiccator to cool to room temperature. These were then re-weighed and this process was repeated until the mass was constant. The ashings were

dissolved in 5 ml of 0.1 M HCl (BDH Aristar grade) and then filtered using Whatman No.1 filter paper. The filter papers were washed with the HCl solution and the filtrate made up to 25 ml, forming the stock solutions. These were diluted 10 and 30 times to ensure that all analyte concentrations were within the calibration range. The diluted samples and the stock solutions were then analysed using the ICP-OES providing a triplicate analysis per crucible.

3.1.2 Steady-state Experiments

A temperature controlled water bath was let to equilibrate at the desired temperature using a Thermomix 1460 heater stirrer for 4 hours prior to starting the experiment. To prevent heat loss and evaporation from the surface of the insulated water bath insulating spheres (Gallenkamp) were used. The flask used in the experiments (brewing flask) was a plastic conical flask (500 ml) containing 400 ml of MilliQ water and a teflon coated magnetic stirrer. The bottom of the flask was heated and moulded into a gentle concave shape so as to house the magnetic stirrer at the centre for efficient stirring of the liquor. It was sealed with a lid that had two holes drilled into it for the fitting of a mercury thermometer and a plastic sampling tube. The end of the tube which was inside the flask consisted of a small cylindrical plastic sheath (inner diameter 5 mm) inside which a Gilson filter (Anachem) was fitted. This prevented the withdrawal of tea leaves which would have blocked the plastic tube. The filter also removed any tiny particles that would have affected the HPLC and Ion Chromatography (IC) columns. Nylon gut was tied through the open end of the plastic sheath to prevent the filter from dislodging. This is because before sampling, air in the syringe was always used to flush the tube and filter. The filter was replaced after each experimental run. The brewing flask was weighed without the thermometer before it was submerged into the bath and allowed to equilibrate to the set temperature. The bath containing the brewing flask is illustrated in Figure 3.1

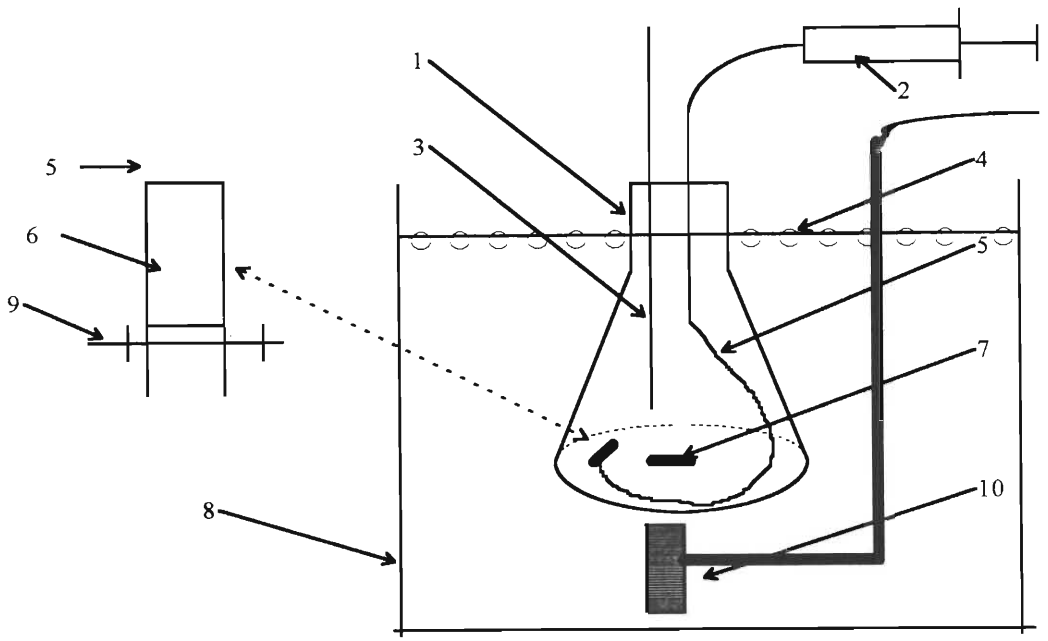

1) Plastic conical flask 2) Plastic syringe 3) Thermometer 4) Anti heat-loss balls

5) Sampling tube 6) Cigarette-like filter 7) Magnetic stirrer 8) Insulated bath walls

9) Nylon gut 10) Underwater magnetic stirrer.

Figure 3.1 The brewing flask and water bath components.

Once the liquid in the brewing flask was at the required temperature, the lid was temporarily removed and a wide bore glass funnel modification of the device used by Spiro and Siddique[64] was used to add a standard amount of tea leaf (4.0 g) into the flask. The tea leaf was accurately weighed on a digital weighing balance. The glass funnel ensured that the tea addition was quick and standardized, ensuring reproducible results. The lid was replaced after the addition to prevent evaporation. An underwater magnetic stirrer with a variable speed control was used to stir the mixture. This process ensured that the concentration of the extracted species and the temperature of the solution was uniform within the flask. After the experiment the stirrer motor container was always removed from the water bath to prevent water creeping into the motor and corroding the parts.

Tea samples (3 ml) were withdrawn from the flask using a 5 ml plastic syringe (Promex). Each sample was then transferred into a plastic polytop from where two samples of 1 ml were accurately measured usinng an Eppendorf pipetteman and placed in two different polytops. Plastic polytops were used for the ICP-OES analyses and the 1 ml samples were diluted with

9 ml of a 0.1 M HCl solution. Glass polytops were used for the IC and HPLC analyses, the 1 ml samples were diluted with 4 ml of MilliQ water for IC analyses and 0.666 ml of methanol (BDH, HPLC Grade) for the HPLC. Methanol was used because the peaks were better resolved as compared to when water was used as the diluting solvent. Experiments at 80 °C were performed in quadruplicate and monitored on the HPLC and ICP-OES, all other experiments performed and monitored using these two instruments were done so in triplicate. Due to limited access to the IC instrument, only duplicate sets of experiments were monitored using the IC throughout the investigations.

Initially a total of 14 samples were withdrawn from the flask, the sampling times being 0.0 (blank), 0.5, 1.0, 1.5, 2.0, 2.5, 3.0, 3.5, 4.0, 5.0, 15.0, 30.0, 45.0, 60.0 and 90.0 minutes. Once it was established that the component was exhibiting the trend shown in Figure 2.1 and the results were reproducible, the sampling times between 5.0 and 60.0 minutes were excluded. The kinetic runs were carried out at different temperatures namely 45 °, 50 °, 60 °, 70 °, 80 ° and 90 °C with a range of leaf particle sizes. At the end of the run, the brewing flask was again weighed with it's contents. The difference in weight was taken as ΔV and used for correction purposes in Equation 28.

The pH of the solution was monitored at the end of each experiment using an Orion Research microprocessor pH/millivoltmeter 811 while the solution was being stirred.

3.1.3 Determination of Partition Coefficients.

Partition coefficients (K) were determined by two different methods for comparative purposes; the graphical and the successive extraction methods. In both methods experiments were performed at 80 °C and using the 0.85-1.00 mm sieving fraction. Preliminary investigations showed that the C_∞ concentration was attained within 60-90 minutes and hence all sampling was done at 90 minutes, and in each case a 4 ml sample was taken. In both methods MilliQ water was used and the samples were treated as described before for analysis on the various intruments.

3.1.3.1 The Graphical Method

A slight modification was made to the method used by Spiro and Selwood[66]. These workers added incremental amounts of coffee beans to the same liquor. The modified experimental procedure involved a fresh brew of tea for each mass of tea leaf. The masses used were 1.0, 1.5, 2.0, 3.0, 3.5 and 4.0 g. These experiments were carried out in duplicate.

3.1.3.2 The Successive Extraction Method

The successive extraction method involved extraction of soluble constituents from a sample of tea leaves with fresh volumes V of water and monitoring the respective equilibrium concentrations. The experimental conditions were similar to the kinetic runs already described. In this case the sample withdrawn was split into three 1 ml aliquots for analysis with the HPLC, ICP-OES and IC using the Eppendorf. After sampling and measuring the pH of the tea, the tea liquor was decanted into a clean plastic sieve and the tea solution used to wash all the tea leaves from the flask into the sieve The wet swollen leaves were carefully dried with clean tissue paper until they did not stick together from the cohesive properties of the liquor but moved freely over one another, care was taken not to squeeze the leaves. A second 400 ml of MilliQ water was in the meanwhile equilibrating to 80 °C, and once the leaves were free of tea liquor they were placed into a clean brewing flask and this water was introduced to the system with immediate stirring. Trying to introduce the leaves to the water in the usual way resulted in problems with the still damp leaves sticking to the glass funnel. The tea was allowed to brew again for another 90 minutes, before sampling and the pH measured again. The solution was then decanted and the leaves dried as described above.

The swollen leaves were then put into a preweighed pycnometer and their combined mass determined. The pycnometer was then filled with MilliQ water (50 cm^3 at 20 °C) and kept at 20 °C for 30 minutes in a temperature controlled water bath. The trapped bubbles were removed by gently shaking the flask, and adding more water before the stopper was inserted. The pycnometer was dried and then weighed to 4 decimal places using a digital weighing balance. Hence the mass and density of the wet swollen leaves were determined.

After each experiment all the glassware and plasticware used was rinsed with tap water to remove excess tea liquor. Then all these items were completely submerged into a cleaning solution of Extran 20 % (Extran MA 03 phosphate free, Merck). This detergent is a non-ionic phosphate free cleaning solution. The syringes were all rinsed thoroughly in the solution and one of them used to flush the sampling tube with the detergent solution. The glassware and plasticware was allowed to soak overnight, before rinsing with tap water followed by a 0.1 M HCl solution. These were finally rinsed with MilliQ water and then dried in an oven at 105 °C, including the plasticware which were all high temperature resistant.

3.2 Analysis of Cations and Phosphorus

3.2.1 Introduction

The ICP-OES was chosen for the analysis of cations and phosphorus present in Rooibos Tea due to the efficiency with which it is able to analyse a range of species[70]. This is a significant advantage over other instruments like Flame Atomic Absorption Spectrophotometry (FAAS) and Graphite Furnace Flame Atomic Absorption Spectrophotometry (GFAAS). Disadvantages of using both of these instruments include the time needed for multi-element analyses owing to their single element capabilities[71]. The former instrument is also known for it's poor precision whilst the latter for it's small dynamic concentration range. The other advantage is that the ICP-OES can cope with a much larger range of sample concentrations. This is important when one considers that the concentrations of the species undergoing an infusion do vary quite significantly requiring a large calibration range.

3.2.2 The Principles of the ICP-OES.

There are various components which comprise the Inductively Coupled Plasma Optical Emission Spectrometry (ICP-OES). These are shown in the schematic diagram in Figure 3.2.

Figure 3.2 Typical components of an ICP-OES.

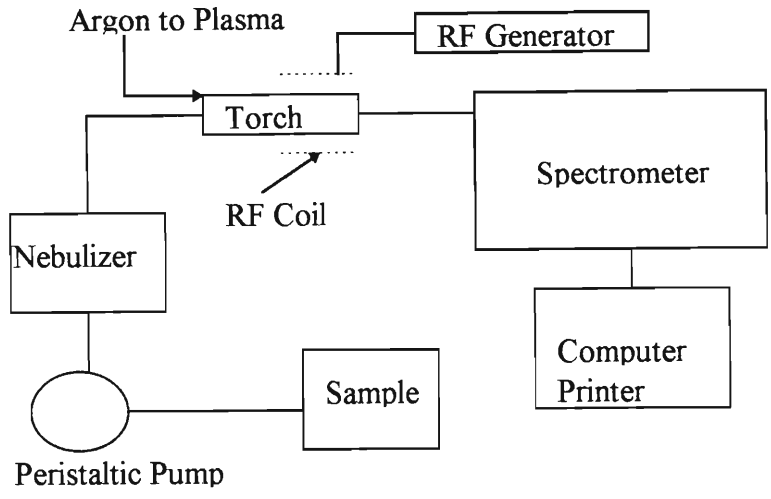

These instruments are used for the determination of mineral species that will emit characteristic radiation on excitation. This includes all metals and some non-metals such as phosphorus.

Initially the sample is aspirated via a peristaltic pump to a nebuliser. The function of the nebuliser is to convert the sample, which will be in the form of a solution, into an aerosol. There are many different types of nebuliser[72], the cross-flow, concentric and ultra-sonic nebulisers. This research involved the use of the latter two. The differences lie in the analyte transport efficiency[73] of the nebulisers, with the ultrasonic being far more efficient than the concentric (pneumatic) nebuliser, resulting in much greater intensities for respective concentrations on the ultrasonic nebuliser. The ideally dry, analyte laden aerosol is then transported from the nebuliser by an inert carrier gas, usually argon, and introduced into the plasma. The plasma is by definition a conducting gaseous mixture of electrons and cations[74], and is sparked by a Tesla coil. It is sustained *via* Ohmic resistance which is the result of the interaction of the cations and electrons with the fluctuating magnetic field supplied to the coil from the Radio Frequency (RF) generator. Harbouring the plasma is a quartz torch which is cooled also by argon, as it yields temperatures between 6000 K and 10000 K [74]. Plasma temperatures and energy are such that the analyte species are thermally exited to the point of emission, and this is monitored with the spectrometer. An atomic or ionic spectrum is emitted

by the analyte that has two dimensions[75]. Firstly the wavelength at which the emission is made is used to determine the elemental composition, and secondly, the intensity of the emitted radiation is proportional to concentration. The spectrometer is usually composed of a monochromator to monitor the emission wavelength, a photomultiplier to boost the signal and a photodetector for detection of the radiation. These are all controlled by a computer.

Preliminary work on the ICP-OES involved optimisation in terms of the signal to background ratio (SBR) and the signal to noise ratio (SNR). The operating power, argon plasma flow, auxiliary argon flow and nebuliser pressure were varied independently and their effects on the SNR and SBR noted as seen while analysing for Mn. Mn is considered by many to be an analyte that is representative of a broad spectrum of elements with respect to it's behaviour in an ICP-OES[76]. The instrument possesses a Rapid Scan function which allows the rapid detection of any species that the instrument is capable of monitoring. Intensity versus wavelength plots are produced at the expected wavelength of each species. A peak represented either the presence of an analyte or an interferent. By monitoring at different wavelengths for the suspected species and spiking with appropriate standards one is able to determine whether or not the suspected species is an interferent or not.

3.2.3 Experimental Conditions for the ICP-OES in the Current Work.

The optimum conditions for use in the current work are reflected in Table 3.1 along with the ICP-OES instrument specifications. In the table, the two values given for the nebuliser pressure and pump speed refer to nebulizers (1) and (2) as listed.

The elements identified in Rooibos Tea using the Rapid Scan function of the instrument are shown in Table 3.2 and the respective lines were chosen according to their prominence, freedom from spectral interference and range of calibration curve linearity. The peak search window is the wavelength range scanned for a peak for that particular species. The window was made narrow enough to ensure that the correct peak intensity was measured.

Table 3.1 ICP-OES specifications and it's operating conditions.

Instrument	Liberty 150 AX Turbo (Varian)
Torch mounting	Axial, Low flow
Nebuliser (1)	Ultrasonic (Cetac U-5000AT$^+$)
Nebuliser (2)	Pneumatic (Concentric)
RF Power supply	40.68 MHz
Operating power	1.00 kW
Nebuliser pressure	(1) 200 kPA (2) 240 kPA
Photomultiplier voltage	800 V
Plasma argon flow	15.0 L/min
Auxiliary argon flow	1.50 L/min
Pump speed	(1) 12 rpm (1) 10 rpm

Table 3.2 Mineral ions detected in Rooibos Tea with the ICP-OES rapidscan along with the respective wavelengths and peak search windows.

Element	Wavelength/nm	Peak search window/nm
Aluminium	396.152	0.080
Barium	493.409	0.080
Calcium	317.933	0.040
Copper	324.754	0.040
Iron	238.204	0.040
Lead	405.783	0.080
Magnesium	383.826	0.080
Manganese	294.920	0.040
Phosphorus	213.618	0.015
Potassium	769.896	0.052
Sodium	589.592	0.080
Strontium	407.771	0.080
Zinc	213.856	0.027

Routine maintenance of the ICP-OES involved cleaning the torch once a week depending on the number of samples analysed and their composition (Samples other than Rooibos Tea were also run on the ICP-OES). It was removed as per instruction manual[76] and cleaned by submerging it in aqua-regia overnight, then rinsed with MilliQ water and oven dried at 105 °C. In cases of extreme soiling 2 % HF was used to soak only the soiled section for a few minutes and then the torch was rinsed as before. The optical window was cleaned at the same time using lint free tissues moistened with ethanol. The base plate was removed and

polished with a metal polish (Brasso). It was then rinsed thoroughly with MilliQ water and replaced back into it's position. The peristaltic pump tubing was replaced when necessary. This is because once the tube has perished, it affects the performance of the sample introduction system.

3.2.4 Calibration curves for Cations and Phosphorus analysis.

Riedel-de-Haen FIXANAL solutions for ICP-OES were obtained for all analytes except phosphorus. The FIXANAL solutions came in solutions containing exact amounts (1.000 g) of the analyte concerned and had guaranteed minimum impurity levels. Thus stock solutions of 2000 ppm of each analyte were made by diluting the 1.000 g solutions to exactly 500 ml, using a 0.1 M HCl (Aristar ICP-OES grade) solution. The acid was used in order to preserve the solutions. This acid solution was made using ultra pure deionised MilliQ water obtained through reverse osmosis. Phosphorus stock solution was prepared by dissolving 21.320 g of Dibasic Ammonium Phosphate (BDH) in MilliQ water and diluting this to exactly 1 litre giving a stock solution of 5000 ppm as P. The phosphate was dried in the oven at 105 °C before use. The analytes and their respective standard concentrations (ppm) used to calibrate the ICP-OES are shown in Table 3.3

Table 3.3 Standard solutions (in ppm) used to calibrate the ICP-OES.

Analyte	Standard 1	Standard 2	Standard 3	Standard 4	Standard 5
Na	0.04	0.20	1.00	2.50	5.00
Mg	0.04	0.20	1.00	2.50	5.00
Al	0.04	0.20	1.00	2.50	5.00
Pb	0.04	0.20	1.00	2.50	5.00
Sr	0.04	0.20	1.00	2.50	5.00
Fe	0.04	0.20	1.00	2.50	5.00
Ba	0.04	0.20	1.00	2.50	5.00
Mn	0.04	0.20	1.00	2.50	5.00
Ca	0.08	0.40	2.00	5.00	10.00
P	0.02	0.10	0.50	1.25	2.50
Zn	0.04	0.20	1.00	2.50	5.00
Cu	0.04	0.20	1.00	2.50	5.00
K	0.04	0.20	1.00	2.50	5.00

The standard solutions were run on the ICP-OES and it constructed it's own calibration curves. The procedure included a blank correction using a 0.1 M HCl (Aristar ICP-OES grade) solution as the blank. The ICP-OES was programmed to do a "Dynamic" background correction, and to reject any calibration with a correlation coefficient of less than 0.995. The instrument was calibrated each time before use since extended use of the instrument changed slightly the working conditions in terms of the cleanliness of the sample introduction system, torch, and optical window. As mentioned earlier, two nebulisers were used in the analysis. Initially the concentric nebuliser was used in the determination of total amounts of cations and phosphorus in Rooibos Tea. However this was damaged during routine analysis and this necessitated converting to the use of the ultrasonic nebuliser for kinetic investigations and determination of partition coefficients. The species selected for kinetic investigations and partition coefficient determination were those that exhibited the trend shown in Figure 2.1. These are listed in Table 3.4. in the Ultrasonic Nebuliser column. The calibration equations in the form of $y = mx + c$ using both nebulisers are shown in Table 3.4, where x = concentration (ppm), y = peak intensity, m = slope and c = intercept. The correlation coefficient for each line is given by the R^2 term.

Table 3.4 Calibration equations for concentric and ultrasonic nebulisers in the form of $y = mx + c$.

Element	Concentric nebuliser			Ultrasonic nebuliser		
	Total mineral ion content			Kinetic investigations		
	m	c	R^2	m	c	R^2
Sr	190209.1	4054.486	0.9997			
Mg	96320.26	5366.971	0.9992	942243.7	54014.16	0.9990
Al	277230.5	8327.662	0.9997			
Pb	29248.04	732.2623	0.9992			
Fe	575093.2	33704.64	0.9993			
Na	1174316	-23929	0.9996	16972356	965801.1	0.9991
Mn	219598.4	5718.384	0.9997			
Ca	132629.2	10915.84	0.9995	1493978	97537.51	0.9996
P	28582.25	452.0968	0.9998	371457.4	-9815.14	0.9992
Zn	863233.8	48114.62	0.9992			
Cu	387483	6907.019	0.9999			
Ba	1046241	27842.79	0.9997			
K	34684.02	-2153.13	0.9977	578889.4	-20192.1	0.9989

Calibration graphs for the elements analysed with the ultrasonic nebuliser are shown in Figures 3.3 - 3.7 as reconstructed with the help of Microsoft Excel software.

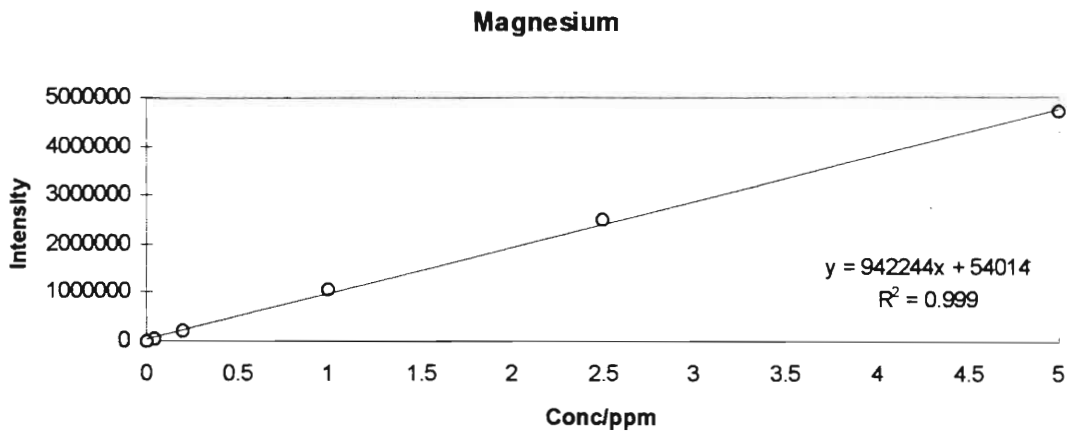

Figure 3.3 Calibration curve for Magnesium

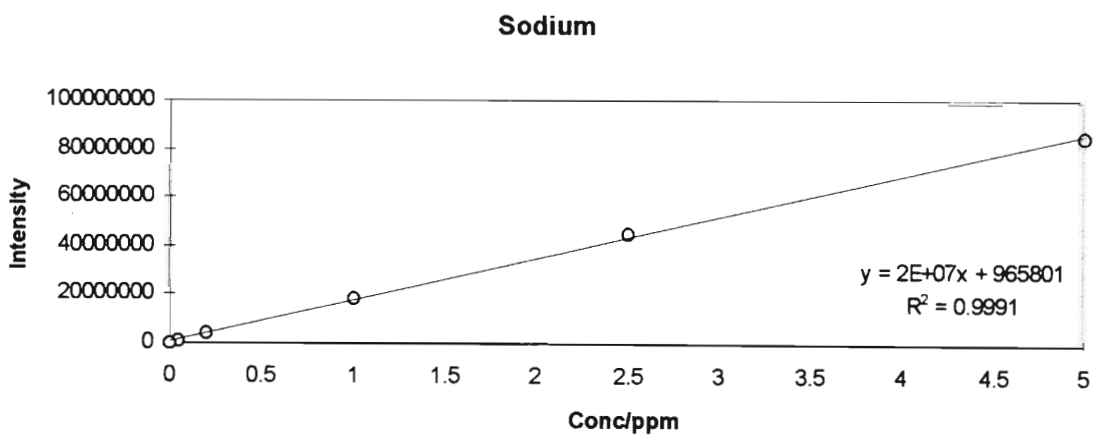

Figure 3.4 Calibration curve for Sodium

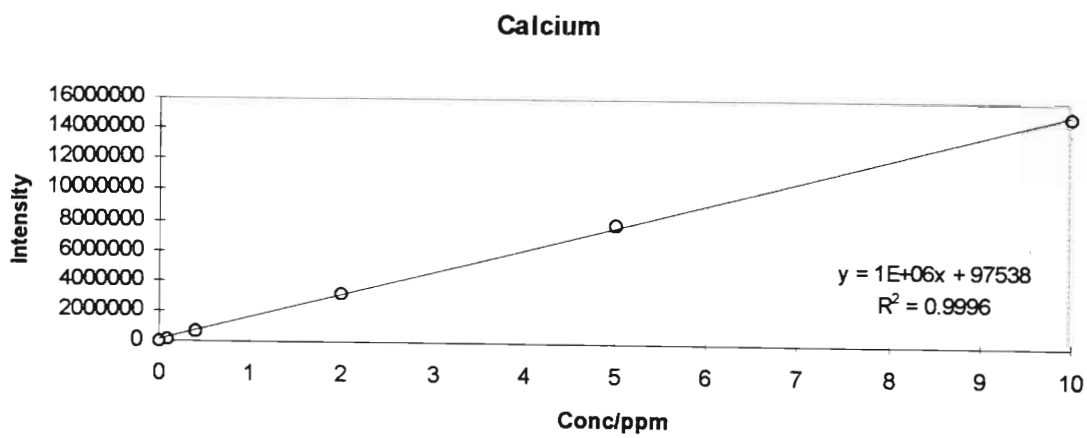

Figure 3.5 Calibration curve for Calcium

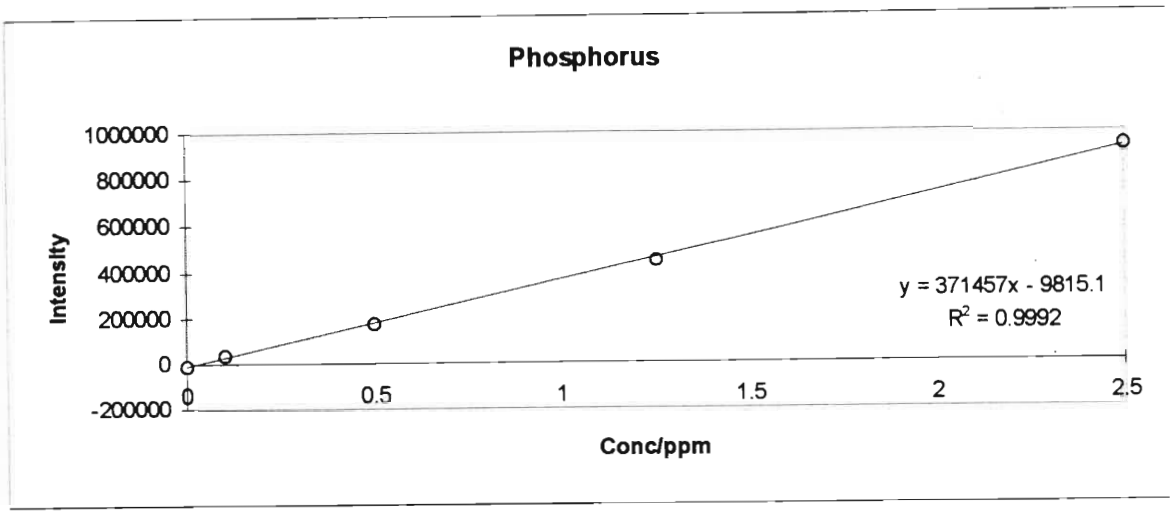

Figure 3.6 Calibration curve for Phosphorus

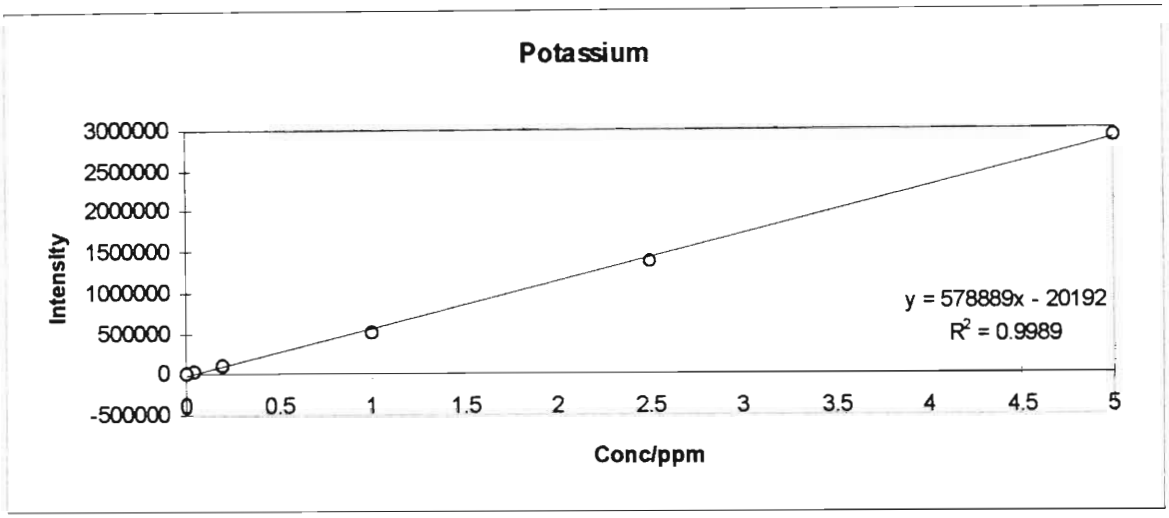

Figure 3.7 Calibration curve for Potassium.

It was necessary to establish whether or not dilutions of samples for ICP-OES analysis was to be done with MilliQ water or with 0.1 M HCl. Dilution with the acid would serve to match the sample and standard matrix since all standards were made up in 0.1 M HCl, and this would contribute to the reliability of the ICP-OES results[70,77]. The ICP-OES standards were made up in 0.1 M HCl (BDH Aristar HCl with MilliQ water) in order to minimise absorption onto container surfaces, critical at trace concentrations. It was found that acidification however, speeded up the precipitation of the tea on standing and cooling. Subsequently a comparison needed to be performed to see whether the acidification would affect the results through precipitation. Rooibos Tea (3.9943g of particle size 1.00-1.40) was brewed in the usual way at 90°C. Samples of 7 ml were withdrawn after 3 and 30 minutes to represent the

lower and higher concentrations respectively. The two samples were each divided into six (1 ml) samples. Three of which were diluted with 9 ml of MilliQ water and the remaining three with 9 ml of 0.1 M HCl solution. The samples treated with HCl produced better results and the anticipated precipitation did not take place prior to analysis. The results of this investigation are discussed in Chapter 4.

3.3 Analysis of Organic Compounds

3.3.1 Introduction

A High Pressure Liquid Chromatography (HPLC) instrument is usually used to monitor non-volatile organic compounds which have different characteristics mostly with respect to polarity, and is thus perfect to monitor the flavonoids of Rooibos Tea. The fundamental advantage of this instrument over many others is that it combines the separation of components and their identification and quantification. Contrast this with other methods which rely on samples being of a pure substance for their identification, such as Nuclear Magnetic Resonance (NMR), and identification and quantification such as UV-Visible Spectrophotometry. Gas chromatography also allows for the separation of compounds within a sample and their identification and quantification, however, GC does not lend itself to the non-volatile compounds of interest in Rooibos Tea. Also, GC instruments generally function with a destructive detector thus removing the possibility of compound isolation. Even for some of the compounds that can be determined by both GC and HPLC, the latter is still more powerful in that UV-Visible spectrums of the pure compounds can be obtained during routine analysis. These advantages combined with the low detection limits of HPLC prompted the choice of this instrument for the present work.

3.2.2 The Principles of the HPLC

The components comprising the average HPLC instrument are seen in Figure 3.8 , except for the temperature controlled water bath whose function is normally performed by a conventional column heater.

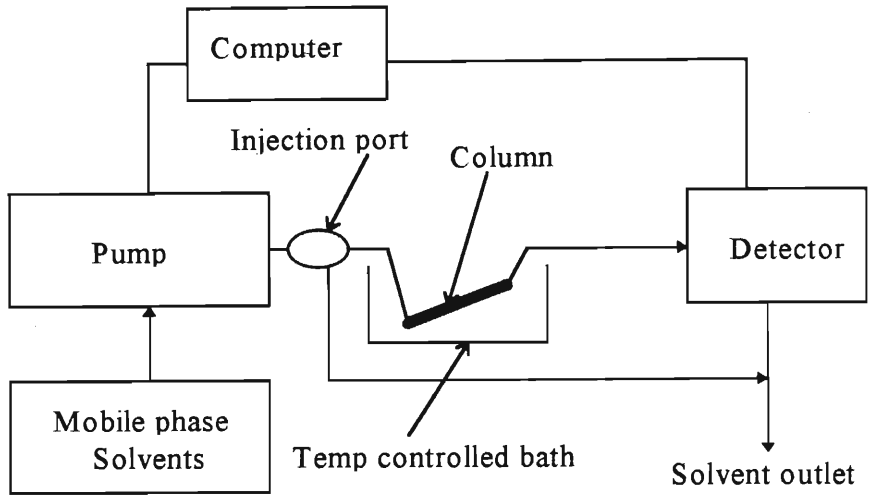

Figure 3.8 Typical components of an HPLC.

The mobile phase as used in HPLC consists of a solvent, or mixture of solvents that effectively carry the injected sample through the instrument during analysis. Many HPLC systems have the option of handling a mixture of more than one solvent as the mobile phase, one solvent being the case for an isocratic elution, and some can handle mixtures of up to four different solvents. These solvents are kept in separate containers where they are sparged with an inert gas (usually helium) to remove dissolved gases before use. On command the solvents are pumped at specific speeds and mixed together by proportioning valves to give the mobile phase desired in terms of polarity, flow rate and pressure. Modern pumps can not only mix solvents to give a mixture of specific polarity for isocratic elution, but also perform gradient elutions which help in overcoming the general elution problem[78]. The mobile phase carries the sample through the system. Once the required mobile phase is being pumped the sample can be injected, which can be done by autosamplers or manually. Most injection ports have a fixed loop injection system to limit errors due to varying injection volumes. After injection the sample is carried by the mobile phase through the column and this results in a separation of constituents.

The separation of the species injected onto the column is a function of many parameters [79] and can be explained when one considers the equilibrium distribution ratio (K) of the components

between the mobile phase (C_m) and stationary phase (C_s). When $K = 1$ the solute is equally distributed between the phases[80].

$$K = \frac{C_s}{C_m}$$

Analyte molecules can only move through the column when they are in the mobile phase. Subsequently molecules that are more strongly held by the stationary phase and are less soluble in the mobile phase will move through the column at a slower rate than those that behave otherwise, hence the separation. The constituents are separated and the detector shows them as peaks on a chromatogram. A problem experienced with chromatography is the broadening of these peaks which represent the solute bands. Broadening is a function of thermodynamic and kinetic processes within the column with the bandwidth being affected by three factors namely : eddy diffusion, longitudinal diffusion and resistance to mass transfer[81]. Eddy diffusion involves the movement of solute particles at different velocities and along different path lengths around the stationary phase particles within the column. This contributes to the band broadening. Eddy diffusion can be minimised by using packing material of smallest possible diameter, and packing the column as uniformly as possible. Longitudinal diffusion describes the axial random molecular motion of solute particles within the mobile phase. This phenomenon becomes significant at low mobile phase velocities. At these velocities high diffusion rates of a solute within the mobile phase causes the solute molecules to disperse axially while moving through the column, broadening the solute band by the time the detector is reached. Resistance to mass transfer, the third contributor to band broadening, refers to the uneven rate at which solute is adsorbed and desorbed from the stationary phase. A consequence of this is that some solute molecules at the front of the band are swept ahead before equlibration occurs as with the bulk of the molecules, and similarly those at the back of the band can be left behind by the moving moblie phase. The overall result being the broadening of the peak. If the rates of mass transfer within the two phases were infinite broadening of this type would not occur, thus the faster the mobile phase moves the less time there is for equilibrium to be approached and the greater the resistance to mass transfer contribution to broadening [79]. In order to obtain a Gaussian shaped peak, the three processes described above must be minimised.

There are two types of chromatography systems for HPLC, normal phase and reversed phase. These terms refer to the selection of stationary and mobile phase. Traditionally when the stationary phase is polar (eg triethylene glycol or water) and the mobile phase is non-polar (eg hexane or isopropyl ether) the system is referred to as normal phase. When the stationary phase is non-polar (eg bonded octyl or octyldecyl siloxane packings) and the mobile phase is moderately polar (eg water or methanol) the system is referred to as reversed phase. The least polar analyte species is eluted first in normal phase chromatography and increasing the solvent polarity decreases elution time. In reversed phase the most polar constituent is eluted first and decreasing the solvent polarity decreases the retention time of the species.

Upon leaving the column the separated species enter the detector. Most HPLC detectors are based on absorption of ultra-violet and visible radiation. Some instruments incorporate for example deuterium and tungsten lamps to cover this range while others will make use of photodiodarray detectors. With these detectors one can identify samples from their peak retention times at a specific wavelength, or even from their actual UV-Visible spectrums if the entire wavelength range is scanned. This requires comparison to standards or at least a proven documented method. These advanced systems are computer controlled.

3.3.3 The Development of the Mobile Phase and Sample Preparation.

Initially investigations into the optimum mobile phase composition and sample preparation were undertaken. The mobile phase systems found in the literature for flavonoid analyses were tried. The first was a gradient elution system (aqueous formic acid and methanol) described by Joubert[5] for the analysis of Rooibos Tea which involved long retention times. The second, also a gradient elution system (aqueous formic acid and methanol), was one described by van Sumere *et al* [82] which was more successful in that the last peak retention time was significantly reduced but it was still to long for a large number samples. Thirdly an isocratic elution system (2-propanol-tetrhydrofuran-water) as described by Pietta *et al* [83] was tried. This system was aimed at removing the slightly sloped baseline associated with a

gradient elution whilst reducing the sample run time. This method was unacceptable because even the peaks from the standard solutions were not resolved. It was decided then to modify the elution system described by Joubert[5] and van Sumere[82] in search for good resolution with a much shorter retention time.

Investigations were also carried out on the effect of flow rate and temperature on the column pressure. The use of a modified van Sumere gradient elution[82] at a flow rate that gave acceptable resolution (1.5 ml/min) produced column pressures likely to damage the column (*c.a.* 4500 psi). This was attributed to the increase in viscosity[84] of the water methanol mixture as 40% methanol composition was approached. The column temperature was then varied along with flow rate in search of conditions giving the best peak resolution. Although column heating slightly affects the chemistry of the separation process, this technique is often used to decrease the viscosity of the solvent mixture. Thus the pressure of the system at the required flow rate can be brought to within acceptable limits.

The mobile phase which was developed and used throughout the experimental work was a gradient elution as tabulated in Table 3.5 and illustrated diagrammatically in Figure 3.9. Solvent A was methanol (Merck; HiperSolv for HPLC) and solvent B was 5 % (v/v) formic acid (Merck, 98 - 100 %), in water (MilliQ). All solvents, except the formic acid which attacked the filters causing contamination, were filtered using 0.45 μm filters (Micropore) prior to use.

Table 3.5 Mobile phase composition in terms of percentages (v/v) of the respective solvents.

Time/min	% Methanol	% (5% formic acid in water)
0	15.0	85.0
4	15.0	85.0
8	30.0	70.0
15	40.0	60.0
18	50.0	50.0
20	50.0	50.0
23	15.0	85.0
28	15.0	85.0

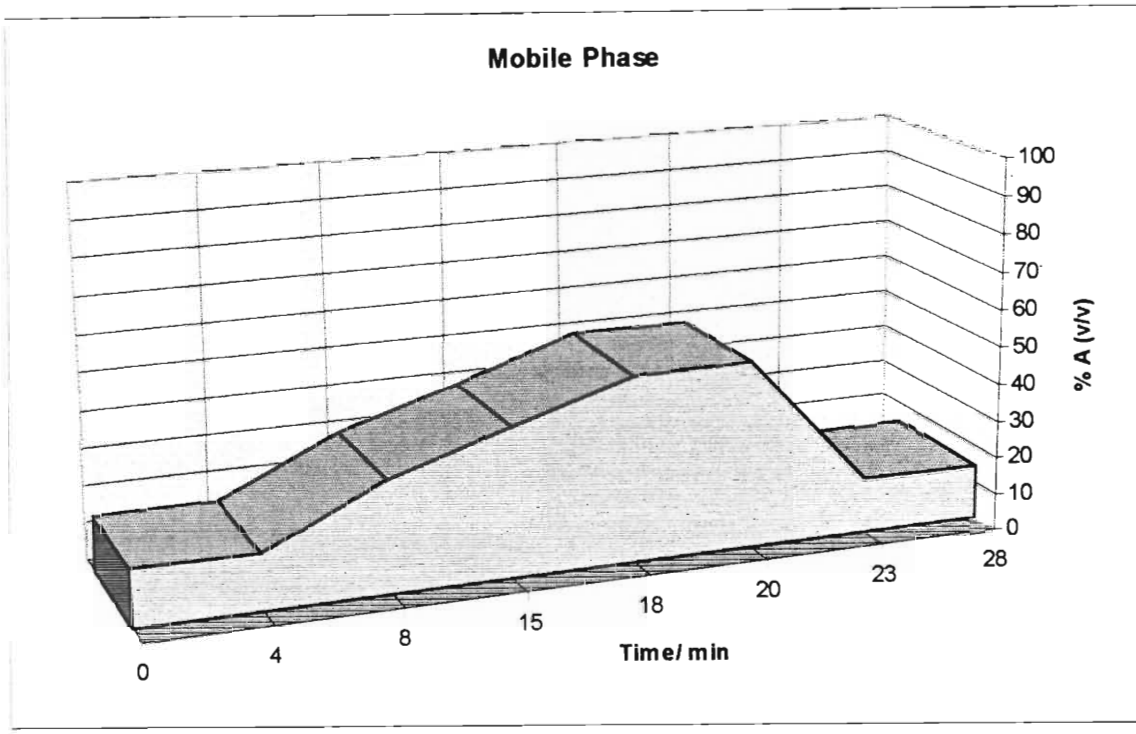

Figure 3.9 Pictorial representation of the gradient elution system for the mobile phase, where A represents methanol and B represents 5 % (v/v) formic acid in water.

Sample preparation was performed with the aim of firstly removing peaks for which there were no standards in order to simplify the chromatogram, and secondly to concentrate the sample and provide some form of filtration. Investigation involved adding fixed amounts of sorbent materials (silica and alumina (Both from Merck)) to tea samples, freeze drying them and then eluting with ethyl acetate with the aim of eluting the same components extracted by Joubert[5]. The ethyl acetate was then removed under vacuum and the solid that remained behind was dissolved in a known amount of methanol. When the solid was dissolved in a 40 % methanol : water (v/v) solution the chromatogram peaks were observed to be sharper than if only one of the solvents was used. This process was time consuming and the chromatogram peaks obtained from the highest concentration samples were very small. The method had also an element of error due to the number of steps involved. Analytichem *Bond Elut LRC* C_{18} cartridges were then tried instead of the alumina and silica. In this case the method of extraction involved using different methanol-water compositions with the hope

of extracting only certain compounds per composition of eluent. This method was not successful, as a result a straight injection of the sample was used. This gave an acceptable chromatogram with few peaks unresolved.

3.3.4 Identification of Peaks

To be able to carry out kinetic studies, the peaks of the chromatogram had to be identified. This was achieved by using pure samples of the suspected peaks as identified by Joubert [5]. The standards were p-hydroxybenzoic acid (**1**), protocatechuic acid (**2**), vanillic acid (**3**), p-coumaric acid (**5**), caffeic acid (**6**), ferulic acid (**7**), rutin (**14**) and aspalathin (**21**). All the standards were obtained from Aldrich, except protocatechuic acid (Fluka) and aspalathin (Courtesy of Prof. D. Ferreira, University of the Orange Free State, Bloemfontein, South Africa). These were used as supplied. Samples and standards were run separately and their UV spectrums were determined by scanning from 210 nm to 450 nm for each chromatogram. Each standard was identified in the sample by comparing the retention times of the sample and standard peaks. The sample was also spiked with a standard and the change in peak size and the resulting UV spectrum monitored. The remaining peaks were not identified because of lack of standard samples.

Vanillic and caffeic acid could not be resolved, neither could ferulic and supposedly orientin as found also by Joubert[5]. It was clear from the spectrum of ferulic acid that the peak in the sample was not pure ferulic acid, hence it was assumed that the co-eluting peak was orientin as found by Joubert[5], whose mobile phase was very similar to the one used in the current work. Rutin and iso-quercitrin were not found to co-elute, as was the case for Joubert[5] . Only a small shoulder was found on the rutin peak and attributed to iso-quercitrin. Integration, described in section 3.3.5 as performed by the instrument, adequately takes the presence of this shoulder into account when calculating the area. The p-coumaric peak was also found to be contaminated although this was not observed by Joubert[5]. Due to the above mentioned co-elution and with the p-hydroxybenzoic acid concentration being at detection limit level of the instrument even in the most concentrated solution, protocatechuic acid, aspalathin and rutin were the only organic compounds chosen for kinetic investigation. The

normalised (with respect to peak height) UV-spectra annd chromatograms for protocatechuic acid, aspalathin and rutin are shown in Figures 3.10a to 3.12a and 3.10b to 3.12b respectively.

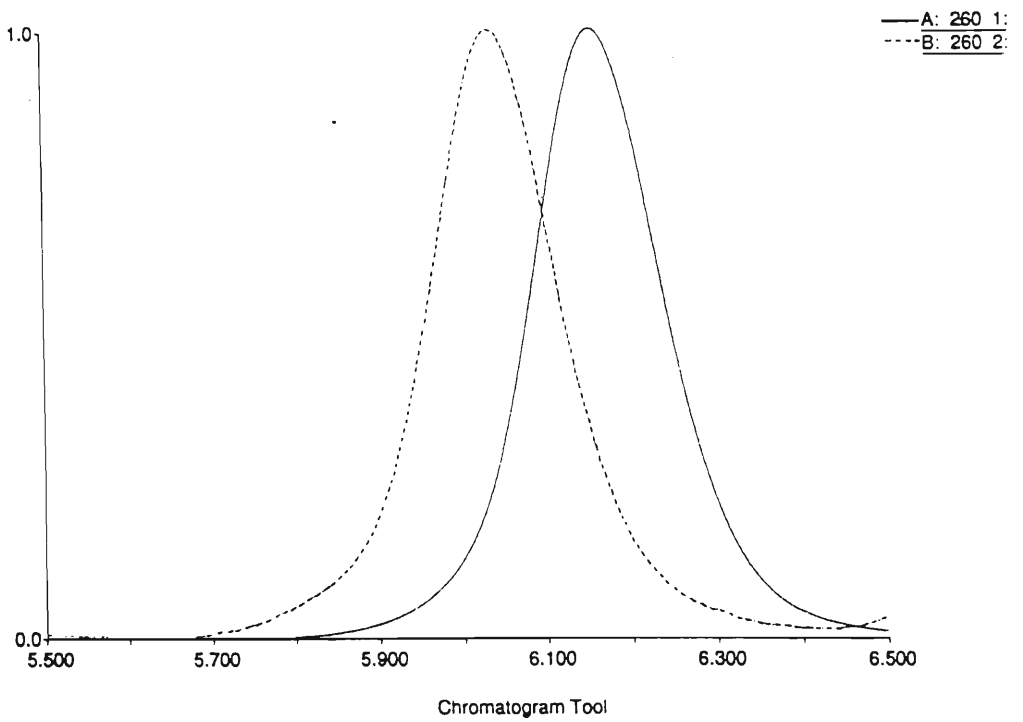

Figure 3.10a The normalised chromatogram of protocatechuic acid where trace (A) is that of the pure standard and trace (B) is of an actual tea sample brewed at 80 °C.

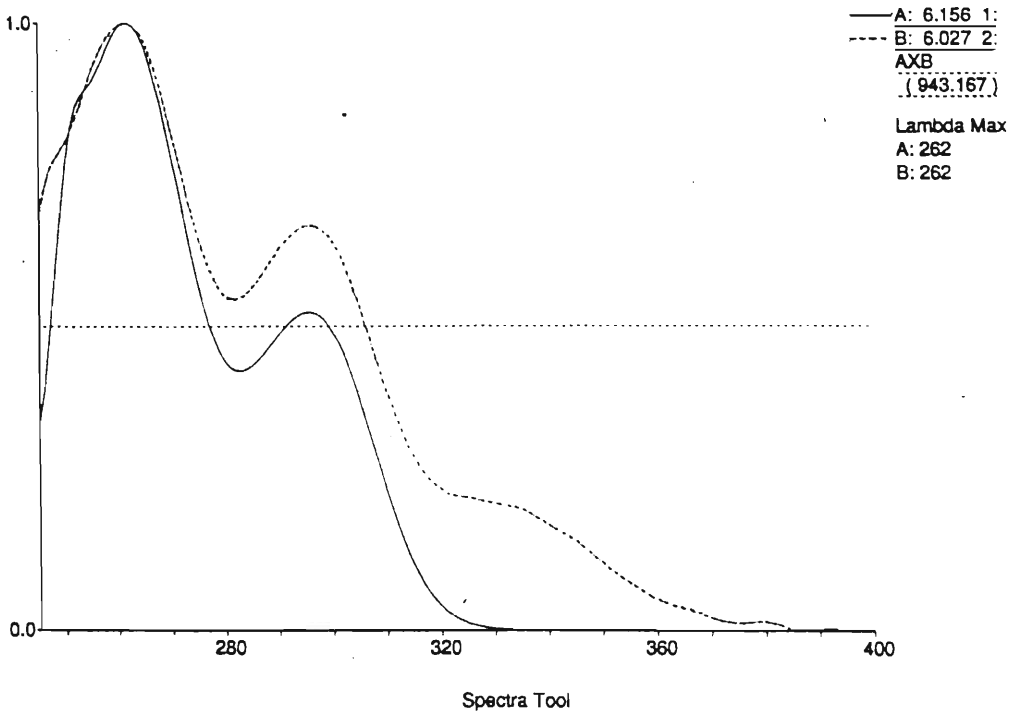

Figure 3.10b The normalised UV-Spectra of protocatechuic acid where trace (A) is that of the pure standard and trace (B) is of an actual tea sample brewed at 80 °C at the same retention time.

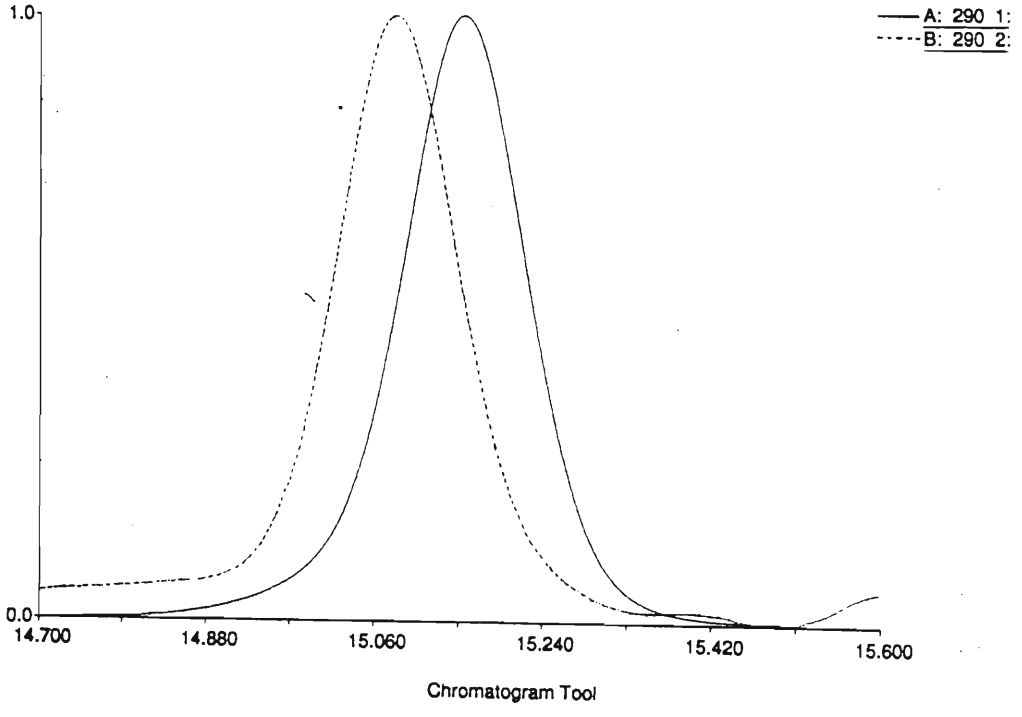

Figure 3.11a The normalised chromatogram of aspalathin where trace (A) is that of the pure standard and trace (B) is of an actual tea sample brewed at 80 °C.

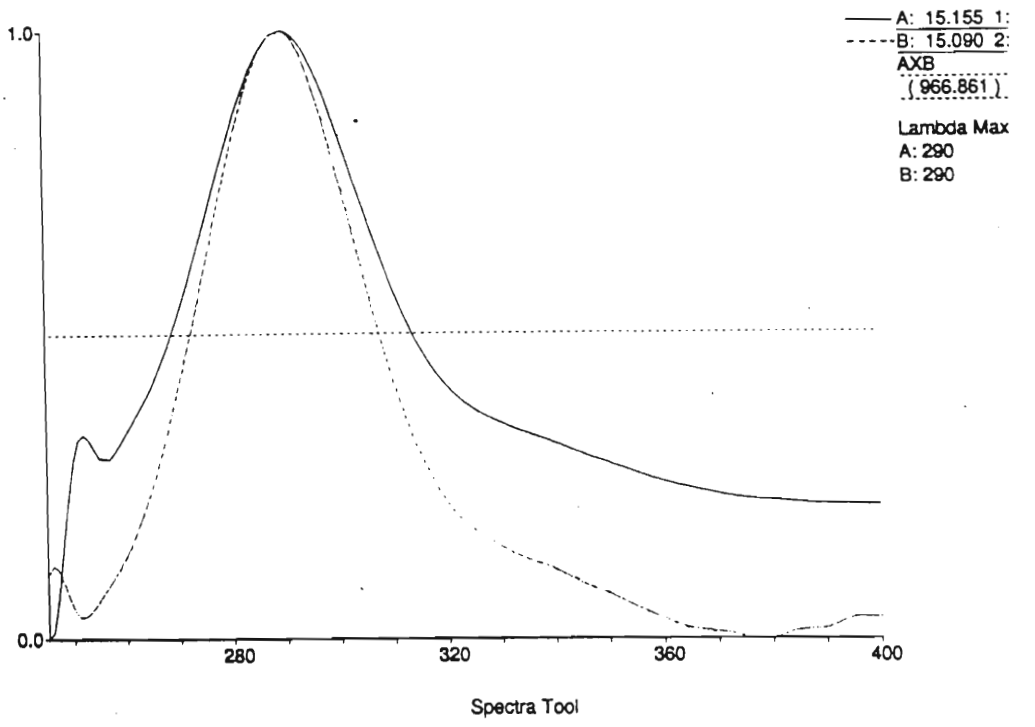

Figure 3.11b The normalised UV-Spectra of aspalathin where trace (A) is that of the pure standard and trace (B) is of an actual tea sample brewed at 80 °C at the same retention time.

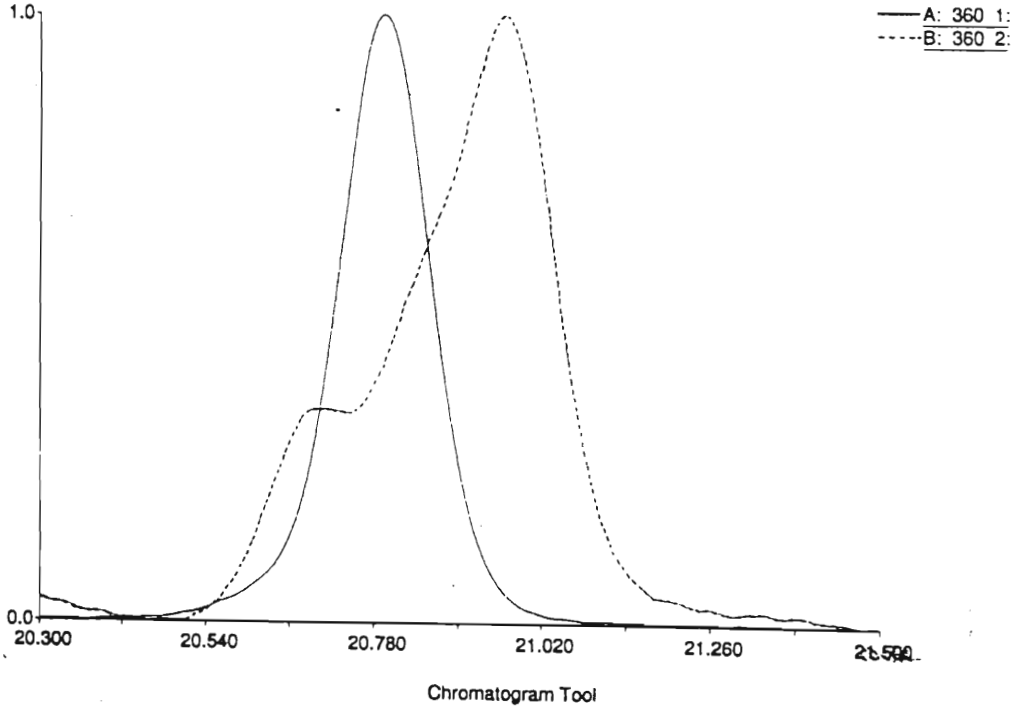

Figure 3.12a The normalised chromatogram of rutin where trace (A) is that of the pure standard and trace (B) is of an actual tea sample brewed at 80 °C.

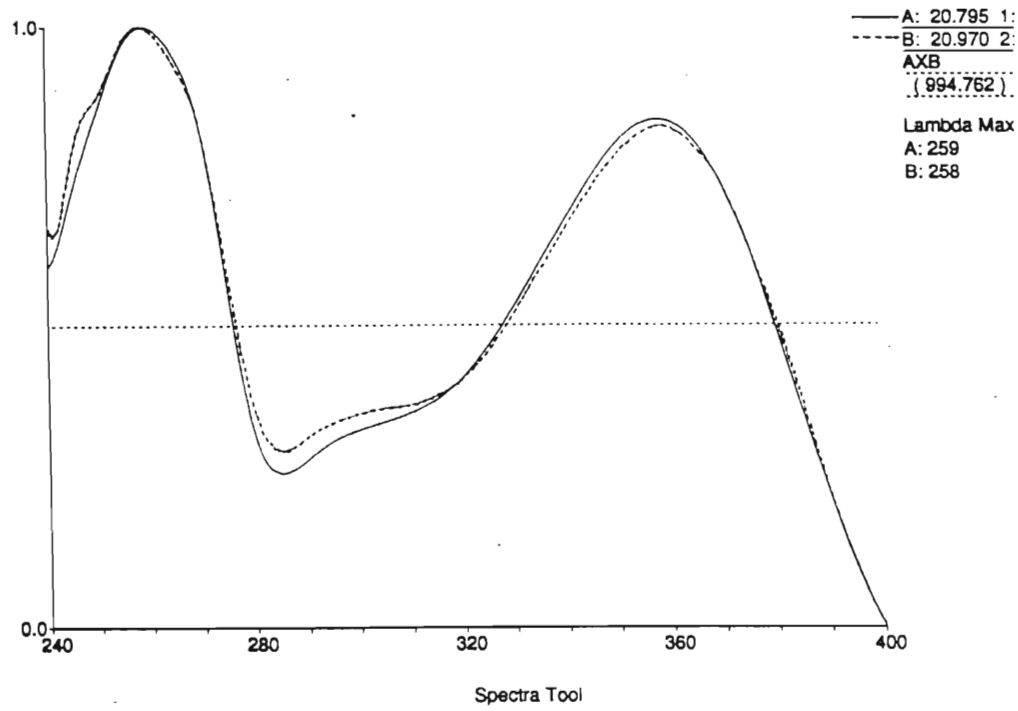

Figure 3.12b The normalised UV-Spectra of rutin where trace (A) is that of the pure standard and trace (B) is of an actual tea sample brewed at 80 °C at the same retention time.

The UV-spectra of the three compounds chosen showed the maximum wavelengths (λ_{max}) to be 262 nm for protocatechuic acid, 290 nm for aspalathin and two peaks for rutin the first one at 259 nm and the second 360 nm. These values agreed very well with data available in the literature[85,86,87]. The optimum wavelengths used in the current investigation were 260, 290 and 360 nm respectively. In the case of protocatechuic acid the wavelength was fixed at 260 nm because the detector could only be set at wavelengths of multiples of five. Rutin was analysed at 360 nm because the baseline was better than at 259 nm. Integration at the selected wavelengths ensured flat baseline and absence of interferents except in the case of rutin. Figure 3.13 represents a three dimensional chromatogram for Rooibos Tea at the selected wavelengths, while Figure3.14depicts those of the three standards.

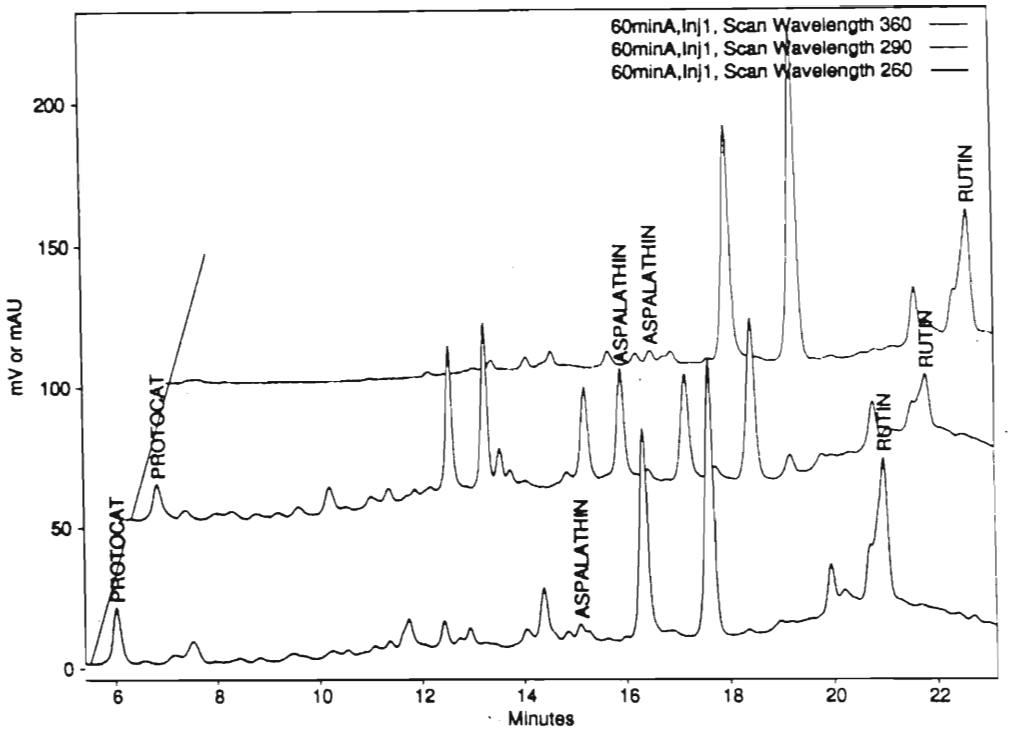

Figure 3.13 Typical chromatogram of Rooibos Tea as seen at 260, 290 and 360 nm.

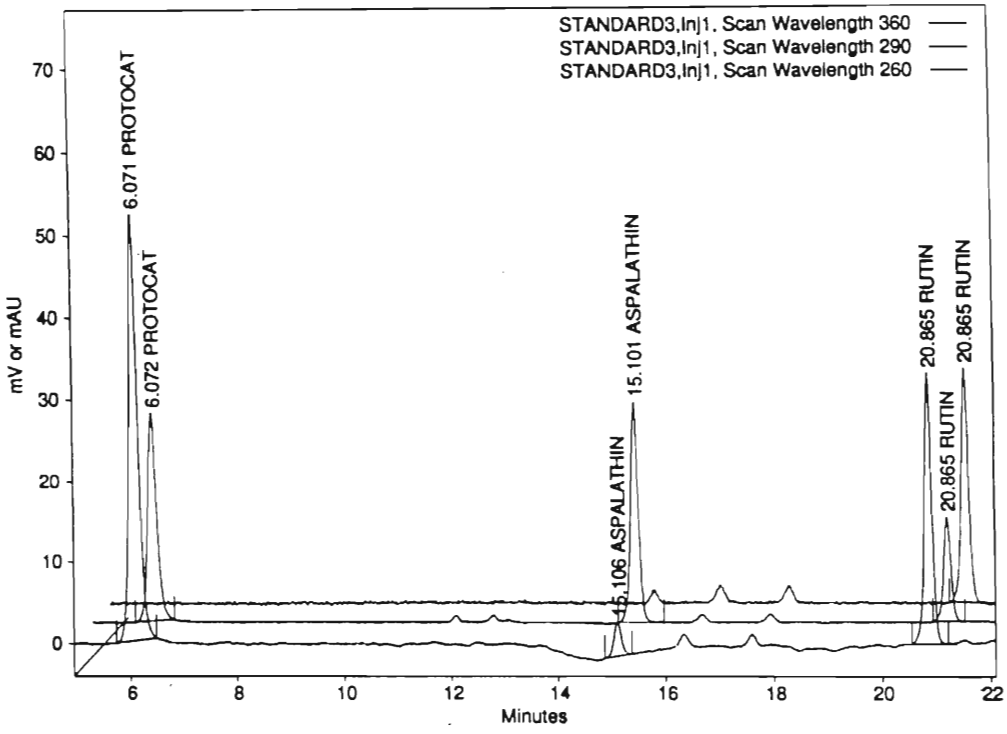

Figure 3.14 The chromatogram of a standard solution containing protocatechuic acid, aspalathin and rutin as seen at 260, 290 and 360 nm.

3.3.5 Summary of the Experimental Conditions for HPLC in the Current Work.

The mobile phase is as described in section 3.3.3. The organic compounds investigated were protocatechuic acid, aspalathin and rutin, with the detector set at three different wavelengths namely 260, 290 and 360 nm. HPLC instrumental specifications and analytical conditions used in the analyses are shown in Table 3.6.

After completing the analysis a standard instrument shutdown was performed. This involved gradual change of the mobile phase to 100 % methanol and holding this elution for 15 minutes. The aqueous formic acid bottle was replaced with a bottle of filtered MilliQ water, which was sparged for 14 minutes with helium gas. The methanol in the column was then gradually changed to 100 % water, and the elution held there for 10 minutes. Finally the solvent composition was brought to 50 % methanol-water and the column and the instrument flushed always for 10 minutes. The column was always parked in this condition. This was done so as to prevent any corrosion and mould growth taking place in the column and inside the instrument. Between various experiments a mixture of isopropanol-water 50 % (v/v) was pumped through the column at 0.2 ml/min for one day. This was done to clean out any constituents that may have remained in the column after the normal cleaning procedure.

Table 3.6 The HPLC component specifications and conditions during routine analyses.

Instrument	Thermo Separation Products
Detector	Spectra System UV3000 (Scanning)
Lamp for 190 nm - 450 nm scan	Deuterium
Lamp for 360 nm - 800 nm scan	Tungsten
Pump	Spectra System P2000 (2 solvents)
Injection valve	Rheodyne 6 port
Fixed loop volume	20 µl
Software	tsp PC 1000
Heater for column bath	Thermomix 1460
Guard column	Nucleosil 100-5 C_{18} (10 mm)
Column	Nucleosil 100-5 C_{18} (Macherey-Nagel)
Column length x inner diameter	250 x 4 mm
Stationary phase	Silica bonded C_{18} alkyl chains
Particle size	5 micon
Column Temperature	27.5 °C
Flow rate	1.0 ml /min

Pressure range	2000 psi - 3300 psi
Detector scanning range	210 nm - 450 nm
Data interval	5 nm
Data rate	5.43 Hz
Integration time	24.00 min
Sample run time	28.00 min

3.3.6 Calibration curves for the Organic Compounds

Standard solutions were made for protocatechuic acid (**2**), rutin (**14**) and aspalathin (**21**) from stock solutions of 106, 101 and 101 ppm respectively . The stock solutions were prepared by weighing 106, 101 and 101 mg of protocatechuic acid, aspalathin and rutin respectively into clean polytops. These were dissolved in a ready made, helium sparged solution of methanol-water 40 % (v/v) and washed into a 100 ml volumetric flask and made up to the mark. The methanol-water solution was sparged with helium to remove dissolved gases including oxygen which has been found by Fereirra *et al*[26] to oxidise aspalathin. The oxidation was actually observed when aspalathin was dissolved in a methanol-water solution which had not been helium sparged, but the effect was only noticeable after 12 hours at room temperature. The decomposition is assumed to occur in the same manner as described in section 1.3.1.5. [26,86]. A total of six standard solutions were then prepared from the stock solution. The standards and the stock solutions were always refrigerated at -10 °C when not in use, and when not in the freezer the standards were kept in ice. These precautions were taken to curb any possible reaction that may lead to the degradation of the samples. These standard concentrations (ppm) and their respective areas (μV-sec) are shown in Table 3.8. Included in the table is the slope (m) of the linear plot and the correlation coefficient (R^2). Since all plots passed through the origin there were no intercepts.

Table 3.8 The standard concentrations and area counts for the calibration of the listed compounds using HPLC. Protocatechuic acid, aspalathin and rutin were analysed at 260, 290 and 360 nm respectively.

Standard	**Protocatechuic acid**		**Aspalathin**		**Rutin**	
	Conc./ppm	Area/(μVs)	Conc./ppm	Area/(μVs)	Conc./ppm	Area/(μVs)
1	26.50	2333815	25.25	1091215	25.25	1096151
2	13.25	1168761	12.63	543903	12.63	548948
3	6.63	621006	6.31	286337	6.31	285776
4	3.31	317571	3.16	149498	3.16	149116
5	1.66	150083	1.58	68700	1.58	69919
6	0.83	81309	0.79	69919	0.79	38194
m	88464		43340		43560	
R^2	0.9995		0.9996		0.9997	

Using an external calibration method the HPLC constructed it's own calibration curves plotting area against concentration. The calibration program which is part of the PC 1000 software, incorporated a blank subtraction whereby the "blank" chromatogram is subtracted point for point from all subsequent chromatograms until another blank is injected. Hence the absence of an intercept in the calibration curve equations. The calibration plots for the three compounds as drawn using Microsoft Excel software are shown in Figures 3.15 - 3.17.

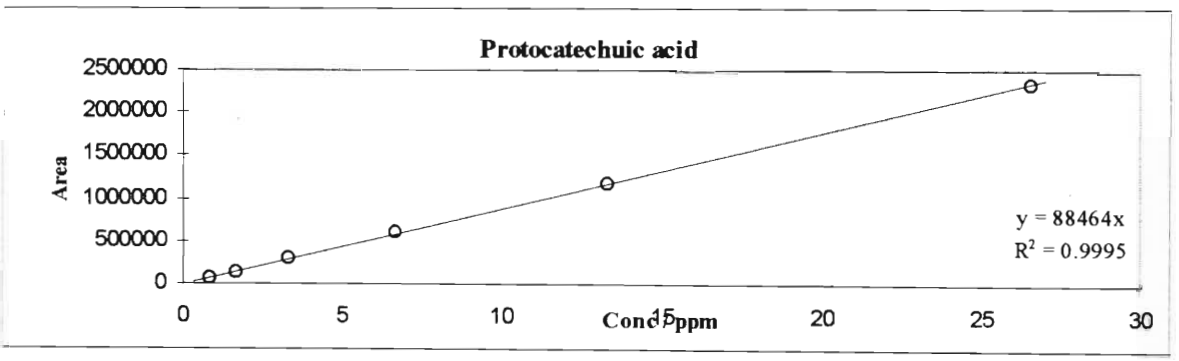

Figure 3.15 The calibration curve for protocatechuic acid determined at 260 nm.

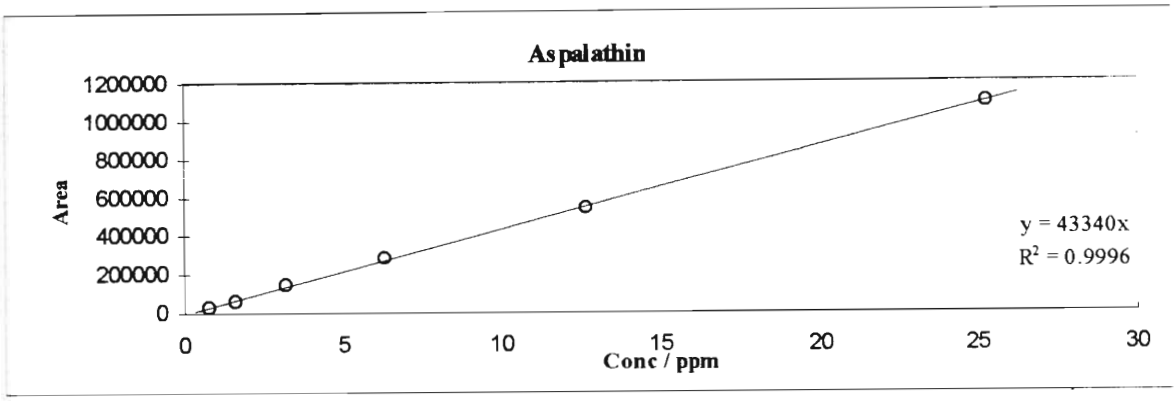

Figure 3.16 The calibration curve for aspalathin determined at 290 nm.

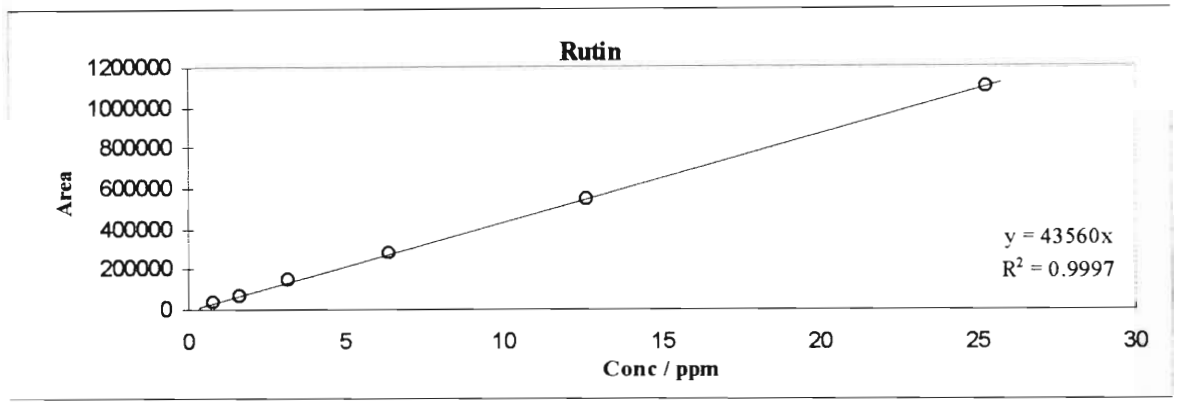

Figure 3.17 The calibration curve for rutin determined at 360 nm.

All peak integration was performed automatically by the PC1000 software. The software determined the peak area by fitting a triangle to the peak from the peak dimensions hence calculating the area. This method successfully coped with the shoulder on the rutin peak as shown in Figure 3.18. The allocation by the software of where the peak starts and ends was always checked and corrected manually, and the peak re-integrated when necessary using the "gravity" feature in the PC 1000 software.

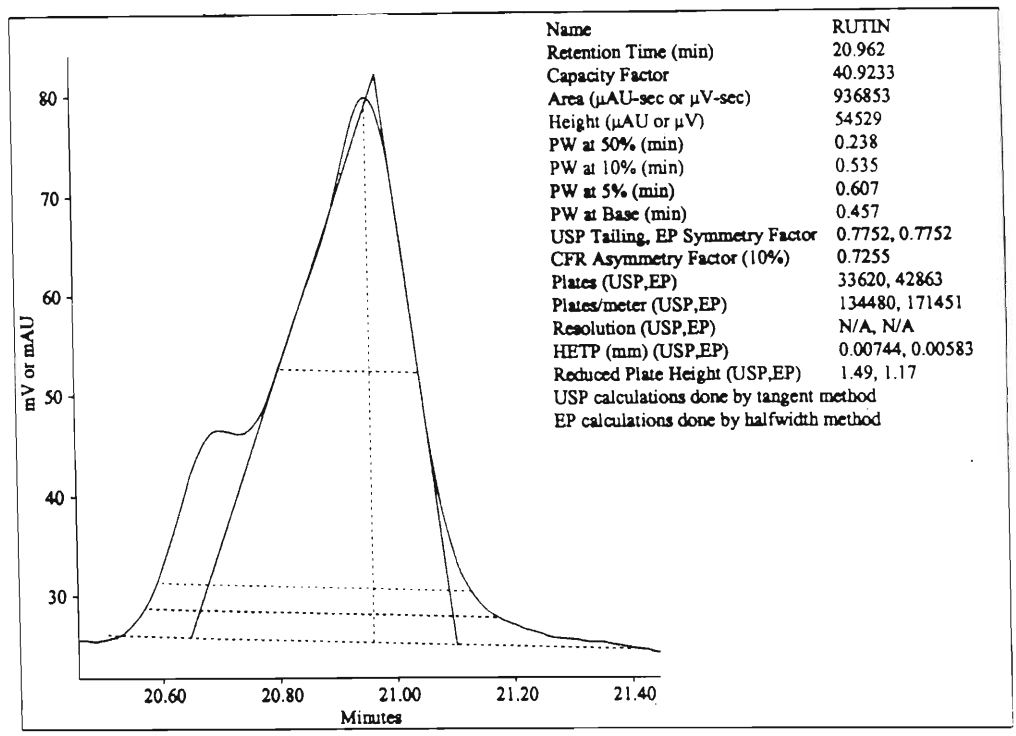

Figure 3.18 An attempt to demonstrate the integration technique employed by the HPLC in determining the peak area of rutin.

Two sets of standards were run intermittently during the five months of data collection. The calibration curves for the three compounds were found to be reproducible over the entire period, with all relative standard deviations of the slope being less than 2.4 %. The mean calibration curves in terms of Area (µV-sec) = Slope x Concentration (ppm) were determined. The average value of the slopes with their corresponding standard deviations in brackets were found to be 90010 (± 2.35 %) for Protocatechuic acid, 44682 (± 1.74 %) for Aspalathin and 43817 (± 1.27 %) for Rutin.

3.4 Analysis of Anions

3.4.1 Introduction

Ion chromatography (IC) is a single instrument technique yielding rapid sequential qualitative and quantitative analysis of anions. Other methods of monitoring anions include colorimetric and titration based procedures. IC has a distinct advantage over colorimetric analysis of anions in that it precludes many chemical interferences often encountered in the latter method, and the multi-species capabilities of IC and it's reliability far surpass the performance

of titration based methods. As a result IC is the most frequently used separation mechanism for anions as well as cations in solution.

3.4.2 The Principles of the IC.

The principle components that make up an Ion Chromnatography (IC) instrument are illustrated in Figure 3.19.

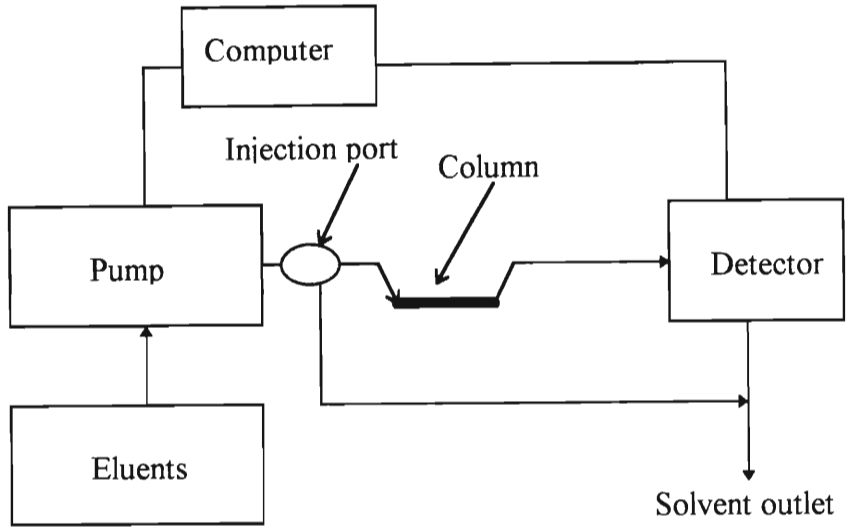

Figure 3.19 Typical components of an IC instrument.

The samples are generally aqueous solutions, these need to be prefiltered and in cases where a high organic content is suspected cleaned with C_{18} extraction cartridges. The eluants or mobile phase used are generally dilute solutions of salts, acids or bases or a combination of these, with pH playing a crucial role in eluant preparation[88]. Once the mobile phase is circulating the sample is injected manually or by autosampler, and the separation process begins as the sample reaches the column. The column packing material is dependent on whether analysis is for cations or anions[89]. A cation-exchange resin is used for M^+ analysis and is generally a strong-acid type resin functionalised with sulfonic acid groups or a weak-acid type with carboxylic acid groups. Anion-exchange resins contain basic amine functional groups attached to a polymer molecule. Strong-base exchangers are quaternary amines while weak-base exchangers are secondary or tertiary amines. All of these resins need to be insoluble in an aqueous medium. When the resin is immersed into this media the following type of exchange equilibrium is established between the mobile and stationary phases.

$$x\underset{\text{solid}}{RSO_3^-H^+} + \underset{\text{solution}}{M^{x+}} \leftrightarrow \underset{\text{solid}}{(RSO_3^-)_xM^{x+}} + \underset{\text{solution}}{xH^+}$$

Where M^{x+} is a cation and R represents that part of the resin molecule containing one sulfonic acid group. Similarly the process involving a typical anion resin can be expressed as follows where A^{x-} is an anion.

$$x\underset{\text{solid}}{RN(CH_3)_3^+OH^-} + \underset{\text{solution}}{A^{x-}} \leftrightarrow \underset{\text{solid}}{[RN(CH_3)_3^+]xA^{x-}} + \underset{\text{solution}}{xOH^-}$$

The separated ions are then monitored with a detector, most of which are based on conductivity. A limitation encountered for many years with IC is that the high electrolyte concentrations needed to elute most species in reasonable time tended to swamp the detector with respect to conductance, greatly reducing detector sensitivity. The solution to this is the suppressor column which is fitted immediately following the ion-exchange column. It is packed with a second resin and serves to convert the ions of the eluting solvent into a molecular species of limited ionisation, without affecting the conductivity of the analyte ions. The analyte species are then identified by their peak retention times as compared to those of standards and quantified according to conductivity from calibration data.

3.4.3 Experimental Conditions for IC in the Current Work.

Since the Chemistry Department did not have access to reliable IC equipment, samples were analysed by a commercial organisation (Umgeni Water Analytical Laboratory Services). The organisation restricted our access to the method of analysis, and all details that we did have access to are documented below.

Table 3.9 describes the IC apparatus and specifications as supplied by Umgeni Water Laboratory Services.

Table 3.9 IC Apparatus and specifications

Column	IC PAK A Anion column (Millipore PN WATO 07355).*
Detector	Waters M430 conductivity detector.
Pump	Waters M510/ M501 (dual piston).
Autosampler	WISP M710B or M712 or WATERS 717. 0-200 µl sample loop and auxiliary loop.
Manual injection (emergency)	RHEODYNE 20 µl loop.
Solvent clarification kit	2 l buchner flask and funnel HPVL 0.45 µm 47 mm diameter filters.
Sample clean-up (for high organic content)	Sep-Pak C_{18} extraction cartridges.
Solvent reservoirs	Polyethylene
Air supply	High quality compressed air for WISP
Systems controller	Millennium Chromatography Manager.

* Comprised of packed spherical beads of a polymethacrylate resin functionalised with quaternary ammonium groups.

The eluant was comprised of a mixture of Lithium hydroxide, Boric acid, D-gluconic acid, Butanol, Acetonitrile and MilliQ water. The needle wash solution was a mixture of Methanol and MilliQ water. Organic modifiers are added to the eluant to control microbial activity, reduce eluant viscosity and facilitate passage of organics through the column.

3.4.4 IC Standard Preparation

A composite stock solution for anions Cl^-, NO_3^-, NO_2^- and SO_4^{2-} anions was made up using KCl, $NaNO_3$, KNO_2 (all from UNIVAR) and K_2SO_4 (Riedel De Haen) respectively. These salts were all oven dried at 105 °C for 4 hours prior to weighing. An external calibration method was employed where the peaks appeared at retention times as displayed in Table 3.10.

Table 3.10 The peak retention times as observed using the IC.

Anion Species	Retention time / minutes
Cl^-	3.32
NO_2^-	4.43
NO_3^-	7.09
SO_4^{2-}	12.98

A typical chromatogram of a Rooibos Tea samplebrewed at 80 °C is shown in Figure 3.20.

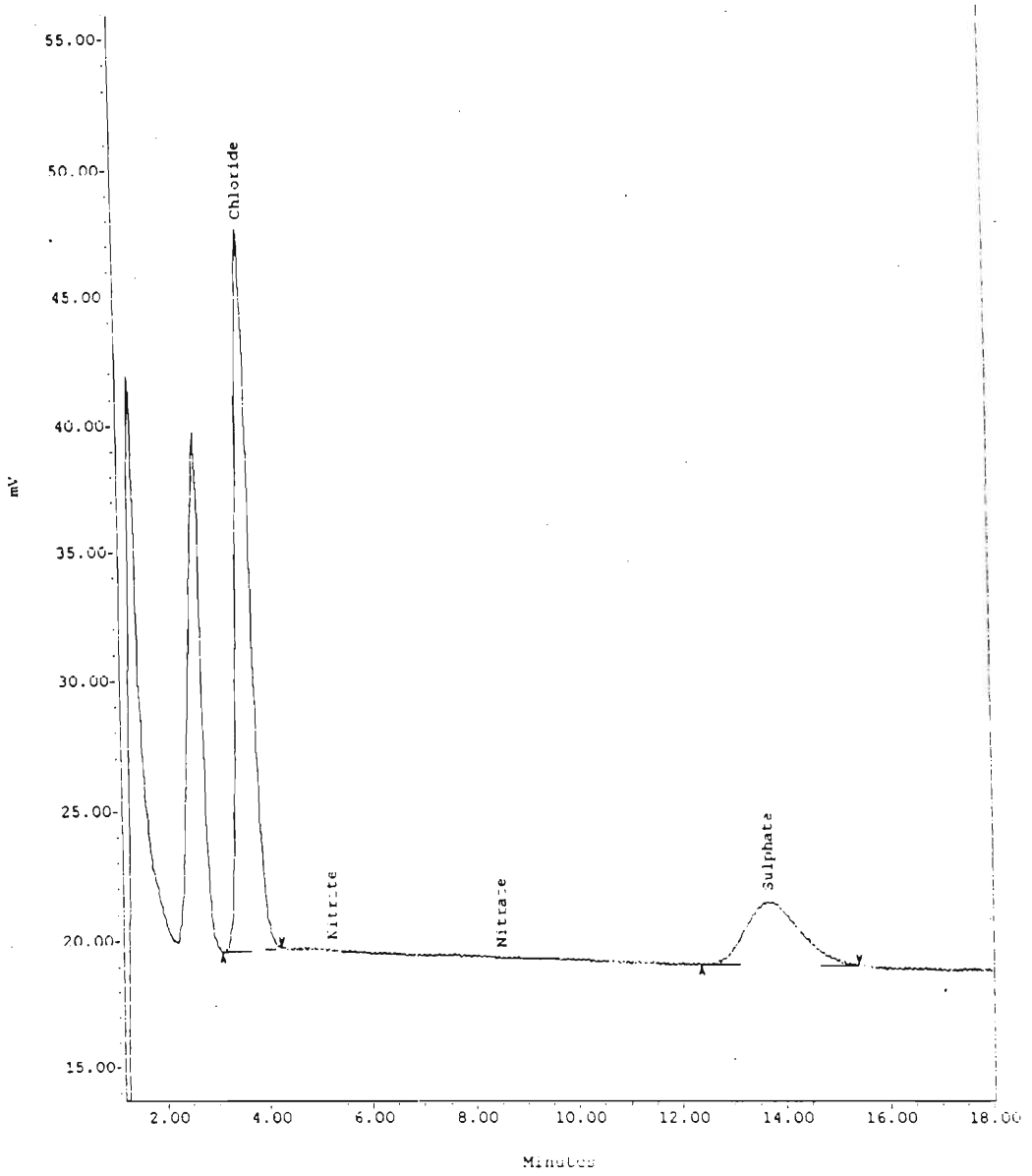

Figure 3.20 A typical IC chromatogram for a Rooibos Tea sample brewed at 80 °C.

CHAPTER 4

4 RESULTS AND DISCUSSION

4.1 Total Mineral Content of Rooibos Tea

The experimental procedure described in section 3.1.1 was used to determine the total mineral ion content of Rooibos Tea. Known amounts (4 g) of tea were ashed in two different types of crucible, 6 of vitreous silica and 3 of platinum, as suggested by Bock[69]. The resulting sample solutions were then analysed with the ICP-OES. Results obtained for all the elements were reproducible using the silica crucibles. However, the platinum crucibles gave reproducible results for only the alkali, alkaline-earth elements and phosphorus. Results obtained from the platinum crucibles for all the transition metals monitored for were not reproducible and hence omitted from the mean values. The average mineral ion concentrations determined are given in Table 4.1 along with the standard deviations.

Table 4.1 Mean mineral ion concentrations, from n number of samples, of Rooibos Tea as found with ICP-OES are presented in μg/g of dry tea with the respective standard deviations.

Element	Mean concentration (μg/g)	n
Sr	12.0 ± 0.3	6
Al	90.4 ± 3.1	6
Pb	1.6 ± 1.2	6
Fe	77.4 ± 5.6	6
Mn	75.7 ± 4.2	6
Zn	8.6 ± 1.3	6
Cu	3.0 ± 0.2	6
Ba	4.2 ± 0.1	6
Ca	2330 ± 124	9
P	703 ± 33	9
Mg	2450 ± 145	9
Na	5025 ± 375	9
K	3789 ± 261	9

There appears to be a dramatic difference between the mineral content of Rooibos Tea and that of Japanese green tea and certain black teas[70]. Rooibos Tea contains much more Na and Mg than do the Japanese green tea and the black tea. Ca content is higher in Rooibos Tea than in the black tea and similar levels of Ca can be found in the Japanese green tea. Rooibos Tea showed lower concentrations of P, Al, Mn, Fe, Cu and Zn than did both other teas. It is important to note, however, that mineral ion concentrations within the tea will vary with the location of the plant, the amount of fertiliser and type of fertiliser used in caring for the plant.

4.2 Acidification of samples for ICP-OES analysis

Rooibos tea extracts tend to show precipitation after standing for periods of time or with cooling. This precipitation is affected by a decrease in pH and takes on two forms depending on the circumstances surrounding the precipitation. On standing, the yellow precipitate seems "stringy" in accordance with Jouberts[90] findings that the precipitation is related to substances of high molecular weight and polymeric substances like proanthocyanidins. If however the pH is lowered with HCl, the yellow precipitate seems distinctly more powdery. This difference in precipitation may be due to the difference in the time period involved in the precipitation process, which is much shorter with the acid present or due to the presence of the acid itself. To minimise adsorption of mineral ions on the surface of the containers, the ICP-OES standards were made up in 0.1 M HCl (BDH Aristar HCl with MilliQ water). This is critical when monitoring trace concentrations. Subsequently, all the tea samples from a kinetic run were diluted with 0.1 M HCl solution so as to limit the ion adsorption and to match the sample and standard matrices. Thus an investigation into the effect of acidifying the tea samples was carried out.

The tea was brewed in the usual way as described in section 3.1.2 at 90° C and samples drawn after 3 and 30 minutes to represent the lower and the higher concentration range respectively. The two samples were each divided into 6 aliquots and half of the aliquots were diluted with MilliQ water and the other half diluted with the 0.1 M HCl solution. No

precipitate was formed in the samples diluted with the acid as suspected. All the samples were then analysed using ICP-OES. The results are tabulated in Table 4.2.

Table 4.2 A comparison of water (MilliQ) and acid (0.1M HCl) dilution of both a 3 minute sample and a 30 minute sample. All values (in ppm) are means from a triplicate analysis.

Element	3 Minute sample (ppm)		30 Minute sample (ppm)	
	Water dilution	Acid dilution	Water dilution	Acid dilution
Sr	< 0.07	< 0.07	< 0.07	< 0.07
Mg	5.12 ± 0.43	5.19 ± 0.09	9.73 ± 0.28	10.36 ± 0.62
Al	< 0.06	< 0.06	0.15 ± 0.02	0.160 ± 0.019
Pb	< 0.05	< 0.05	< 0.05	< 0.05
Fe	< 0.14	< 0.14	< 0.14	< 0.14
Na	21.3 ± 2.0	23.18 ± 0.14	31.3 ± 1.4	34.7 ± 2.0
Mn	0.15 ± 0.02	0.148 ± 0.003	0.258 ± 0.012	0.282 ± 0.013
Ca	3.80 ± 0.36	3.90 ± 0.14	4.59 ± 0.16	4.81 ± 0.38
P	2.76 ± 0.28	2.78 ± 0.08	3.94 ± 0.11	4.06 ± 0.28
Zn	< 0.12	< 0.12	< 0.12	< 0.12
Cu	0.067 ± 0.005	0.08 ± 0.02	0.067 ± 0.005	0.062 ± 0.003
Ba	< 0.05	< 0.05	< 0.05	< 0.05
K	22.88 ± 2.12	23.67 ± 0.35	30.7 ± 1.0	33.1 ± 1.9

Thus all the ICP-OES samples were acidified and run within one day to avoid any possibility of precipitation.

4.3 Equilibrium Studies

4.3.1 Determination of Partition Coefficient using the Graphical Method

A graphical method was used to determine the partition coefficient of various species infusing from the tea leaves. This method made use of the relationship:

$$\frac{1}{C_\infty} = \frac{1}{KC_0} + \frac{\rho V}{mC_0} \qquad (36)$$

as described in section 2.4.1. C_0 represents the initial component concentration within the leaf after penetration by water, and before any extraction of the component. The partition coefficient, equilibrium concentration, volume of water used, mass of the wet tea leaves and density of the wet swollen leaves are represented by K, C_∞, V, m, and ρ respectively. Experiments were performed in duplicate using five different masses of Rooibos Tea. The equilibrium samples were taken after 90 minutes and their concentrations determined. These mean equilibrium concentrations and the masses used are listed in Table 4.3. Using these mean values, graphs of $1/C_\infty$ versus $1/m$ were plotted, (Microsoft Excel) and were found to be linear. Two of the graphs are shown in Figures 4.1 and 4.2. Once the slopes and intercepts were obtained from the graphs, values of C_0 and K were calculated. Knowing C_0, the mass concentration of the component in the dry tea leaf (x_0) could be calculated from[66]:

$$x_0 = \beta\, C_0 M / \rho$$

Where β is the wet mass : dry mass ratio of the tea leaves, M is the molecular mass of the component and ρ is the density of the swollen wet leaves. These values are listed in Table 4.3.

Table 4.3 Tabulated are the tea leaf masses and the equilibrium concentrations they yielded. Also tabulated is the intercept (ppm^{-1}) and slope (kg/ppm) obtained from the graphs of the various components along with the calculated x_0 (g/kg), C_0 (mol/dm^3) and K values. A negative partition coefficient is meaningless and thus omitted from the table.

mass / g	Mean Equilibrium concentrations (ppm)							
	Na^+	K^+	Mg^{2+}	Ca^{2+}	Prot	Asp	Rutin	HPO_4^{2-}
3.9979	23.9051	24.1427	9.1500	5.0192	3.8479	13.0602	26.8741	2.6743
3.5002	21.6161	21.7450	7.9861	4.3895	3.6233	12.8080	28.5109	2.4358
2.9999	14.0488	14.8076	6.4023	3.4443	2.9908	10.9368	23.6857	1.8925
1.9995	9.6701	10.0768	4.0161	2.8407	2.0178	7.3867	15.4354	1.4981
1.5004	6.6148	6.2468	2.6096	2.5196	1.4121	5.5621	11.8404	1.0393
1.0000	2.3268	5.2455	1.3854	1.8749	0.5758	1.9780	4.5435	0.9350
	Mean slope, intercept and calculated values as obtained from graphs from duplicate analyses.							
intercept	-0.023 ± 0.007	-0.031 ± 0.009	-0.033 ± 0.004	0.106 ± 0.019	-0.026 ± 0.021	0.008 ± 0.004	0.003 ± 0.004	0.036 ± 0.048
slope x 10^3	0.26 ± 0.02	0.28 ± 0.02	0.56 ± 0.01	0.44 ± 0.03	1.08 ± 0.05	0.26 ± 0.01	0.12 ± 0.01	1.36 ± 0.11
C_0	1.539 ± 0.096	1.435 ± 0.107	0.708 ± 0.016	0.916 ± 0.066	0.370 ± 0.016	1.560 ± 0.060	3.284 ± 0.220	0.295 ± 0.024
x_0	3.522 ± 0.220	3.282 ± 0.245	1.620 ± 0.036	2.096 ± 0.151	0.846 ± 0.038	3.570 ± 0.138	7.514 ± 0.503	0.674 ± 0.055
K	-	-	-	0.010 ± 0.002	-	0.081 ± 0.045	0.096 ± 0.108	0.096 ± 0.130

Total mineral ion concentration (x_0) has been determined *via* the graphical method for partition coefficient determination. However, ICP-OES analysis of Rooibos Tea for determination of total mineral ion concentration has also been performed (section 4.1), the results from which are considered to be reliable. Comparison of the two values will reflect the credibility of the graphical method as a means of determining total component concentration within the tea leaf. Values obtained from both methods are given in Table 4.4 along with the percentage differences.

Table 4.4 A comparison of total mineral ion concentrations as obtained using the ICP-OES and *via* the graphical method for partition coefficient determination.

Element	$x_{0\,(\text{ICP-OES})}$ (μg/g)	$x_{0\,(\text{Graphical method})}$ (μg/g)	Difference (%)
Na^+	5025	3522	30
K^+	3789	3282	13
Mg^{2+}	2450	1620	34
Ca^{2+}	2330	2096	10

As the table shows, the values differ by between 10 and 34 %. Consequently, the reliability of total component concentrations obtained using the graphical method remain questionable.

Also, all the intercepts found with this method were small and easily influenced by experimental error. As seen in the Table 4.4, some of the intercepts are negative. This suggests that the graphical method is prone to significant error, since a negative intercept implies a negative equilibrium concentration, which is impossible. As a result, the partition coefficients derived in this manner are also prone to error as they are calculated using the intercept values. The K values obtained range from 0.010 to 0.096. These values imply that the concentrations of the various components in the tea liquor are between 10 and 100 times less than the concentrations of the components within the tea leaf, at equilibrium at 80 °C. Figures 4.1 and 4.2 show typical graphs of plots yielding positive and negative intercepts respectively.

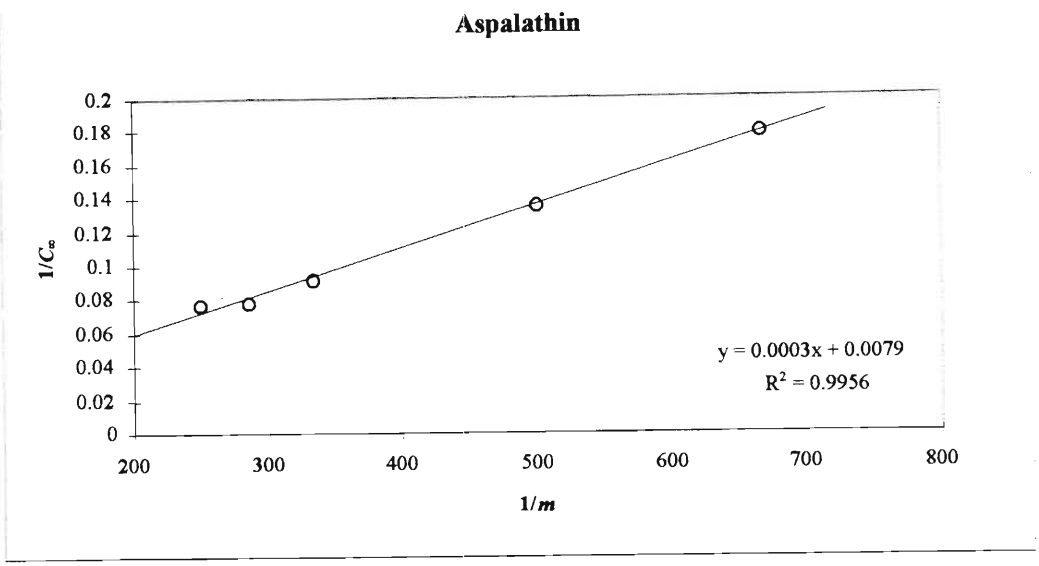

Figure 4.1 Plotting $1/C_\infty$ versus $1/m$ for the determination of the aspalathin partition coefficient. This graph highlights the small positive intercept.

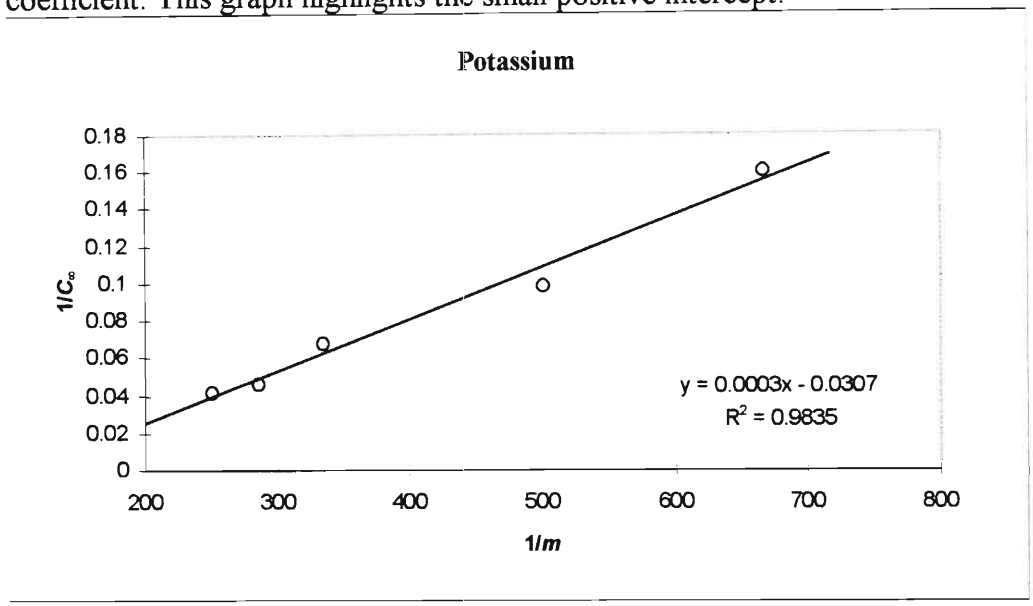

Figure 4.2 Plotting $1/C_\infty$ versus $1/m$ for the determination of the potassium partition coefficient. This graph highlights the small negative intercept.

Spiro and Chen[91] in their work on Rose hip tea, and Spiro and Selwood[66] in their coffee infusion investigations, also found the intercepts and thus partition coefficients unreliable from this method. It appears then that the graphical method is limited both in terms of providing total component concentrations as well as partition coefficients. Subsequently, the latter two workers developed another technique for partition coefficient determination, the successive extraction method as described in section 4.3.2.

4.3.2 Determination of Partition Coefficeient using the Sucessive Extraction Method

Since the graphical method could not provide reliable partition coefficients, an alternative method for the determination of partition coefficients was employed[66]. The experimental procedure is as described in section 3.1.3.2 The brewing temperature was 80 °C and the mass of tea used was 4 g. The first equilibrium sample, $C_{\infty 1}$, was taken after 60 minutes. The water-swollen leaves were infused into a fresh volume of water and the extraction process repeated. The second equilibrium sample, yielding $C_{\infty 2}$, was taken after one hour. The mass (m) and density (ρ) of the swollen wet leaves were also determined. All the obtained values were substituted into Equation 42, where V represented the water volume used in the extraction, and the partition coefficients determined.

$$K = \frac{m}{\rho V}\left(\frac{C_{\infty 1}}{C_{\infty 2}} - 1\right) \qquad (42)$$

The experiment was repeated three times. The mean ratio of wet to dry tea leaves mass (β) was found to be 2.43 ± 0.06. Mean density values for the swollen wet leaves (ρ_{swo}) and the dry leaves (ρ_{dry}) were obtained using a pycnometer. Water was used in the pycnometer as the solvent for the wet swollen leaves, and toluene (AR, Merck) for the dry unswollen leaves. Values for ρ_{swo} and ρ_{dry} were found to be 1.063 ± 0.001 and 1.102 ± 0.005 gml^{-1} respectively. The average equilibrium concentration values (ppm), and the calculated partition coefficients and their respective standard deviations are given in Table 4.5. Only two extractions were carried out since very little of the species would infuse into the solution at the third extraction.

The β value calculated here for Rooibos Tea of 2.43 ± 0.06, is larger than that found by Spiro and Chen[91] for Rose-hip tea of 1.635. The density of swollen wet Rooibos Tea compares favourably with that found by Spiro and Chen of 1.019 g/ml for a similar sieving fraction[91] of Rose-hip tea. Knowing β, we can determine a swelling factor from :

$$\beta = \frac{m_{swo}}{m_{dry}} = \frac{\rho_{swo} V_{swo}}{\rho_{dry} V_{drry}} = \frac{1.063 V_{swo}}{1.102 V_{dry}}$$

Substituting the β value into the above equation, the swelling factor is determined to be :

$$V_{swo} = 2.52\ V_{dry}$$

This indicates that Rooibos Tea leaves swell by a factor of 2.52 when submerged in water, and this value is very close to that found by Spiro and Chen[91] of 2.4 for rose-hip tea.

Table 4.5 First ($C_{\infty 1}$) and second ($C_{\infty 2}$) extraction equilibrium concentrations, and the resultant partition coefficients for the monitored cations, anions and organic components.

Mineral	Equilibrium Concentrations (ppm)		*K* mean
	$C_{\infty 1}$	$C_{\infty 2}$	
Mg^{2+}	8.30 ± 0.02	0.14 ± 0.05	**1.473 ± 0.642**
Na^{+}	23.65 ± 0.37	1.52 ± 0.29	**0.340 ± 0.061**
Ca^{2+}	5.71 ± 0.20	1.18 ± 0.10	**0.088 ± 0.007**
K^{+}	25.89 ± 0.59	1.15 ± 0.06	**0.492 ± 0.011**
Protocatechuic acid	3.51 ± 0.09	0.23 ± 0.01	**0.331 ± 0.028**
Aspalathin	13.78 ± 0.14	1.29 ± 0.07	**0.222 ± 0.017**
Rutin	28.40 ± 1.51	3.02 ± 0.21	**0.193 ± 0.015**
$H_2PO_4^{-}$	3.14 ± 0.07	0.09 ± 0.01	**0.752 ± 0.101**
Cl^{-}	33.33 ± 3.31	5.80 ± 5.13	**0.079 ± 0.033**
SO_4^{2-}	8.80 ± 0.71	0.80 ± 0.00	**0.228 ± 0.019**

All the equilibrium concentration values of the various species tabulated in Table 4.5 were found to be reproducible, except for the chloride ion which showed large variations. Of the obtained *K* values, magnesium has the highest value of 1.47, while the chloride ion has the lowest value of 0.079. The high value of Mg^{2+} may be due to the fact that its extraction may be pH dependent. In a normal extraction (Particle size 1.40 -1.00 mm sieve, at 80 °C) the pH was found to be 4.6 at equilibrium. When a second extraction was performed with the same tea leaves and fresh water, the pH was found to be 5.10. The low concentration of Mg^{2+} found in the solution after the second extraction could be due to this difference in pH, and hence the very high *K* value. The difference in pH values between the first and second extractions is plausible when one considers that a large proportion of the organic acids extracted initially, are present in much lower concentrations during the second extraction.

Some trends are noticed within the groups of species. The singularly charged cations; Na^{+} and K^{+} show higher *K* values than that for Ca^{2+}, with K^{+} being the highest. This trend could also be related to the hydrated radii of the ions. Diffusion coefficients (D_{aq}) for the ions in

aqueous media as presented in section 4.4.7, show that the singularly charged ions concerned have much smaller hydrated radii than the doubly charged Mg^{2+}. Unfortunately a D_{aq} value for Ca^{2+} was not obtained, but it is feasible that this doubly charged ion of similar size to sodium will also have a larger hydrated radius than the respective singularly charged ions.

All the organics (protocatechuic acid, aspalathin and rutin) are neutral and the partition coefficient value is possibly dependant on the molecular mass, and hence the size of each species. Or, the trend could also be as a result of the difference in polarity of the species which increases in the following order : Rutin > aspalathin > protocatechuic acid, as found with the elution order on the HPLC. The more polar protocatechuic acid, possibly due to the carboxylic acid functional group, more readily dissolves in the polar water solvent than do the other two.

Of the anions, the singularly charged Cl^- ion has the lowest partition coefficient, followed by the sulfate ion and the orthophosphate ion having the largest value. There is no partition coefficient trend within the three groups of species namely; cations, anions and organics.

4.3.3 Determination of Partition Coefficient using Total Mineral content values.

Due to the uncertainty of the partition coefficient for Mg^{2+} as determined in section 4.3.2, and for the sake of verifying the results given in Table 4.5, an alternative method was used to calculate the partition coefficients. The method involved the use of the total mineral content values C_0, as determined by ICP-OES in section 4.1. Knowing C_0 and the equilibrium concentrations within the bulk solution (C_∞), the concentration in the leaf at equilibrium (C_∞^*) can be determined from (variables defined in section 4.3.2)

$$C_0 V_{dry} \rho_{dry} = C_\infty V \rho_{soln} + C_\infty^* V_{swo} \rho_{swo}$$

Substituting these values into Equation (2) of chapter 2, the partition coefficients were calculated for four replicates (inclusive of an extra $C_{\infty 1}$ value) and the average values are tabulated in Table 4.6. The C_∞ values used in this calculation were the equilibrium concentrations listed as $C_{\infty 1}$ in Table 4.5. The C_0 values are the same values given in Table 4.3 in μg/g, and converted into ppm using the exact mass (W) of tea used for the infusion (4

g) and the exact volume (V) of water (400 ml). The former partition coefficient values were subject to many variables including the difference in pH between the first and second extraction, the analyte coating on the tea leaf surface before the second extraction and the assumption that the tea samples were equally dried in each experiment. In comparison, this approach provides a direct means of determining the partition coefficients with minimal error. Unfortunately, only species responsive to the ICP-OES were analysed in this manner.

Table 4.6 The equilibrium concentrations in ppm of the species monitored on the ICP-OES and their respective standard deviations (Analysis in quadruplicate). Also tabulated are the average partition coefficient values and the corresponding standard deviations.

Element	C_o	C_∞^*	C_∞	**Mean K**
Na^+	50.432 ± 0.129	21.025 ± 0.069	23.454 ± 0.421	**1.116 ± 0.026**
K^+	38.871 ±0.100	15.869 ± 0.031	25.726 ± 0.501	**1.621 ± 0.035**
Mg^{2+}	24.419 ± 0.063	10.315 ± 0.029	8.273 ± 0.047	**0.802 ± 0.007**
Ca^{2+}	23.223 ± 0.060	9.875 ± 0.045	6.384 ± 1.439	**0.647 ± 0.172**
HPO_4^{2-} **(P)**	6.977 ± 0.018	2.915 ± 0.009	3.102 ± 0.087	**1.064 ± 0.036**

All K values determined using this method are higher than those from the successive extraction method except for magnesium. As with the successive extraction method, the K values for the singularly charged cations ions are larger than those for the doubly charged cations. The concentration of potassium in the bulk solution at equilibrium is almost twice that in the leaf, this is reflected in the high value of K. Natesan and Ranganathan[92] have reported similar ratios of potassium in solution to that in the leaf, for Orthodox teas from Nilgris and CTC teas from Anamallais, to be 1.9 and 2.2 respectively. The ratios of sodium reported were 1.2 and 2.2 for the same teas respectively, the former being similar in magnitude to that obtained using this method. All these ratios were determined after 5 minutes of infusion. Even this method for the determination of the partition coefficient will be subject to some error, since for many of the species only part of the C_o will have been exchangeable. This may account for the relatively high partition coefficients obtained.

4.4 Kinetic Studies

4.4.1 Determination of Rate Constants of infusion at 80°C

Kinetic studies were carried out on species that showed first order behaviour. These were identified by infusing tea in the usual way (4 g tea, 400 ml MilliQ water, using 1.40-1.00 mm sieving) and taking a full range of samples as described in section 3.1.2. All samples were analysed as described in sections 3.2, 3.3 and 3.4, for cations and phosphorus, organics and anions respectively, and plots of concentration versus time drawn. The species that yielded the typical first order plots exemplified in Figure 2.1, were sodium, potassium, magnesium, protocatechuic acid, aspalathin, rutin, and phosphorus.

The C_∞ values for each species were obtained from the plots before correcting for sampling and evaporation. If one is to obtain a correct overall rate constant (k_{obs}), the C_∞ value used in Equation 17 needs to be corrected for water loss. Using 0.97183 gml^{-1} [99] as the density of water, ΔV and V values were calculated for use in Equation 28. If ΔV_T represents the total volume of water lost during the experiment, then ΔV is calculated from this by dividing through by the number of samples taken and multiplying the outcome by the number of samples required too reach equilibrium. The number of samples required to reach equilibrium were obtained by comparing which of the uncorrected concentration values were closest to the corrected values. While water is lost through sampling and evaporation, so too is analyte lost. The number of moles lost with each sample (ΔT), is calculated using Equation 26, and Equation 28 was used to calculate the total correction for C_∞. Correction for water loss was also performed on all individual observed concentrations using Equation 30. Table 4.7 tabulates the values of ΔV, ΔT, C (uncorrected) and C (corrected) for the relevant sample times.

Table 4.7 Typical correction for water loss data, shown here for sodium. All concentrations are presented in ppm, and ΔT is also presented in ppm for comparison. In this instance, ΔV_T was 41.37 ml and ΔV 2.75 ml for 15 samples.

Time / s	Observed Conc./ppm	ΔT / ppm	Corrected Conc. /ppm
0	0.000	0.00	0.00
30	7.50	0.07	7.50
60	10.05	0.10	10.04
90	12.14	0.11	12.10
120	13.00	0.12	12.94
150	14.04	0.13	13.95
180	14.47	0.14	14.37
210	15.56	0.15	15.41
240	15.51	0.15	15.36
300	16.13	0.18	15.95
900	20.84	0.20	20.37
1800	21.92	0.21	21.37
2700	22.91	0.22	22.29
3600	22.55	0.22	21.96
5400	23.53	0.23	22.85

Figures 4.3 - 4.9 illustrate the concentration - time relationships obtained for the respective species. The different symbols used in these graphs represent the duplicate analyses performed. Reproducibility is seen to be reasonable. Due to the limited access to the IC instrument, the only samples analysed were those that were required for the determination of rate constants. The concentrations obtained were fitted into Equation 17 and found to produce reproducible linear plots. It was therefore concluded that the Cl^- and SO_4^{2-} ions obeyed first order extraction. The corresponding concentration data, given as a mean of 3 values, is given in Tables 4.8-4.10 with the corrected concentration shown in brackets.

Table 4.8 Concentration (ppm) versus time (sec) data for the cations as obtained during an infusion at 80 °C. Corrected (for water loss) concentration values are given in brackets.

Species	Na^+	K^+	Mg^{2+}
Time/sec	Concentration (corrected) / ppm		
0	0.000 (0.000)	0.000 (0.000)	0.000 (0.000)
30	7.503 (7.503)	9.714 (9.714)	1.114 (1.114)
60	10.053 (10.036)	11.514 (11.502)	2.140 (2.133)
90	12.143 (12.097)	13.154 (13.119)	3.023 (3.004)
120	13.003 (12.939)	14.464 (14.402)	3.462 (3.434)
150	14.043 (13.950)	15.274 (15.190)	4.085 (4.040)
180	14.473 (14.365)	15.604 (15.508)	4.147 (4.099)
210	15.563 (15.410)	16.654 (16.515)	4.489 (4.427)
240	15.513 (15.363)	16.864 (16.715)	4.559 (4.494)
300	16.133 (15.949)	17.634 (17.442)	5.050 (4.958)
900	20.843 (20.366)	21.174 (20.762)	6.904 (6.697)
1800	21.923 (21.372)	23.044 (22.503)	7.997 (7.714)
2700	22.913 (22.287)	22.844 (22.318)	8.830 (8.484)
3600	22.553 (21.957)	25.064 (24.354)	8.928 (8.574)
5400	23.533 (22.849)	23.624 (23.043)	9.892 (9.452)

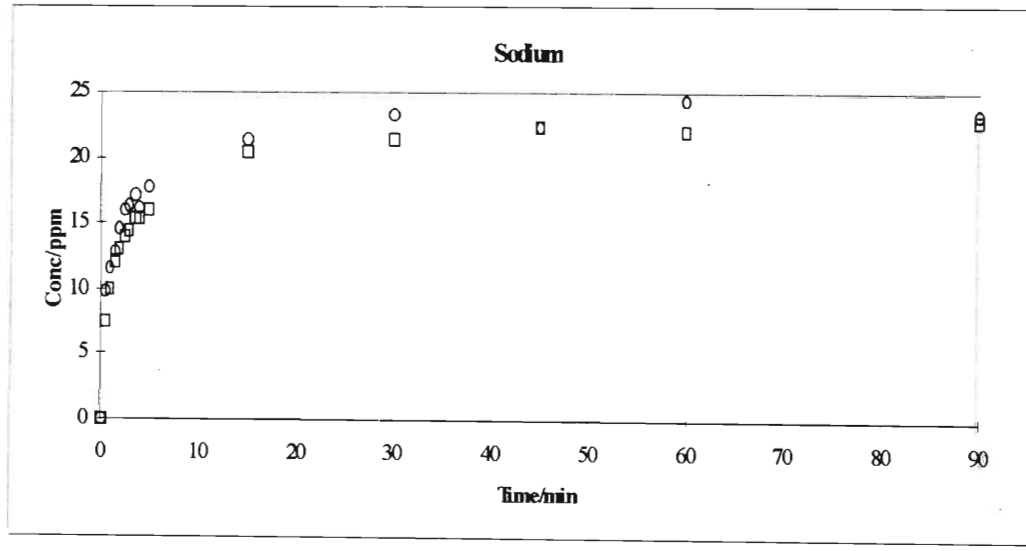

Figure 4.3 Plot of concentration (ppm) versus time (min) for sodium, showing the typical trend of rapid initial concentration increase, and leading up to the equilibrium concentration (C_∞) seen at the profile plateau occurring between 60 and 90 minutes. The different symbols used represent the duplicate analyses performed.

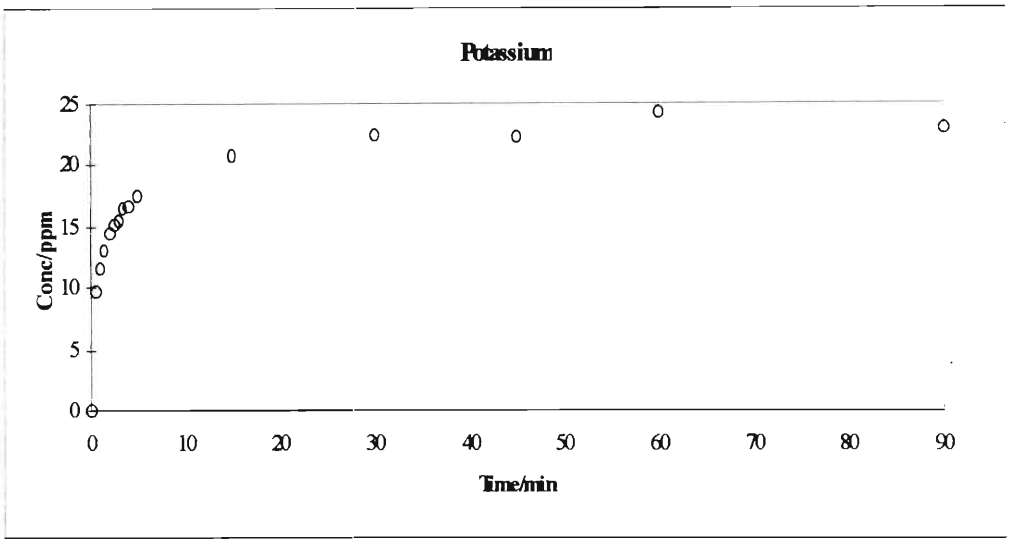

Figure 4.4 Plot of concentration versus time for potassium, showing the typical trend of rapid initial concentration increase, and leading up to the equilibrium concentration (C_∞) seen at the profile plateau occurring between 60 and 90 minutes

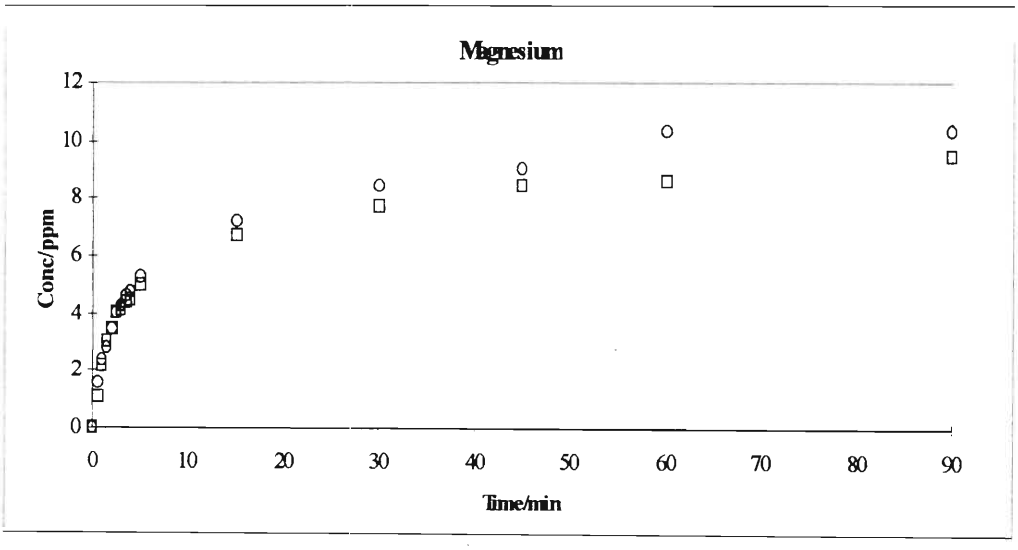

Figure 4.5 Plot of concentration versus time for magnesium, showing the typical trend of rapid initial concentration increase, and leading up to the equilibrium concentration (C_∞) seen at the profile plateau occurring between 60 and 90 minutes. The different symbols used represent the duplicate analyses performed.

Table 4.9 Concentration (ppm) versus time (sec) data for the organics during an infusion at 80 °C. Corrected (for water loss) concentration values are given in brackets.

Species	Protocatechuic acid	Aspalathin	Rutin
Time/sec	Concentration (corrected) / ppm		
0	0.000 (0.000)	0.000 (0.000)	0.000 (0.000)
30	1.142 (1.142)	2.693 (2.693)	5.383 (5.383)
60	1.610 (1.606)	3.921 (3.912)	7.709 (7.693)
90	1.833 (1.826)	4.583 (4.566)	9.015 (8.981)
120	2.037 (2.026)	5.123 (5.095)	10.064 (10.008)
150	2.182 (2.167)	5.522 (5.482)	10.625 (10.554)
180	2.402 (2.380)	6.153 (6.091)	12.075 (11.954)
210	2.533 (2.505)	6.470 (6.395)	14.121 (13.915)
240	2.647 (2.614)	6.727 (6.640)	14.289 (14.075)
300	2.815 (2.773)	7.290 (7.172)	14.439 (14.217)
900	3.669 (3.574)	10.897 (10.555)	21.283 (20.636)
1800	3.750 (3.649)	12.167 (11.738)	25.800 (24.842)
2700	3.894 (3.782)	13.052 (12.555)	25.517 (24.580)
3600	3.996 (3.876)	13.396 (12.871)	25.628 (24.682)
5400	4.094 (3.965)	12.449 (12.009)	29.702 (28.391)

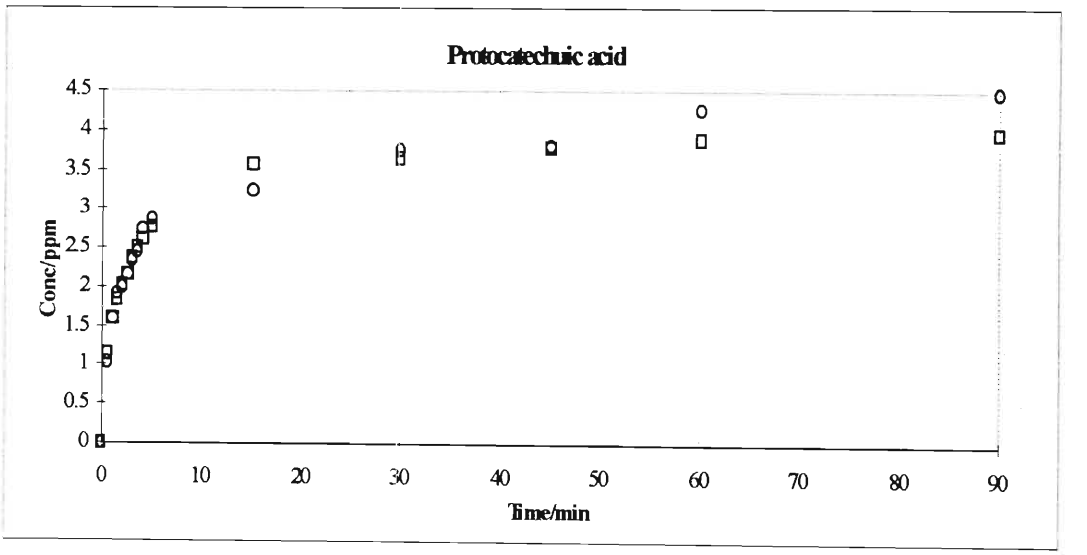

Figure 4.6 Plot of concentration versus time for protocatechuic acid, showing the typical trend of rapid initial concentration increase, and leading up to the equilibrium concentration (C_∞) seen at the profile plateau occurring between 60 and 90 minutes. The different symbols used represent the duplicate analyses performed.

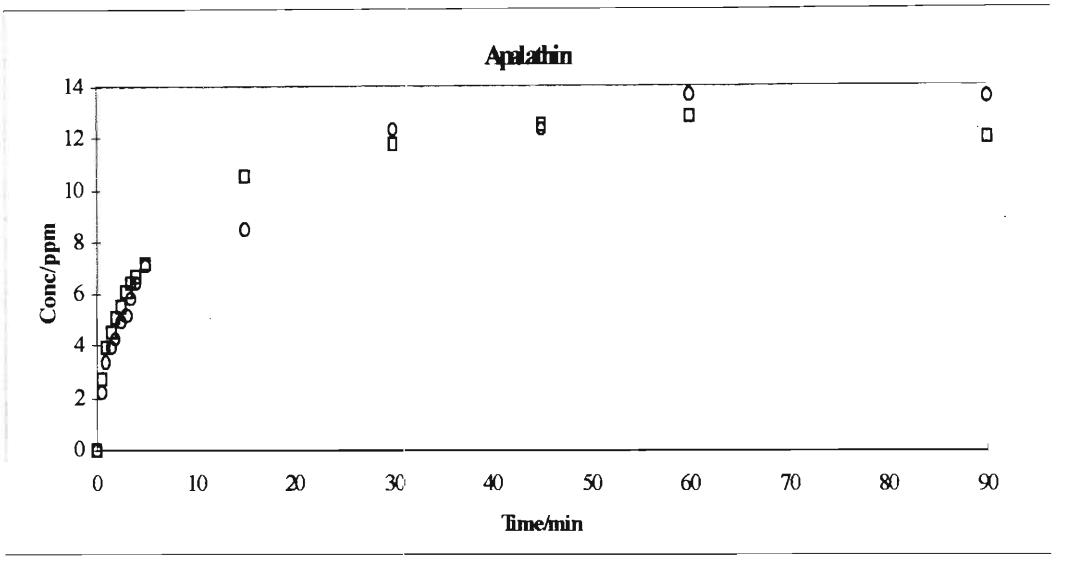

Figure 4.7 Plot of concentration versus time for aspalathin showing the typical trend of rapid initial concentration increase, and leading up to the equilibrium concentration (C_∞) seen at the profile plateau occurring between 60 and 90 minutes. The different symbols used represent the duplicate analyses performed

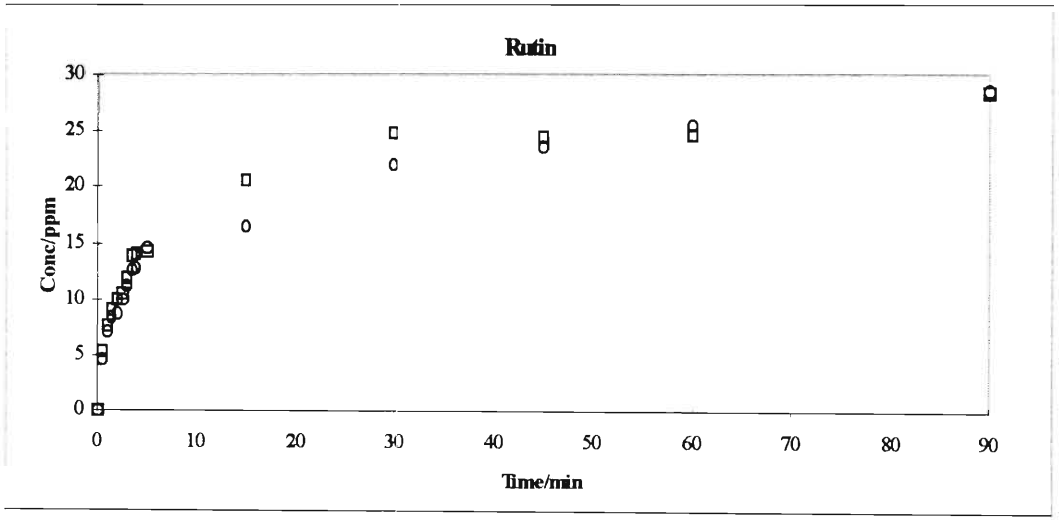

Figure 4.8 Plot of concentration versus time for rutin, showing the typical trend of rapid initial concentration increase, and leading up to the equilibrium concentration (C_∞) seen at the profile plateau occurring between 60 and 90 minutes. The different symbols used represent the duplicate analyses performed.

Table 4.10 Concentration (ppm) versus time (sec) data for the anions during an infusion at 80 °C. Corrected (for water loss) concentration values are given in brackets.

	Cl^-	HPO_4^{2-}	SO_4^{2-}
Time/sec	Concentration (corrected) / ppm		
0	0.000 (0.000)	0.000 (0.000)	0.000 (0.000)
30	27.700 (27.700)	1.357 (1.357)	2.750 (2.750)
60	20.300 (20.333)	1.555 (1.553)	3.150 (3.145)
90	22.250 (22.258)	1.858 (1.852)	4.100 (4.083)
120	33.850 (33.633)	2.000 (1.991)	3.750 (3.740)
150	26.800 (26.763)	2.188 (2.174)	5.000 (4.958)
180	28.200 (28.119)	2.286 (2.269)	5.550 (5.490)
210	29.550 (29.417)	2.281 (2.264)	5.800 (5.731)
240	46.500 (45.614)	2.295 (2.277)	5.350 (5.301)
300		2.404 (2.380)	
900		3.194 (3.121)	
1800		3.296 (3.216)	
2700		3.564 (3.464)	
3600		3.428 (3.339)	
5400	32.450 (32.276)	3.586 (3.483)	9.300 (9.050)

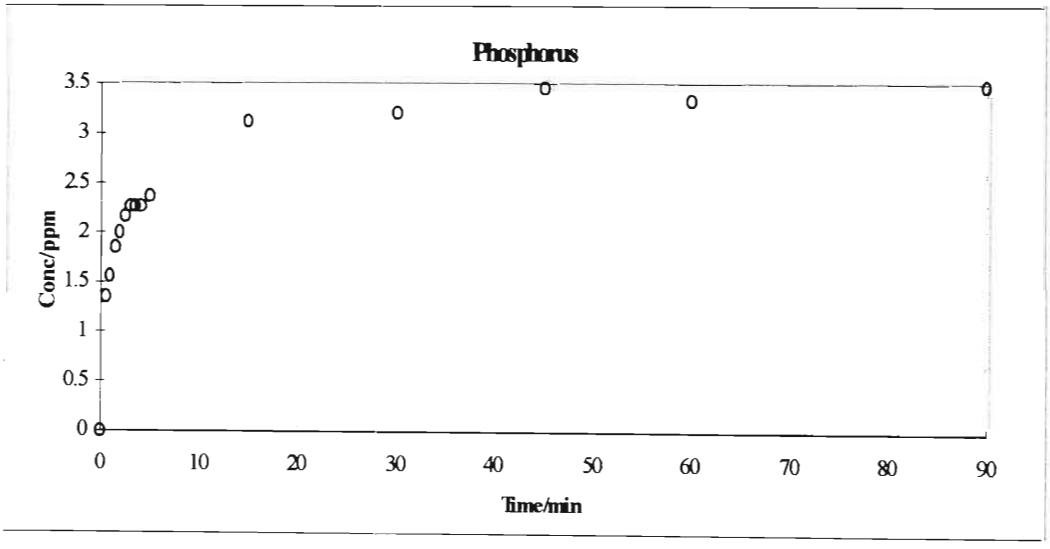

Figure 4.9 Plot of concentration versus time for phosphorus (orthophosphate), showing the typical trend of rapid initial concentration increase, and leading up to the equilibrium concentration (C_∞) seen at the profile plateau occurring between 60 and 90 minutes.

These plots clearly show that the concentrations of the various species rise rapidly initially and then asymptotically approach a limiting equilibrium concentration (C_∞). The shape of these curves closely resembles those already published for similar infusions[91]. In the case of aspalathin, Figure 4.7 shows that the concentration value begins to decline after 90 minutes. This observation can be attributed to the oxidation of aspalathin to (2R)- and (2S)-2,3-dihydro-iso-orientin [27] (section 1.3.1.5), and or to conversion to an as yet unidentified brown substance in the presence of oxygen and sunlight[6]. Under these circumstances the 90 minute C_∞ value was used when required.

The corrected values of C_∞ and C were fitted into Equation (17),

$$\ln\left(\frac{C_\infty}{C_\infty - C}\right) = k_{obs}\, t \qquad (17)$$

and the k_{obs} values obtained by plotting the ln function against time. The values obtained using Equation (17) and the resulting mean k_{obs} are tabulated in Tables 4.11-13. The graphs were plotted using Microsoft Excel software and can be seen in Figures 4.10 –12.

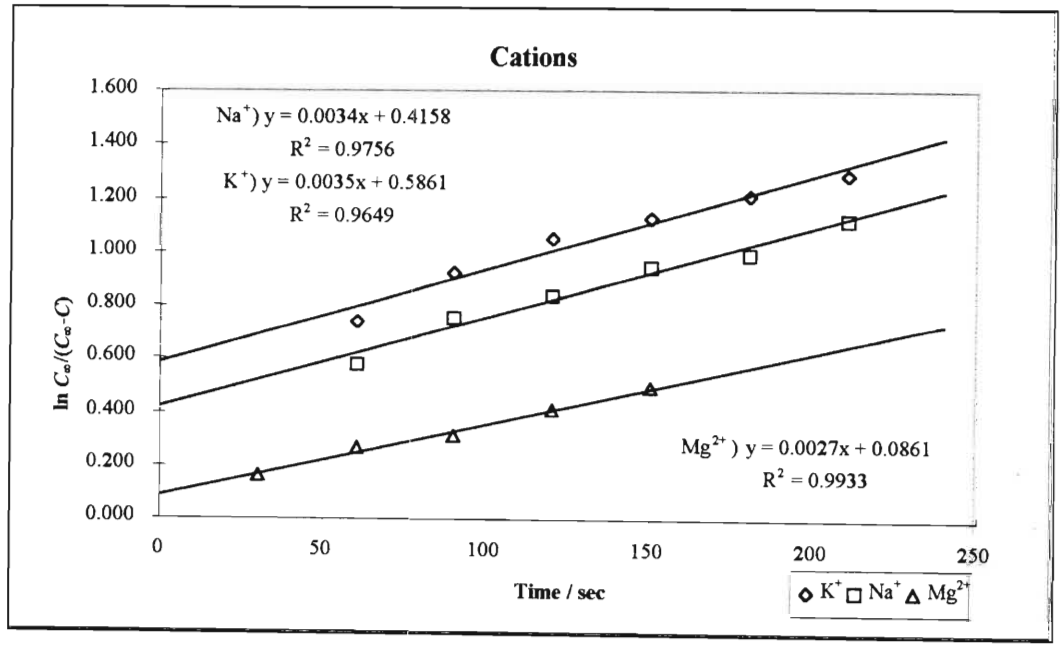

Figure 4.10 Typical linear plots for the monitored cations at 80 °C, also shown are the line equations and the Pearson's correlation coefficient as determined by linear regression.

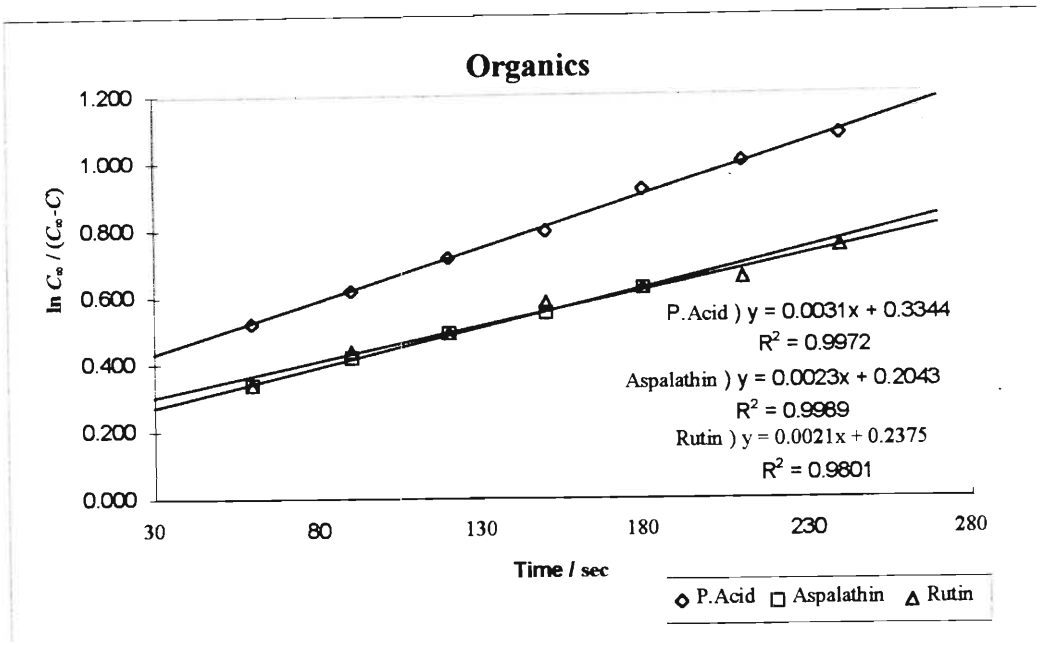

Figure 4.11 Typical linear plots for the monitored organics at 80 °C, also shown are the line equations and the Pearsons correlation coefficient as determined by linear regression.

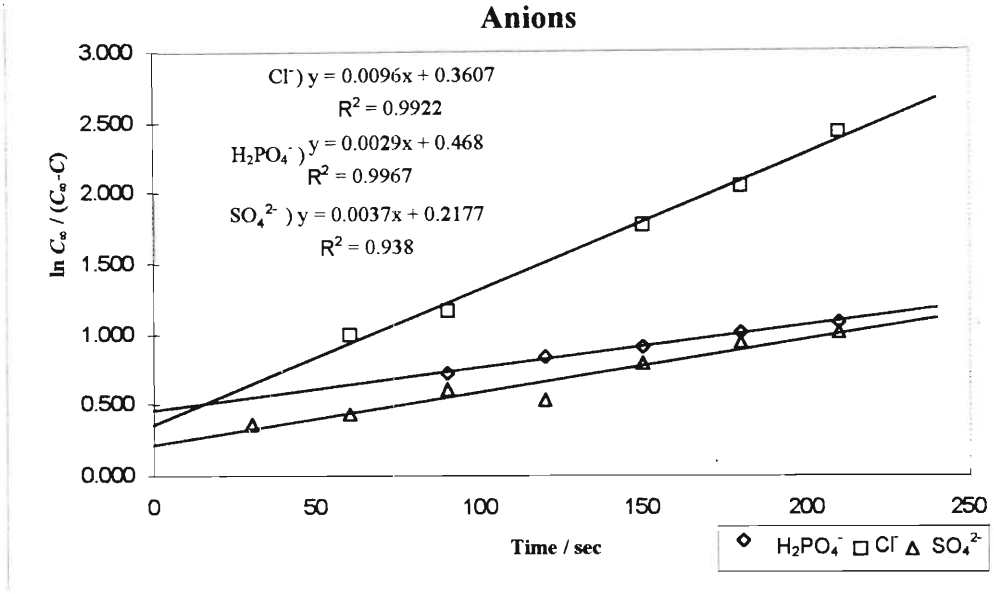

Figure 4.12 Typical linear plots for the monitored anions at 80 °C, also shown are the line equations and the Pearson's correlation coefficient as determined by linear regression. A point was omitted on the Cl^- plot due to the contamination of that specific sample.

A summary of the results is given in Tables 4.11-13. The theory, through Equation (17), suggests that the line should pass through the origin. This was not the case as seen in the first order plots presented in Figures 4.10-12, as has been reported in many other situations[66, 91, 93, 95, 98] where a semi-empirical intercept (*a*) was found in each instance. Price and Spiro[93]

suggested that the intercept is the result of a complex infusion process. These workers postulate that the intercept is affected by the loss of solubles, the leaf structure and it's uptake of water at the beginning of the infusion process. Price and Spitzer[95] suggest that the intercepts serve as indicators of the quality of the data and deviations from the model employed. Note that an intercept of $a = 0.5$ implies that about 25 % of the soluble component is present in the solution at $t = 0$. An intercept corrected rate constant k_{eqn} can be calculated in two steps: Firstly, once a and k_{obs} have been obtained the half life ($t_{1/2}$) can be calculated[94] from

$$t_{1/2} = (\ln 2 - a)/k_{obs}$$

Secondly, substituting the value of $t_{1/2}$ back into Equation (17) and setting $C = 0.5\ C_\infty$ will yield the value of k_{eqn}. The half life $t_{1/2}$ and k_{eqn} values given in Tables 4.11-13 were calculated according to a method devised by Price and Spitzer[95], and although they represent essentially the same data are both given to aid assessing the impact of the non-zero intercept.

Table 4.11 The table shows, for cation extraction at 80°C, typical values obtained from Equation (17). Only the points used in the linear plots are shown.. Also given are the mean (from at least a triplicate analysis) C_∞, a, k_{obs}, $t_{1/2}$ and k_{eqn} values.

Species	Na^+	K^+	Mg^{2+}
Temp/°C	80	80	80
Time/s	$\ln\left(\frac{C_\infty}{C_\infty - C}\right)$		
30			0.163
60	0.578	0.742	0.263
90	0.754	0.923	0.315
120	0.835	1.051	0.411
150	0.943	1.129	0.495
180	0.991	1.210	
210	1.122	1.286	
	Mean Values		
C_∞ / ppm	24.25 ± 0.32	24.01 ± 1.47	9.61 ± 0.71
a	0.537 ± 0.035	0.434 ± 0.039	0.120 ± 0.027
$k_{obs}/10^{-4}\ s^{-1}$	34.9 ± 0.9	33.8 ± 0.3	25.3 ± 1.7
$t_{1/2}$ / s	44.7	76.6	226.4
$k_{eqn}/10^{-4}\ s^{-1}$	155.0	90.5	30.6

Table 4.12 The table shows, for the extraction of the organics at 80°C, typical values obtained from Equation (17). Only the points used in the linear plots are shown hence the omission of certain points. Also given are the mean (from at least a triplicate analysis) C_∞ , a, k_{obs} , $t_{1/2}$ and k_{eqn} values.

Species	Protocatechuic acid	Aspalathin	Rutin
Temp/°C	80	80	80
Time/s	$\ln\left(\frac{C_\infty}{C_\infty - C}\right)$		
60	0.519	0.341	0.340
90	0.617	0.415	0.439
120	0.715	0.490	0.491
150	0.791	0.554	0.581
180	0.917	0.622	0.622
210	0.999		0.652
240	1.077		0.743
	Mean Values		
C_∞ / ppm	3.92 ± 0.03	12.97 ± 0.07	28.56 ± 1.24
intercept	0.350 ± 0.011	0.200 ± 0.050	0.204 ± 0.032
$k_{obs}/10^{-4}$ s^{-1}	30.4 ± 1.5	22.0 ± 0.4	19.9 ± 1.4
$t_{1/2}$ / s	112.9	224.3	246.2
$k_{eqn}/10^{-4}$ s^{-1}	61.4	30.9	28.2

Simple kinetic theory[96] states that the diffusion of a (spherical) component is inversely related to the square root of it's mass. If we compare from the data above, the square root of the masses of, for example, aspalathin and rutin (0.861) and the ratio of their half lives (0.912) we find that these values are in good agreement with a 6 % difference. Similarly the square root of the ratio of the masses for rutin and protocatechuic acid is 1.990 and the ratio of the half lives is 2.181 and these values are also in agreement with a 9 % difference. This is quite possibly the case for all the components listed above. These results support the assumption that the rate-determining step of the infusion process is a diffusive one, as was found by Price and Spitzer[95].

Table 4.13 The table shows, for anion extraction at 80°C, typical values obtained from Equation (17). Only the points used in the linear plots are shown hence the omission of certain points. Also given are the mean (from at least a duplicate analysis) C_∞ , a, k_{obs} , $t_{1/2}$ and k_{eqn} values.

Species	$H_2PO_4^-$	Cl^-	SO_4^{2-}
Temp/°C	80	80	80
Time/s	$\ln\left(\frac{C_\infty}{C_\infty - C}\right)$		
30			0.362
60		0.994	0.427
90	0.726	1.170	0.600
120	0.833		0.533
150	0.905	1.767	0.794
180	1.004	2.049	0.933
210	1.083	2.424	1.003
	Mean Values		
C_∞ / ppm	3.17 ± 0.25	50.21	8.93 ± 0.14
intercept	0.435 ± 0.024	0.308	0.194 ± 0.024
$k_{obs}/10^{-4}$ s^{-1}	31.2 ± 1.7	112.4	38.0 ± 0.7
$t_{1/2}$ / s	82.7	34.3	131.5
$k_{eqn}/10^{-4}$ s^{-1}	83.8	202.4	52.7

4.4.2 Comparison of Rate Constants

Table 4.14 shows rate constants obtained for each of the species analysed, and the calculated k_{eqn} values. From the rate constants for the cations, it is apparent that k_{obs} and k_{eqn} show the same trend: $K^+ > Na^+ > Mg^{2+}$. It is possible that this is related to the hydrated radii of the cations since it is known that K^+ has a smaller hydrated radius than Na^+[97], and that the ionically smaller doubly charged Mg^{2+} will have the largest hydrated radius of the three. A similar trend is found with the D_{aq} (presented in section 4.4.8) where D_{aq} $K^+ > Na^+ > Mg^{2+}$,

implying that the larger the hydrated radius, the slower will be the diffusion in an aqueous media and the slower the rate of infusion.

Table 4.14 Values of k_{obs} and k_{eqn} obtained from infusion experiments at 80 °C, are listed for comparative purposes for the cations, organics and anions.

Species	k_{obs}	k_{eqn}
Cations		
Na^+	33.8	90.5
K^+	34.9	154.9
Mg^{2+}	25.3	30.6
Organic compounds		
Protocatechuic acid	30.4	61.4
Aspalathin	22.0	30.9
Rutin	19.3	28.2
Anions		
Cl^-	112.4	202.4
$H_2PO_4^-$	31.2	52.7
SO_4^{2-}	38.0	83.8

The organics show a trend in k_{obs} and k_{eqn} that inversely follows molecular weight with protocatechuic acid > aspalathin > rutin. This could simply relate to the molecular volumes of the compounds. On the other hand the trend could be related to polarity, with protocatechuic acid being most polar followed by aspalathin and then rutin, as seen from their elution order from a reversed phase system.

An anionic trend is also evident with both k_{obs} and k_{eqn} occurring in the order of $Cl^- > SO_4^{2-} > H_2PO_4^-$. This is reflected in the respective hydrodynamic radii as implied by the D_{aq} values with $Cl^- < SO_4^{2-} < H_2PO_4^-$. It is interesting that k_{obs} and k_{eqn} for Cl^- are about three times as large as those for SO_4^{2-} and $H_2PO_4^-$, and in fact about three times as large as all the other values except k_{eqn} K^+.

Overall, k_{obs} values within the groups overlap with those in other groups excluding Cl^-. It is difficult to make educated assumptions as to the relationships between various cations, anions and organics. It would appear that Cl^- infuses faster than any of the other monitored constituents, and will be involved in more complicated relationships if any at all. There appears to be no direct effect on infusion by the charge of the constituent, besides affecting

the hydrated radius of certain ions. Differences from 17 % to 77 % are found between k_{obs} and k_{eqn} values. These differences are large compared to those found for Japanese Green Tea (Sen Cha Uji Tsuyu)[95] which varied between 0 and 17 %. This can be attributed to the much larger intercepts obtained in the current work as compared to those reported for the Japanese Green Tea. Intercepts will directly affect the calculated $t_{1/2}$ values, and hence the k_{eqn} values.

Most rate constants given in literature are based on investigations at 80°C, and thus it is expedient to compare these values with the rate constants obtained in this work at 80°C as seen in Table 4.14 above. Literature reported rate constants determined at 80°C using different sieving fractions, were converted to reflect those that would have been obtained using a 1.40-1.00 mm sieving fraction[94]. This was achieved knowing that $k_{obs} \propto 1/d^2$ from Equation (22). The value of d was taken to be the mean of the upper and lower sieving fraction limits. Values for Rooibos Tea and those reported in literature are given in Table 4.15

Table 4.15 Comparison of Rooibos Tea rate constants with literature values at 80°C.

	Tea type				
	Rooibos Tea	**Japanese Green**	**Rose-hip Tea**	**Black Assam**	**Green Chun Mee**
Species	k_{obs} / (10^{-4} s^{-1})				
Na^+	34	-	-	-	-
K^+	35	-	24	166	197
Mg^{2+}	25	-	11	83	116
Cl^-	112	-	-	394	546
HPO_4^{2-}	31	-	24	259	190
SO_4^{2-}	38	-	33	297	340
Organic Range	20-30[a]	116-164[b]	23-33[c]	197[d]	245[d]
pH[e]	4.6	-	4.1	4.8	5.6

[a] Protocatechuic acid, aspalathin and rutin.
[b] Price and Spitzer[95] (Epicatechin, Epigallocatechin, Epicatechin gallate and Epigallocatechin gallate).
[c] Spiro and Chen[91] (Range representing values from German, Chilean and French teas)
[d] Spiro and Lam[98].
[e] Measured at equilibrium.

It appears that only the data from the Rose-hips tea investigations compares favourably with that obtained in the present work. The values for the cations and anions are on the whole slightly greater than those for Rooibos Tea, except for magnesium. The range of infusion rate constants for L-ascorbic acid in German, Chilean and French Rose-hip teas compares well with the range of organic compounds investigated in Rooibos Tea. However, the rate constants for the flavanols from Japanese Green Tea as investigated by Price and Spitzer[95] are very different, with values over 5 times as large as those found for Rooibos Tea flavanols. Similarly the rate constants for cations, anions and caffeine for Black Assam Bukial and Green Chun Mee teas range between 3-10 times those of Rooibos Tea. This difference can be attributed to the fact that the teas are very different and undergo very different manufacturing processes. In the Green and Black tea cases, the leaf is subjected to a tearing process which opens the leaf and makes the infusion path for water in and species out of the leaf matrix much easier. Also, the difference in leaf structure between the plant species could account for the difference in rate constants. The pH results obtained for Rooibos Tea are comparable with those found for the other teas except Green Chun Mee tea, whose pH value was approximately 20 % higher.

4.4.3 Effect of Partition Coefficients on Rate Constants

Partition coefficients (K) were determined in three different ways; the graphical method (detailed in Section 4.3.1), the successive extraction method (Section 4.3.2) and the total mineral content method (Section 4.3.3). Partition coefficients influence rate constants, and as a result corrected infusion rate constants (k') were calculated from the k_{obs} values and the respective partition coefficients using the equation[66]:

$$k' = \frac{k_{obs}}{1 + \frac{\beta w}{\rho K V}}$$

Where β is the ratio of wet to dry tea mass, w (4g) is the dry tea mass, ρ is the density of the swollen wet leaf, and V (400 ml) is the volume of water used to brew the tea. Mean values of β and ρ were found to be 2.43 ± 0.06 and 1.063 ± 0.001 gml^{-1} as reported in Section 4.3.2. The mean values of β and w were used instead of m alone in order to limit the error in the conversion from k_{obs} to k'. The k' values calculated using partition coefficients from total

mineral content (k'_{TM}) and from the successive extraction method (k'_{SE}) are given below in Table 4.16 along with the percentage errors with respect to k_{obs}. Values for k'_{GM} were not calculated because many K_{GM} values could not be obtained as a result of the negative intercepts encountered using the graphical method. are presented in Table 4.16.

All k values are given in 10^{-4} s^{-1}.

Table 4.16 The table shows the effects of the various partition coefficients on k_{obs}, presenting values for k_{obs}, k'_{SE}, k'_{TM} and the percentage differences between the k' values and k_{obs}.

Species	k_{obs}	k'_{TM}	Difference	k'_{SE}	Difference
	x 10^{-4} s^{-1}	x 10^{-4} s^{-1}	%	x 10^{-4} s^{-1}	%
Cations					
Na^+	33.8	33.0	2.6	31.7	6.3
K^+	34.9	34.5	1.2	33.3	4.4
Mg^{2+}	25.3	24.2	4.3	24.9	1.5
Organic compounds					
Protocatechuic acid	30.4			28.5	6.5
Aspalathin	22.0			20.0	9.3
Rutin	19.9			17.8	10.6
Anions					
Cl^-	112.4			106.6	5.1
HPO_4^{2-}	31.2	30.4	2.8	30.3	3.0
SO_4^{2-}	38.0			34.5	9.1

Since the difference between k_{obs} and the corrected rate constants is small, all rate constants will be recorded as k_{obs}.

4.4.4 The Effect of Particle Size on Rate Constants

The effect of particle size on the rate of extraction of solubles from Rooibos Tea during infusion was investigated by observing infusions from five different sieved fractions ranging from 0.250 to 1.40 mm in size. Experiments were conducted in duplicate at 80°C and the rate constants obtained in each case. The kinetic data including the equilibrium concentrations are presented in Tables 4.17-4.19 for the cations, Tables 4.20–4.22 for the organic compounds and Table 4.23 for the orthophosphate ion. These are accompanied by Figures 4.13-4.18 for

the cations, Figures 4.19-4.24 for the organic compounds and Figures 4.25 – 4.26 for the orthophosphate ion, representing the graphs used in the determination of the rate constants. All the presented tables show mean values from duplicate analyses, and the presented graphs are typical plots chosen from the duplicate analyses. The investigation of SO_4^{2-} and Cl^- with respect to particle size was not performed due to the high cost of using the privately owned IC. Table 4.24 is a summary table containing all the infusion rate constants for the various species as obtained for the different sieving fractions.

Table 4.17 Observed and corrected Na^+ concentrations, accompanied by the relevant kinetic data as obtained from the different sieved fractions. Included are the C_∞, a and k_{obs} values.

Sieving	**0.250-0.425mm**	**0.425-0.600mm**	**0.600-0.850mm**	**0.850-1.00mm**	**1.00-1.40mm**
Time/s	**Observed and corrected concentrations / ppm**				
0	0.00 (0.00)	0.00 (0.00)	0.00 (0.00)	0.00 (0.00)	0.00 (0.00)
30	14.06 (14.06)	10.40 (10.40)	12.43 (12.43)	8.68 (8.68)	7.50 (7.50)
60	19.29 (19.25)	14.27 (14.25)	15.87 (15.85)	10.76 (10.74)	10.05 (10.04)
90	21.82 (21.75)	16.45 (16.40)	18.53 (18.47)	12.19 (12.15)	12.14 (12.10)
120	23.81 (23.70)	18.22 (18.13)	20.15 (20.06)	13.75 (13.68)	13.00 (12.94)
150	25.01 (24.86)	19.55 (19.42)	21.01 (20.89)	15.09 (14.98)	14.04 (13.95)
180	25.96 (25.78)	20.79 (20.62)	22.34 (22.18)	15.74 (15.61)	14.47 (14.37)
210	25.58 (25.42)	22.86 (22.60)	23.07 (22.88)	16.13 (15.99)	15.56 (15.41)
240	25.68 (25.51)	22.05 (21.83)	23.45 (23.24)	16.45 (16.29)	15.51 (15.36)
300	28.18 (27.88)	23.54 (23.24)	25.86 (25.52)	17.31 (17.11)	16.13 (15.95)
3600	31.88 (31.35)	30.29 (29.57)	32.77 (32.01)	22.45 (21.94)	22.55 (21.96)
5400	32.82 (32.23)	29.27 (28.62)	28.48 (28.01)	23.67 (23.08)	23.53 (22.85)
Mean Values					
C_∞/ppm	31.98 ± 0.84	27.73 ± 0.90	26.72 ± 1.29	23.21± 0.13	24.01 ± 1.47
a	0.64 ± 0.05	0.44 ± 0.03	0.41 ± 0.11	0.39 ± 0.02	0.43 ± 0.04
$k_{obs}/10^{-4}s^{-1}$	52.4 ± 6.0	49.7 ± 1.2	67.7 ± 8.9	41.2 ± 2.5	33.8 ± 3.1

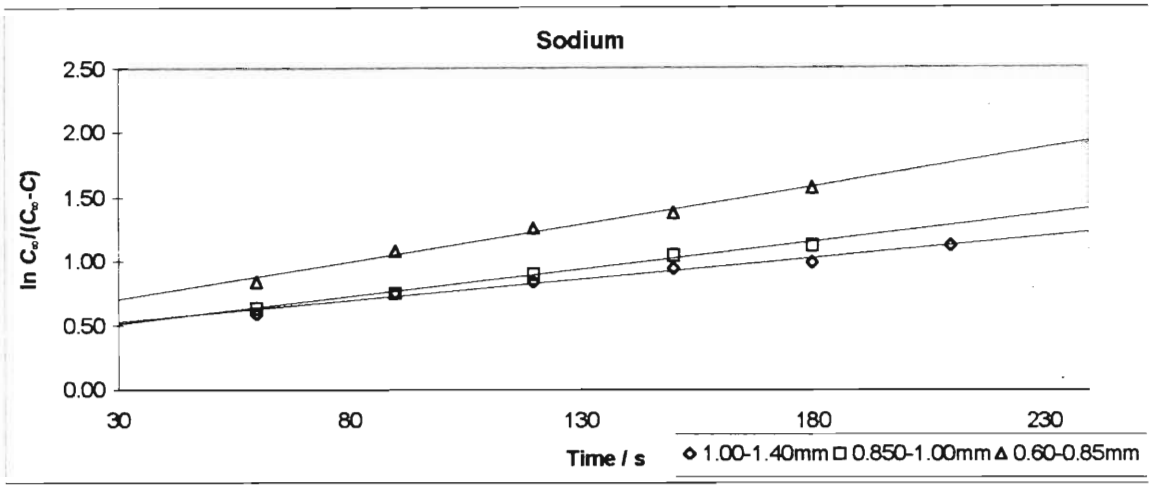

Figure 4.13 Typical plots for Na^+ for 0.60–0.85 mm, 0.85-1.00 mm and 1.00-1.40mm sieved fractions at 80 °C.

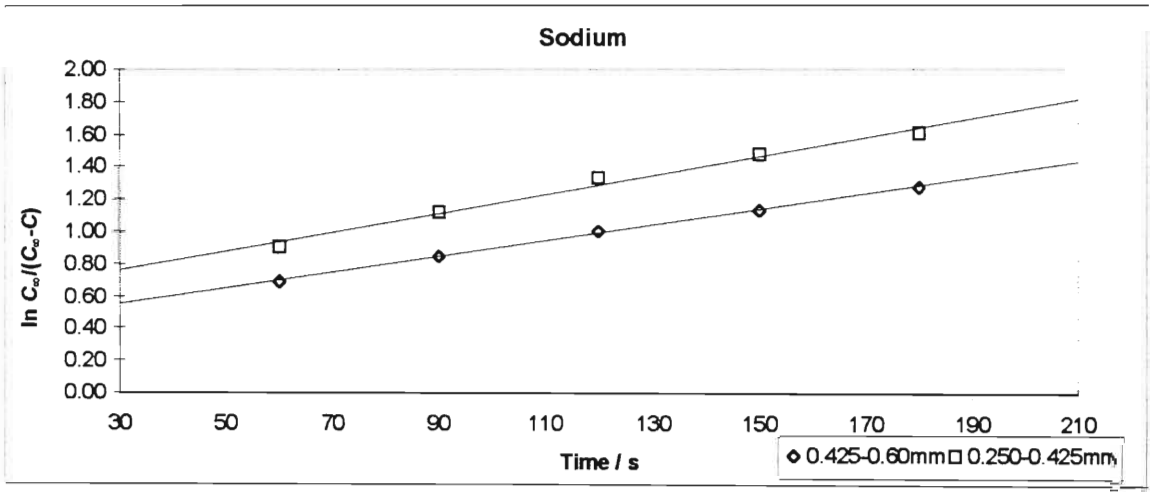

Figure 4.14 Typical plots for Na^+ for 0.250-0.425 mm and 0.425-0.60 mm sieved fractions at 80 °C.

Table 4.18 Observed and corrected K^+ concentrations, accompanied by the relevant kinetic data as obtained from the different sieved fractions. Included are the C_∞, a and k_{obs} values.

Sieving	0.250-0.425mm	0.425-0.600mm	0.600-0.850mm	0.850-1.00mm	1.00-1.40mm
Time/s	Observed and corrected concentrations / ppm				
0	0.00 (0.00)	0.00 (0.00)	0.00 (0.00)	0.00 (0.00)	0.00 (0.00)
30	12.82 (12.82)	11.85 (11.85)	10.74 (10.74)	7.51 (7.51)	8.71 (8.71)
60	18.96 (18.92)	16.04 (16.01)	13.43 (13.41)	10.42 (10.40)	12.91 (12.87)
90	21.08 (21.01)	18.20 (18.14)	15.45 (15.41)	12.00 (11.96)	14.87 (14.81)
120	22.63 (22.53)	20.06 (19.97)	16.99 (16.91)	12.89 (12.83)	16.07 (15.98)
150	23.56 (23.43)	21.18 (21.06)	17.93 (17.83)	13.35 (13.27)	16.73 (16.63)
180	24.28 (24.13)	21.77 (21.62)	18.73 (18.60)	14.31 (14.20)	17.37 (17.25)
210	24.91 (24.73)	22.69 (22.51)	18.88 (18.75)	14.43 (14.32)	17.93 (17.78)
240	25.45 (25.25)	22.26 (22.10)	19.13 (18.98)	14.92 (14.79)	17.94 (17.79)
300	25.87 (25.65)	23.42 (23.19)	21.11 (20.86)	16.57 (16.35)	19.02 (18.82)
3600	29.58 (29.13)	28.93 (28.36)	26.14 (25.58)	19.96 (19.54)	22.42 (22.02)
5400	29.61 (29.16)	28.14 (27.63)	22.10 (21.81)	19.72 (19.31)	25.15 (24.58)
Mean Values					
C_∞/ppm	30.02 ± 0.86	27.63 ± 0.00	23.06 ± 1.25	18.99 ± 0.32	24.25 ± 0.32
a	0.71 ± 0.02	0.54 ± 0.02	0.51 ± 0.01	0.56 ± 0.02	0.54 ± 0.04
$k_{obs}/10^{-4}s^{-1}$	65.2 ± 0.06	53.8 ± 0.02	64.7 ± 15.2	40.4 ± 3.4	34.9 ± 0.9

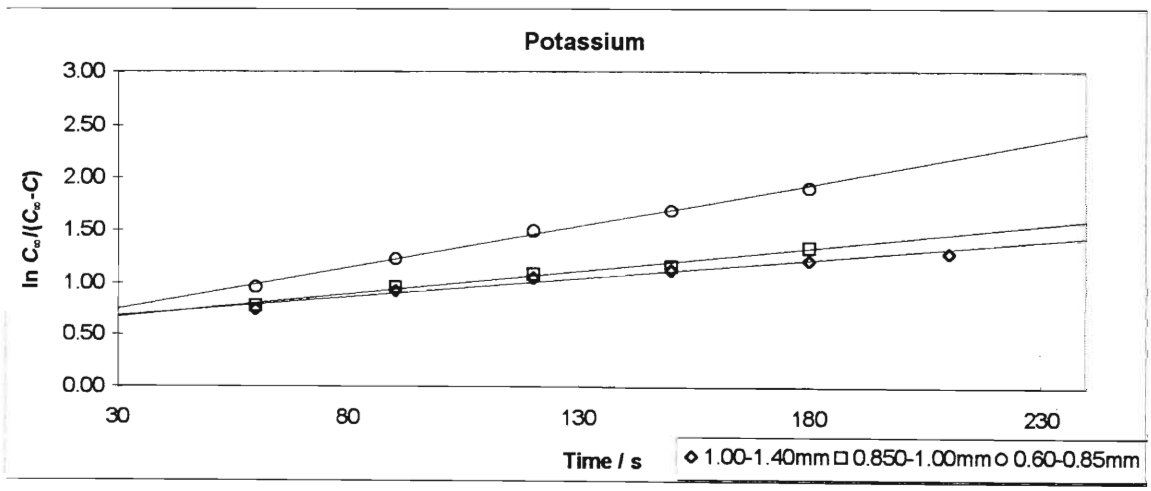

Figure 4.15 Typical plots for K^+ for 0.60–0.85 mm, 0.85-1.00 mm and 1.00-1.40mm sieved fractions at 80 °C.

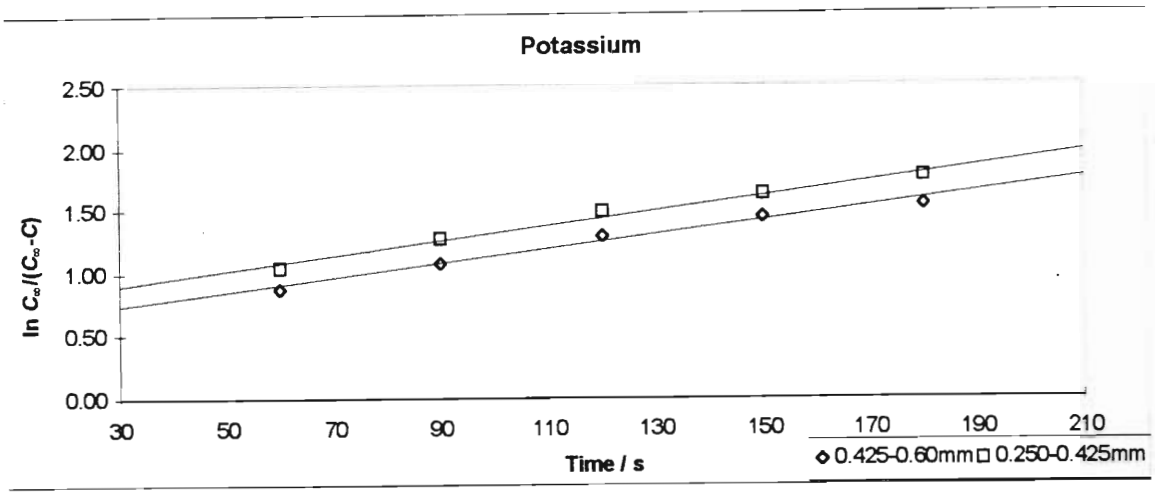

Figure 4.16 Typical plots for K^+ for 0.250-0.425 mm and 0.425-0.60 mm sieved fractions at 80 °C.

Table 4.19 Observed and corrected Mg^{2+} concentrations, accompanied by the relevant kinetic data as obtained from the different sieved fractions. Included are the C_∞, a and k_{obs} values.

Sieving	**0.250-0.425mm**	**0.425-0.600mm**	**0.600-0.850mm**	**0.850-1.00mm**	**1.00-1.40mm**
Time/s	**Observed and corrected concentrations / ppm**				
0	0.00 (0.00)	0.00 (0.00)	0.00 (0.00)	0.00 (0.00)	0.00 (0.00)
30	2.21 (2.21)	1.38 (1.38)	1.80 (1.80)	0.64 (0.64)	1.56 (1.56)
60	3.92 (3.91)	2.70 (2.70)	3.06 (3.05)	1.71 (1.71)	2.40 (2.39)
90	4.76 (4.74)	3.50 (3.48)	3.86 (3.84)	2.42 (2.40)	2.81 (2.80)
120	5.27 (5.23)	4.13 (4.10)	4.30 (4.27)	2.83 (2.81)	3.51 (3.49)
150	5.61 (5.56)	4.36 (4.32)	4.73 (4.69)	3.07 (3.04)	4.08 (4.04)
180	5.94 (5.89)	4.65 (4.60)	5.11 (5.06)	3.39 (3.35)	4.32 (4.27)
210	6.15 (6.09)	4.92 (4.86)	5.21 (5.15)	3.49 (3.44)	4.68 (4.61)
240	6.34 (6.27)	5.06 (5.00)	5.31 (5.24)	3.63 (3.58)	4.84 (4.77)
300	6.82 (6.72)	5.57 (5.48)	5.86 (5.77)	3.90 (3.83)	5.35 (5.25)
3600	11.83 (11.43)	10.13 (9.76)	10.53 (10.16)	6.75 (6.51)	10.79 (10.31)
5400	12.57 (12.12)	10.60 (10.20)	9.73 (9.41)	7.31 (7.04)	10.83 (10.34)
Mean Values					
C_∞**/ppm**	11.47 ± 0.64	10.40 ± 0.21	9.30 ± 0.11	6.97 ± 0.07	9.61 ± 0.71
a	0.10 ± 0.02	0.06 ± 0.02	0.10 ± 0.03	0.10 ± 0.02	0.12 ± 0.03
$k_{obs}/10^{-4}s^{-1}$	42.7 ± 2.8	40.0 ± 0.8	39.8 ± 0.8	30.6 ± 0.1	25.3 ± 0.2

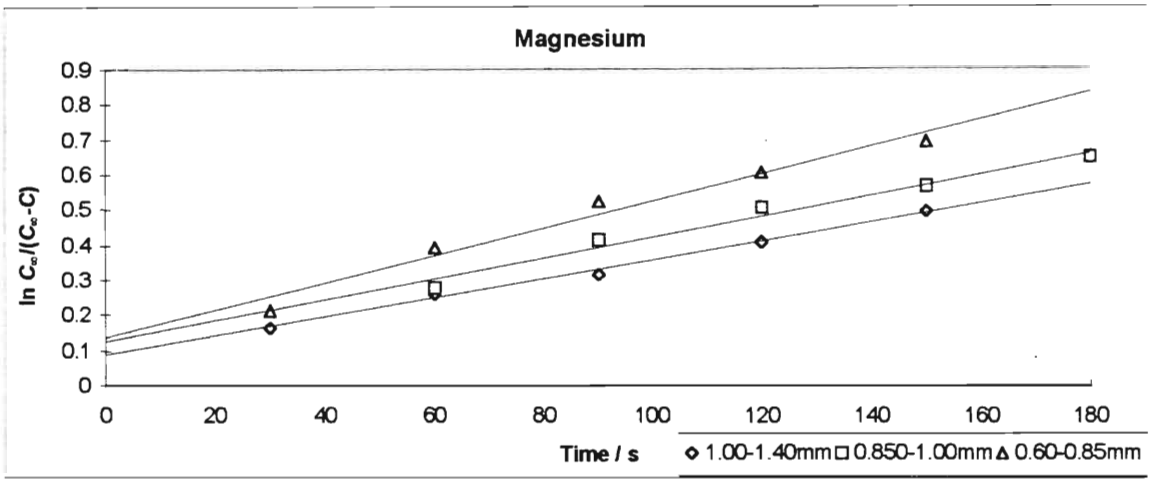

Figure 4.17 Typical plots for Mg^{2+} for 0.60–0.85 mm, 0.85-1.00 mm and 1.00-1.40mm sieved fractions at 80 °C.

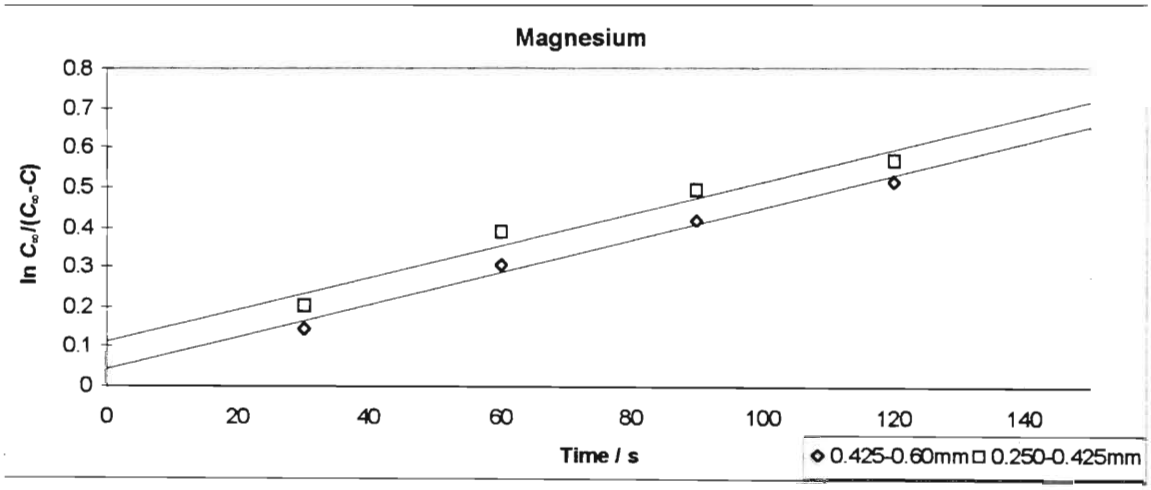

Figure 4.18 Typical plots for Mg^{2+} for 0.250-0.425 mm and 0.425-0.60 mm sieved fractions at 80 °C.

Table 4.20 Observed and corrected Protocatechuic acid concentrations, accompanied by the relevant kinetic data as obtained from the different sieved fractions. Included are the C_∞, a and k_{obs} values.

Sieving	0.250-0.425mm	0.425-0.600mm	0.600-0.850mm	0.850-1.00mm	1.00-1.40mm
Time/s	Observed and corrected concentrations / ppm				
0	0.00 (0.00)	0.00 (0.00)	0.00 (0.00)	0.00 (0.00)	0.00 (0.00)
30	1.70 (1.70)	1.31 (1.31)	1.36 (1.36)	0.92 (0.92)	1.14 (1.14)
60	2.43 (2.43)	1.79 (1.79)	1.69 (1.69)	1.36 (1.36)	1.61 (1.61)
90	2.76 (2.75)	2.14 (2.13)	2.07 (2.07)	1.39 (1.39)	1.83 (1.83)
120	2.96 (2.95)	2.45 (2.43)	2.24 (2.23)	1.57 (1.56)	2.04 (2.03)
150	3.16 (3.14)	2.62 (2.60)	2.40 (2.39)	1.74 (1.73)	2.18 (2.17)
180	3.37 (3.34)	2.83 (2.80)	2.54 (2.52)	1.83 (1.82)	2.40 (2.38)
210	3.48 (3.45)	2.91 (2.88)	2.69 (2.66)	1.92 (1.90)	2.53 (2.51)
240	3.68 (3.64)	2.94 (2.91)	2.74 (2.71)	2.01 (1.99)	2.65 (2.61)
300	3.69 (3.65)	3.25 (3.21)	3.16 (3.11)	2.08 (2.06)	2.82 (2.77)
3600	4.47 (4.38)	4.46 (4.34)	1.13 (1.20)	2.98 (2.90)	4.00 (3.88)
5400	4.77 (4.66)	4.57 (4.45)	4.49 (4.34)	3.39 (3.28)	4.09 (3.97)
Mean Values					
C_∞/ppm	4.72 ± 0.06	4.42 ± 0.03	4.31 ± 0.02	3.30 ± 0.02	3.92 ± 0.03
a	0.48 ± 0.02	0.30 ± 0.01	0.34 ± 0.02	0.38 ± 0.02	0.35 ± 0.01
$k_{obs}/10^{-4}s^{-1}$	42.0 ± 0.2	39.2 ± 0.5	30.5 ± 1.5	23.9 ± 0.4	30.4 ± 0.2

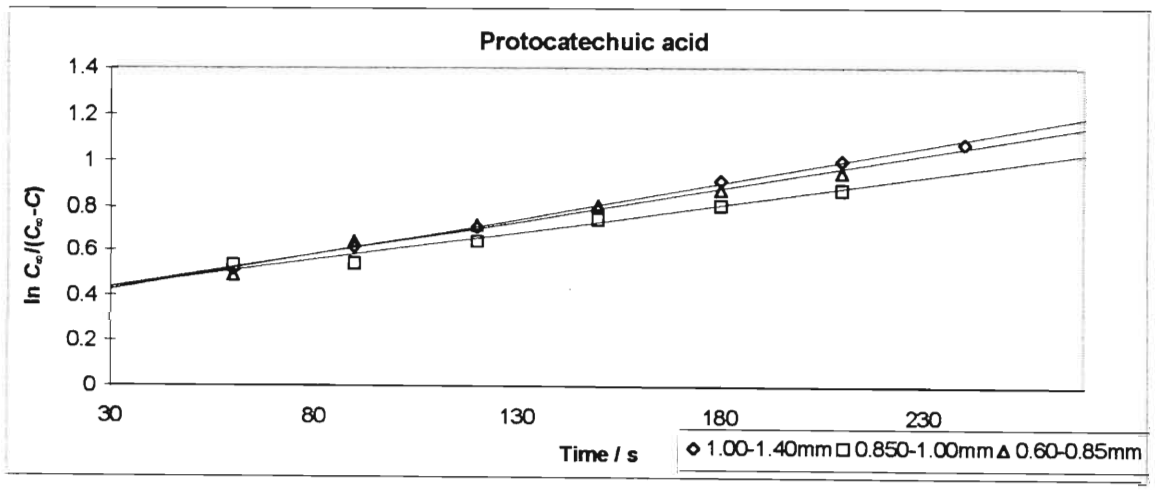

Figure 4.19 Typical plots for Protocatechuic acid for 0.60–0.85 mm, 0.85-1.00 mm and 1.00-1.40mm sieved fractions at 80 °C.

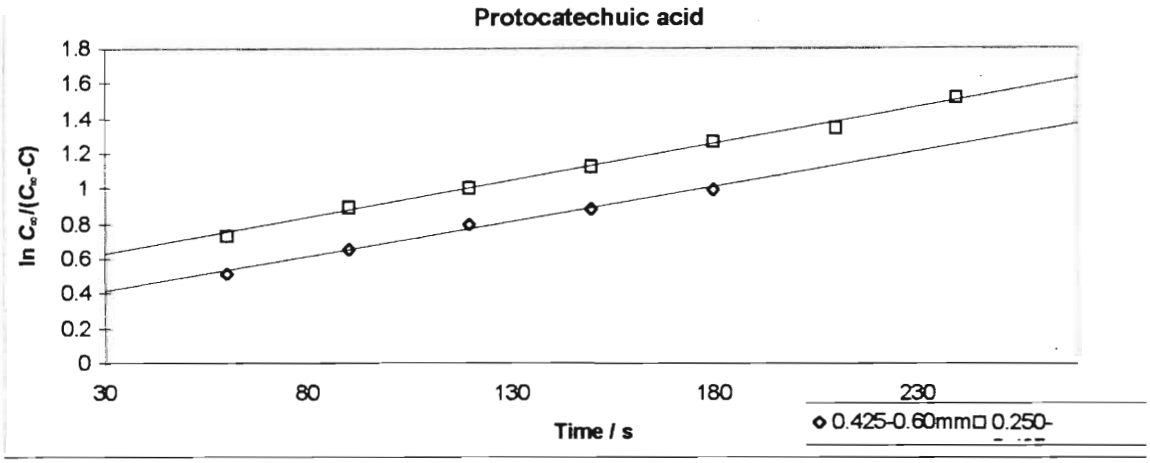

Figure 4.20 Typical plots for Protocatechuic acid for 0.250-0.425 mm and 0.425-0.60 mm sieved fractions at 80 °C.

Table 4.21 Observed and corrected Aspalathin concentrations, accompanied by the relevant kinetic data as obtained from the different sieved fractions. Included are the C_∞, a and k_{obs} values.

Sieving	**0.250-0.425mm**	**0.425-0.600mm**	**0.600-0.850mm**	**0.850-1.00mm**	**1.00-1.40mm**
Time/s	**Observed and corrected concentrations / ppm**				
0	0.00 (0.00)	0.00 (0.00)	0.00 (0.00)	0.00 (0.00)	0.00 (0.00)
30	2.62 (2.62)	2.17 (2.17)	3.03 (3.03)	1.79 (1.79)	2.54 (2.54)
60	3.91 (3.90)	3.55 (3.54)	4.03 (4.02)	2.61 (2.60)	3.77 (3.76)
90	4.65 (4.63)	4.10 (4.08)	4.81 (4.79)	3.03 (3.02)	4.44 (4.42)
120	5.17 (5.14)	5.18 (5.15)	5.32 (5.29)	3.33 (3.31)	5.07 (5.04)
150	5.62 (5.58)	5.60 (5.55)	5.89 (5.85)	3.56 (3.54)	5.57 (5.53)
180	6.08 (6.03)	6.29 (6.21)	6.42 (6.36)	4.06 (4.03)	6.08 (6.02)
210	6.55 (6.48)	6.81 (6.72)	6.83 (6.75)	4.07 (4.03)	6.48 (6.40)
240	7.04 (6.94)	7.07 (6.96)	7.43 (7.33)	4.20 (4.15)	6.98 (6.88)
300	7.25 (7.14)	8.04 (7.88)	7.56 (7.45)	4.61 (4.55)	7.63 (7.49)
3600	11.13 (10.78)	15.55 (14.94)	15.36 (14.77)	6.97 (6.76)	13.47 (13.00)
5400	10.29 (10.00)	15.45 (14.85)	15.03 (14.47)	7.21 (6.99)	12.53 (12.12)
Mean Values					
C_∞**/ppm**	11.81 ± 1.81	14.34 ± 0.60	14.05 ± 0.42	7.43 ± 0.44	12.97 ± 0.07
a	0.23 ± 0.05	0.15 ± 0.02	0.22 ± 0.01	0.32 ± 0.00	0.20 ± 0.05
$k_{obs}/10^{-4}s^{-1}$	36.2 ± 5.8	22.8 ± 0.6	20.4 ± 1.0	26.8 ± 2.8	22.0 ± 0.4

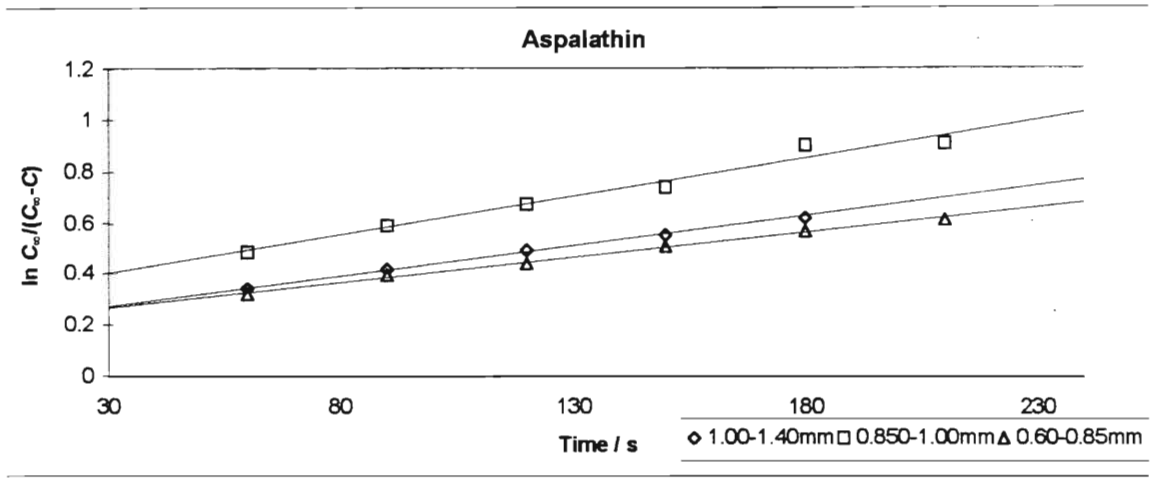

Figure 4.21 Typical plots for Aspalathin for 0.60–0.85 mm, 0.85-1.00 mm and 1.00-1.40mm sieved fractions at 80 °C.

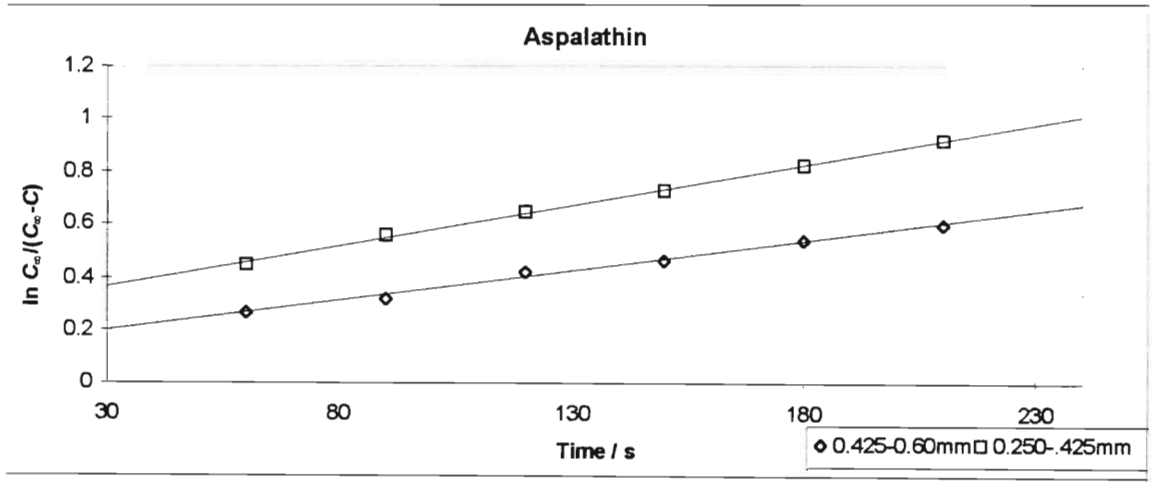

Figure 4.22 Typical plots for Aspalathin for 0.250-0.425 mm and 0.425-0.60 mm sieved fractions at 80 °C.

Table 4.22 Observed and corrected Rutin concentrations, accompanied by the relevant kinetic data as obtained from the different sieved fractions. Included are the C_∞, a and k_{obs} values.

Sieving	0.250-0.425mm	0.425-0.600mm	0.600-0.850mm	0.850-1.00mm	1.00-1.40mm
Time/s	Observed and corrected concentrations / ppm				
0	0.00 (0.00)	0.00 (0.00)	0.00 (0.00)	0.00 (0.00)	0.00 (0.00)
30	6.90 (6.90)	6.72 (6.72)	7.53 (7.53)	3.47 (3.47)	5.31 (5.31)
60	10.75 (10.73)	9.11 (9.10)	9.76 (9.74)	5.43 (5.42)	7.85 (7.83)
90	12.06 (12.01)	11.19 (11.14)	11.67 (11.62)	6.55 (6.52)	9.69 (9.65)
120	13.18 (13.11)	12.96 (12.88)	12.69 (12.62)	7.32 (7.27)	10.58 (10.52)
150	14.12 (14.03)	14.59 (14.47)	14.17 (14.07)	7.72 (7.67)	12.06 (11.96)
180	15.74 (15.59)	15.49 (15.34)	15.27 (15.13)	8.06 (7.99)	12.69 (12.57)
210	16.36 (16.19)	16.07 (15.88)	16.35 (16.17)	8.38 (8.30)	13.14 (13.00)
240	17.58 (17.35)	17.43 (17.18)	17.02 (16.80)	8.84 (8.74)	14.42 (14.22)
300	17.93 (17.68)	19.43 (19.07)	18.25 (17.97)	9.45 (9.32)	15.86 (15.59)
3600	33.45 (32.27)	36.17 (34.77)	35.15 (33.84)	15.21 (14.74)	27.96 (26.99)
5400	35.19 (33.89)	37.83 (36.32)	37.89 (36.40)	15.71 (15.20)	28.11 (27.13)
Mean Values					
C_∞/ppm	28.19 ± 5.69	37.08 ± 0.76	34.58 ± 1.81	14.56 ± 0.64	28.56 ± 1.24
a	0.25 ± 0.02	0.16 ± 0.00	0.22 ± 0.01	0.36 ± 0.01	0.20 ± 0.03
$k_{obs}/10^{-4}s^{-1}$	21.7 ± 3.1	22.1 ± 0.0	20.0 ± 1.9	21.2 ± 0.3	19.9 ± 1.4

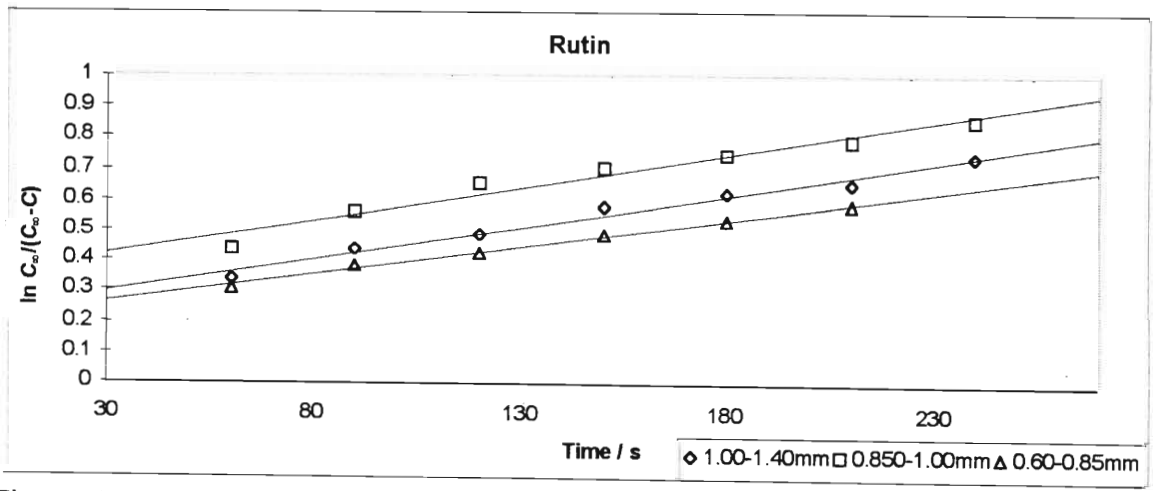

Figure 4.23 Typical plots for Rutin for 0.60–0.85 mm, 0.85-1.00 mm and 1.00-1.40mm sieved fractions at 80 °C.

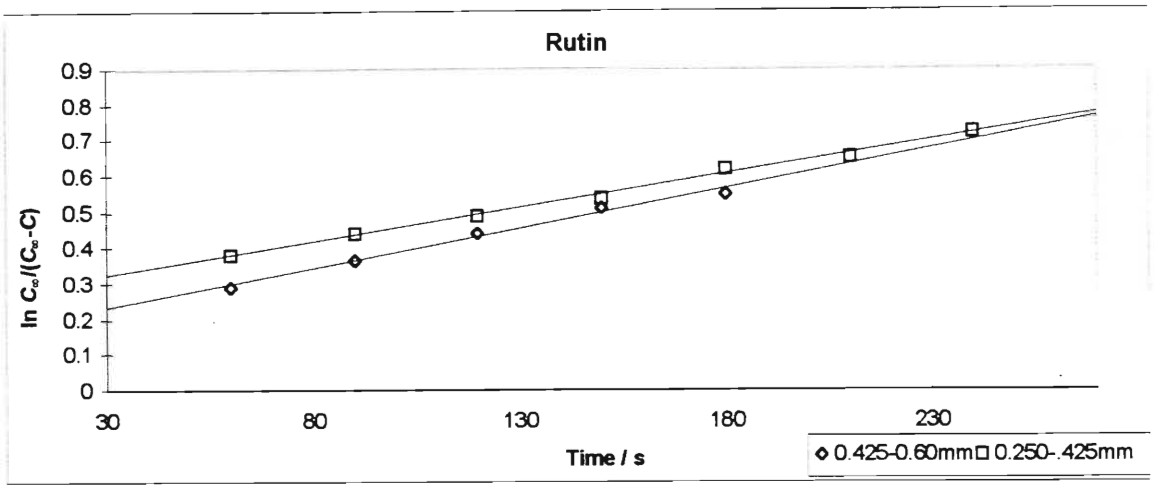

Figure 4.24 Typical plots for Rutin for 0.250-0.425 mm and 0.425-0.60 mm sieved fractions at 80 °C.

Table 4.23 Observed and corrected Orthophosphate concentrations, accompanied by the relevant kinetic data as obtained from the different sieved fractions. Included are the C_∞, a and k_{obs} values.

Sieving	**0.250-0.425mm**	**0.425-0.600mm**	**0.600-0.850mm**	**0.850-1.00mm**	**1.00-1.40mm**
Time/s	**Observed and corrected concentrations / ppm**				
0	0.00 (0.00)	0.00 (0.00)	0.00 (0.00)	0.00 (0.00)	0.00 (0.00)
30	1.73 (1.73)	1.15 (1.15)	1.23 (1.23)	1.10 (1.10)	1.02 (1.02)
60	2.32 (2.32)	1.54 (1.54)	1.59 (1.59)	1.40 (1.39)	1.40 (1.40)
90	2.70 (2.69)	1.79 (1.78)	1.87 (1.87)	1.59 (1.58)	1.63 (1.63)
120	2.98 (2.97)	2.02 (2.01)	1.95 (1.94)	1.73 (1.72)	1.79 (1.78)
150	3.10 (3.08)	2.18 (2.16)	2.09 (2.08)	1.83 (1.82)	1.89 (1.88)
180	3.41 (3.38)	2.24 (2.22)	2.09 (2.08)	1.93 (1.91)	2.01 (2.00)
210	3.31 (3.28)	2.29 (2.27)	2.11 (2.09)	2.01 (1.99)	2.11 (2.09)
240	3.40 (3.37)	2.38 (2.36)	2.14 (2.13)	2.08 (2.06)	2.11 (2.09)
300	3.47 (3.44)	2.54 (2.51)	2.34 (2.32)	2.21 (2.18)	2.23 (2.20)
3600	4.11 (4.03)	3.30 (3.23)	3.13 (3.06)	3.17 (3.09)	2.84 (2.78)
5400	4.32 (4.24)	3.25 (3.18)	3.11 (3.04)	3.21 (3.13)	3.24 (3.15)
Mean Values					
C_∞/ppm	4.38 ± 0.15	3.27 ± 0.09	3.21 ± 0.17	3.00 ± 0.12	3.17 ± 0.25
a	0.401 ± 0.039	0.350 ± 0.050	0.398 ± 0.015	0.357 ± 0.004	0.435 ± 0.024
k_{obs}/10 $^{-4}$s^{-1}	62.7 ± 4..9	56.2 ± 1.2	48.0 ± 3.2	35.9 ± 0.5	31.2 ± 1.7

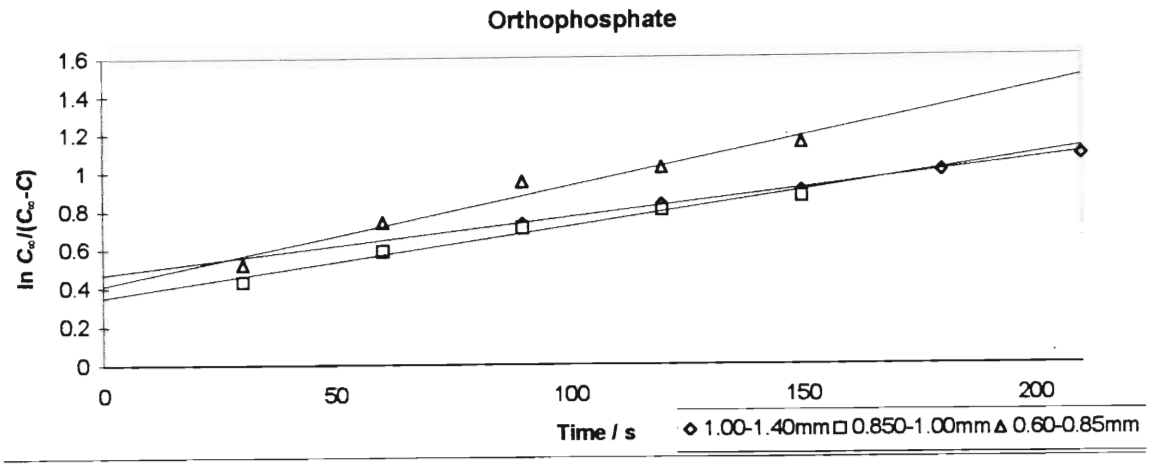

Figure 4.25 Typical plots for HPO_4^{2-} for 0.60–0.85 mm, 0.85-1.00 mm and 1.00-1.40mm sieved fractions at 80 °C.

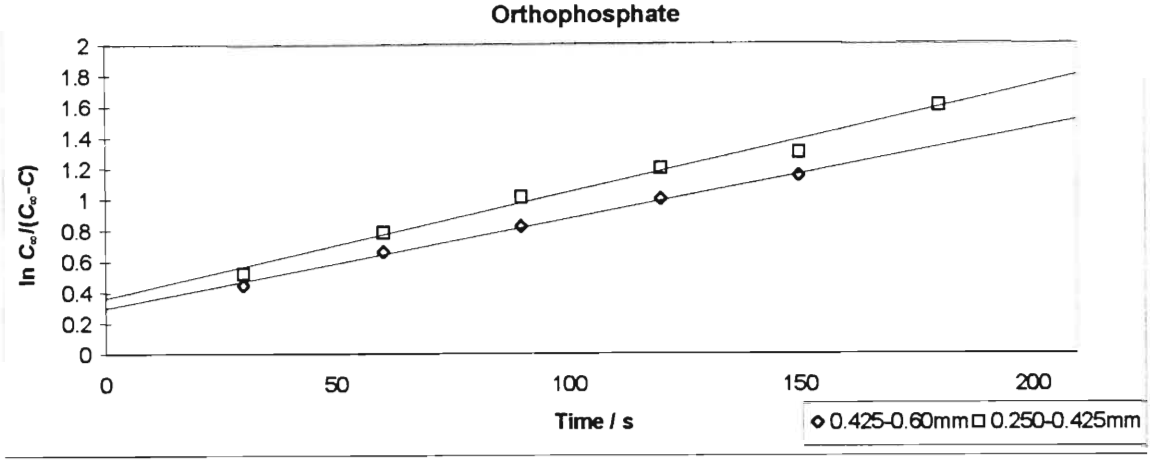

Figure 4.26 Typical plots for HPO_4^{2-} for 0.250-0.425 mm and 0.425-0.60 mm sieved fractions at 80 °C.

Table 4.24 Summary table of infusion rate constants for the cations, organics and the orthophosphate ion for the various sieving fractions used in the particle size investigations.

Species	Particle size (mm)				
	0.250-0.425	0.425-0.60	0.60-0.85	0.85-1.00	1.00-1.40
	Infusion rate constants (k_{obs}) / x 10^{-4} s^{-1}				
Na^+	52.4	49.7	67.7	41.2	33.8
K^+	65.2	53.8	64.7	40.4	34.9
Mg^{2+}	42.7	40.0	39.8	30.6	25.3
Protocatechuic acid	42.0	39.2	30.5	23.9	30.4
Aspalathin	36.2	22.8	20.4	26.8	22.0
Rutin	21.7	22.1	20.0	21.2	19.9
$H_2PO_4^-$	62.7	56.2	48.0	35.9	31.2

Values for the cationic species show that the rate constants increase with decreasing particle size. An anomaly is observed with only one particle size, that being the 0.60-0.85 sieved fraction. The organic species exhibit no general trend. The orthophosphate ion shows an increase in the rate constant with decreasing particle size. Rate constants for protocatechuic acid and aspalathin, for the smallest particle sizes, are approximately 1.3 and 1. 7 time larger than those for the other particle sizes respectively. These results also show that the rate constant for rutin is independent of particle size. In order to explain the trends observed for the cations and the orthophosphate ion, and also to explain the higher rate constants from the smaller particle sizes in the cases of protocatechuic acid and aspalathin, one needs to consider the model used to generate the results. The model treats the tea leaf as a lamina, and assumes that extraction of solutes is only from the lamina's two large surfaces. This is acceptable for large leaf particles, but extraction from the edges of the "lamina" become significant as the leaf size diminishes. In these cases the leaf can be regarded as a small cube, or even a sphere. Under these circumstances, since the rate determining step is diffusion through the leaf as assumed, the rate constant for infusion changes from

$$k_{obs} = \frac{2D}{d^2}\left(1 + \frac{w}{K'V}\right)$$

for a leaf of thickness $2d$, to

$$k_{obs} = \frac{12D}{d^2}\left(1 + \frac{w}{K'V}\right)$$

for a spherical particle of diameter $2d$[93]. Where D is the diffusion coefficient of the soluble constituent within the leaf, w is the mass of tea used and K' represents the notional partition coefficient of the soluble constituent as extracted from the leaf into a volume V of water. This theory predicts an increase in the rate constant of up to 6 times with a decrease in particle size. Ratios of rate constants from different particle sizes as determined in this work ranged from 1.5 to 2 when considering the largest and smallest sieving fractions. Increases of this nature have been reported by Spiro and Price[93] with regard to black tea infusions.

4.4.5 Extraction of Calcium with respect to particle size.

Calcium presents an interesting case for discussion. Kinetic investigation was not performed on Ca^{2+} since it's extraction did not follow a first order trend, nevertheless the metal was monitored during investigations of the particle size effect on tea infusions. Figure 4.27 shows plots of Ca^{2+} concentration with time as found in the same duplicate experiments with the species discussed in section 4.4.4, excluding the 1.00-1.40 mm fraction.

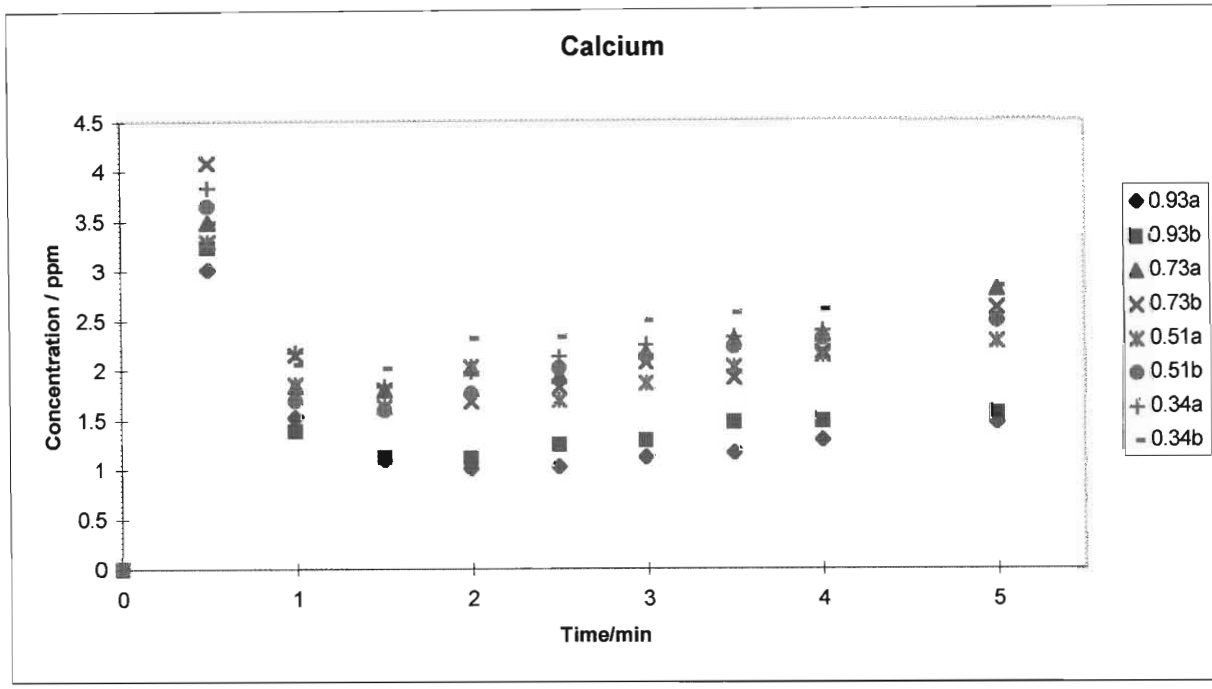

Figure 4.27 Duplicate plots, as represented by two points of the same colour, of Ca^{2+} in the concentration versus time using various particle sizes.

As illustrated by Figure 4.27, the concentration of Ca^{2+} ions in the water is zero as indicated by the point at the origin. After 30 seconds the Ca^{2+} concentration reaches a maximum, followed by a substantial decrease and then a gradual increase after about 90 seconds. This trend is reproducible within the particle sizes as the figure indicates. It is also clear that the trend is particle size dependent. The smaller particle size having higher values than the bigger particle size. This is possibly due to differences in surface area, with the smaller particle size having a greater surface area than that of the larger particle size. One could explain the observed trend if one assumed that the calcium exists in the leaf as a very soluble compound.

This dissolves very rapidly into the aqueous medium to give the high initial concentrations observed. In an aqueous medium the calcium exists as an ion which is re-absorbed into the leaf matrix. Calcium uptake by tea leaf material has been reported for infusions in hard water[98]. Once the re-absorption process is complete, the calcium starts to infuse back into the aqueous medium resulting in the gradual increase of Ca^{2+} concentration.

4.4.6 Determination of Rate Constants over a Temperature Range.

The rate of extraction of the nine species was investigated at six different temperatures (45 °, 50 °, 60 °, 70 °, 80 °, and 90 °C) except for chloride and sulfate for which the 45 °C temperature was omitted. The particle size used was the 1.00-1.40 mm sieved fraction. The experiments were repeated three times (four times at 80 °C) at each temperature, and the concentrations obtained corrected for volume losses. These were fitted into Equation (17). The gradient of all resultant plots gave the overall rate constants (k_{obs}) for the respective temperatures. The results, for the various species, are presented in Tables 4.25-4.33. The values in parenthesis are the concentrations corrected for water loss. These tables also contain the mean kinetic data from the triplicate analyses (quadruplicate in the case of 80 °C) of the equilibrium concentration C_∞, the intercept a, the observed rate constant k_{obs}, the half-life $t_{1/2}$ and the intercept corrected rate constant k_{eqn}. The kinetic plots are shown in Figures 4.28-4.42 in order to demonstrate the linearity and increase in the rate of extraction with increased temperature.

Table 4.25 Observed and corrected concentrations and rate constants for the sodium ion at various temperatures.

Temp/°C	45	50	60	70	80	90
Time/s	Observed and corrected concentrations / ppm					
0	0.00 (0.00)	0.00 (0.00)	0.00 (0.00)	0.00 (0.00)	0.00 (0.00)	0.00 (0.00)
30	2.27 (2.27)	3.81 (3.81)	9.20 (9.20)	6.06 (6.06)	7.50 (7.50)	9.38 (9.38)
60	5.29 (5.26)	6.97 (6.94)	13.20 (13.17)	9.66 (9.63)	10.05 (10.04)	13.39 (13.37)
90	8.17 (8.11)	8.45 (8.41)	15.59 (15.53)	10.78 (10.73)	12.14 (12.10)	15.28 (15.23)
120	9.66 (9.58)	10.16 (10.09)	17.07 (16.98)	12.65 (12.57)	13.00 (12.94)	16.66 (16.58)
150	11.52 (11.39)	11.37 (11.27)	18.30 (18.18)	13.29 (13.19)	14.04 (13.95)	17.74 (17.63)
180	12.86 (12.69)	12.49 (12.36)	19.97 (19.79)	14.30 (14.17)	14.47 (14.37)	18.26 (18.13)
210	13.92 (13.71)	13.22 (13.07)	20.81 (20.60)	14.99 (14.83)	15.56 (15.41)	19.59 (19.41)
240	14.75 (14.50)	14.38 (14.18)	21.53 (21.29)	15.28 (15.10)	15.51 (15.36)	19.99 (19.79)
300			22.70 (22.39)	15.60 (15.41)	16.13 (15.95)	20.62 (20.38)
3600	25.66 (24.90)	24.87 (24.24)	20.27 (20.11)	22.47 (21.87)	22.55 (21.96)	25.23 (24.70)
5400	31.00 (29.96)	25.64 (24.98)	31.40 (30.50)	23.40 (22.74)	23.53 (22.85)	27.05 (26.39)
Mean values of C_∞, a and k_{obs}. Calculated values of $t_{1/2}$ and k_{eqn}.						
C_∞ / ppm	29.99 ± 0.04	26.62 ± 2.45	26.51 ± 3.04	23.95 ± 1.37	24.01 ± 1.47	25.65 ± 0.82
a	0.15 ± 0.09	0.21 ± 0.06	0.28 ± 0.10	0.32 ± 0.05	0.43 ± 0.04	0.49 ± 0.07
$k_{obs}/10^{-4}s^{-1}$	27.4 ± 0.1	29.5 ± 1.7	29.9 ± 2.4	30.3 ± 1.2	33.8 ± 0.3	34.5 ± 0.6
$t_{1/2}$ /s	200.0	163.8	138.0	122.2	76.6	59.5
$k_{eqn}/10^{-4}s^{-1}$	34.65	42.31	50.23	56.74	90.51	116.4

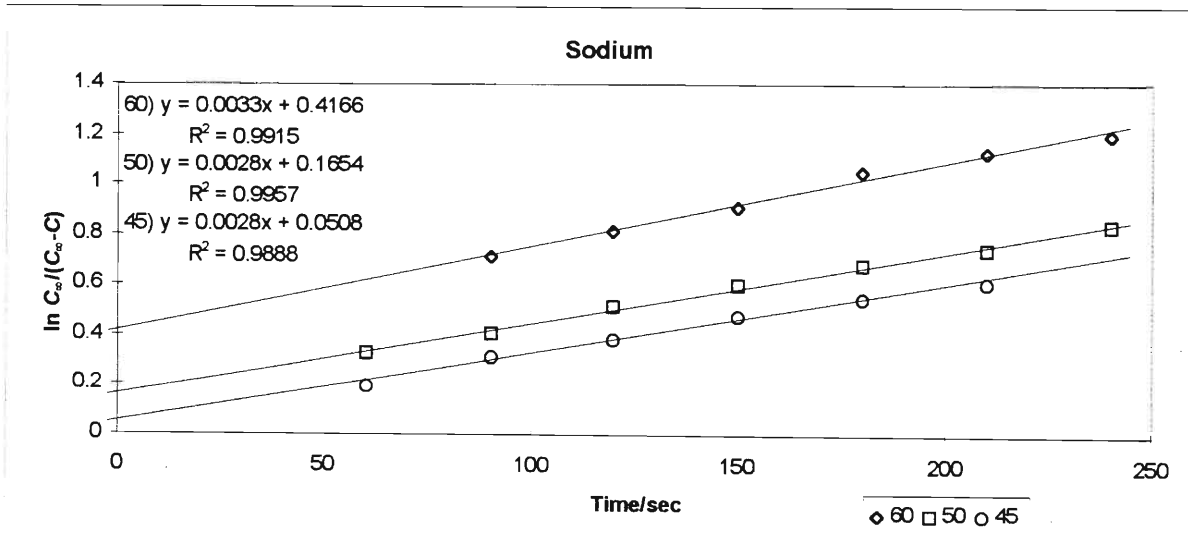

Figure 4.28 Typical kinetic plots for the sodium ion at 45°, 50° and 60°C.

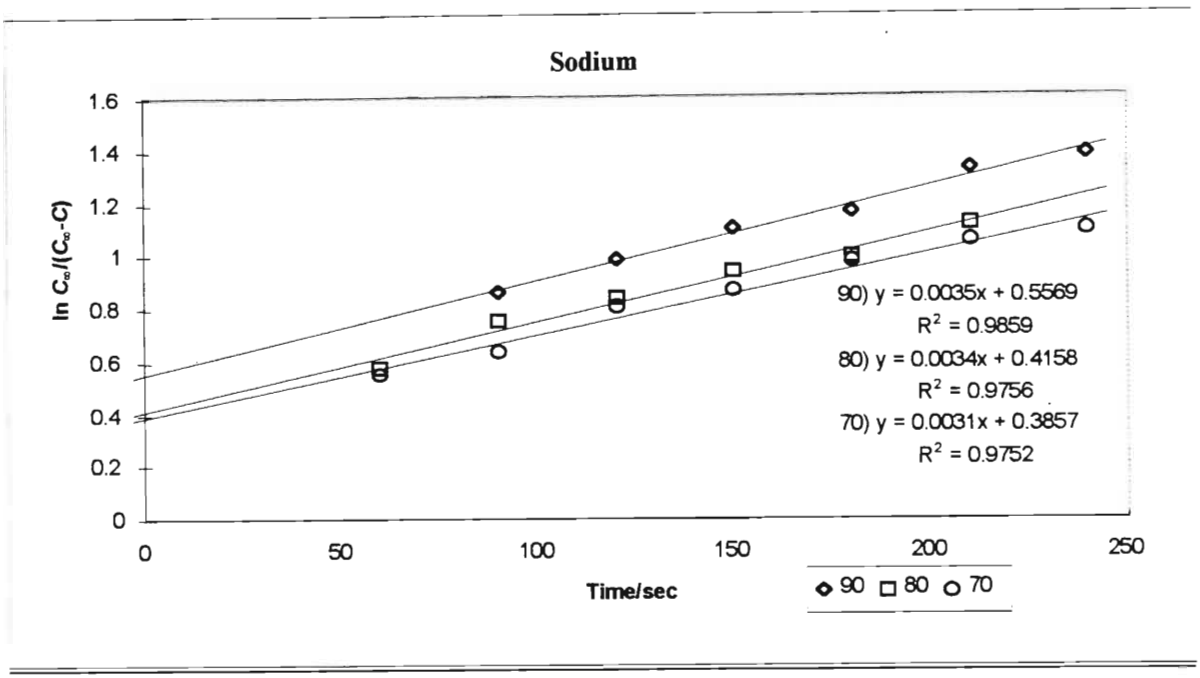

Figure 4.29 Typical kinetic plots for the sodium ion at 70°, 80° and 90°C.

Table 4.26 Observed and corrected concentrations and rate constants for the potassium ion at various temperatures.

Temp/°C	**45**	**50**	**60**	**70**	**80**	**90**
Time/s	Observed and corrected concentrations / ppm					
0	0.00 (0.00)	0.00 (0.00)	0.00 (0.00)	0.00 (0.00)	0.00 (0.00)	0.000 (0.00)
30	4.11 (4.11)	4.46 (4.56)	5.53 (5.53)	6.16 (6.16)	8.71 (8.71)	9.04 (9.04)
60	7.73 (7.70)	7.26 (7.39)	7.78 (7.76)	9.95 (9.92)	12.91 (12.87)	13.42 (13.39)
90	10.20 (10.14)	9.09 (9.25)	9.19 (9.15)	11.25 (11.20)	14.87 (14.81)	16.13 (16.06)
120	11.30 (11.22)	10.79 (10.95)	10.51 (10.45)	12.40 (12.33)	16.07 (15.98)	17.04 (16.95)
150	12.93 (12.81)	11.42 (11.59)	11.50 (11.41)	13.24 (13.15)	16.73 (16.63)	18.10 (17.98)
180	13.59 (13.45)	12.48 (12.64)	12.46 (12.34)	14.09 (13.97)	17.37 (17.25)	18.85 (18.71)
210	14.33 (14.16)	13.27 (13.43)	13.36 (13.21)	14.95 (14.79)	17.93 (17.78)	19.56 (19.39)
240	15.05 (14.85)	13.58 (13.73)	14.22 (14.03)	16.03 (15.82)	17.94 (17.79)	19.78 (19.60)
300			14.86 (14.63)	16.38 (16.16)	19.02 (18.82)	20.79 (20.55)
3600	24.13 (23.51)	22.56 (22.57)	19.54 (19.03)	23.79 (23.12)	22.42 (22.02)	26.99 (26.36)
5400	27.45 (26.66)	22.99 (22.99)	24.94 2(4.08)	24.42 (23.71)	25.15 (24.58)	26.04 (25.48)
Mean values of C_∞, a and k_{obs}. Calculated values of $t_{1/2}$ and k_{eqn}.						
C_∞ / ppm	26.64 ± 0.03	24.15 ± 2.32	23.68 ± 0.39	23.83 ± 0.20	24.25 ± 0.32	25.84 ± 0.37
a	0.30 ± 0.01	0.37 ± 0.10	0.31 ± 0.08	0.35 ± 0.07	0.54 ± 0.04	0.61 ± 0.06
$k_{obs}/10^{-4}s^{-1}$	23.5 ± 1.0	25.2 ± 4.8	27.7 ± 0.8	30.1 ± 1.7	34.9 ± 0.9	37.1 ± 2.0
$t_{1/2}$ /s	166.1	128.1	137.9	115.4	44.7	23.2
$k_{eqn}/10^{-4}s^{-1}$	41.73	54.11	50.28	60.07	154.97	298.59

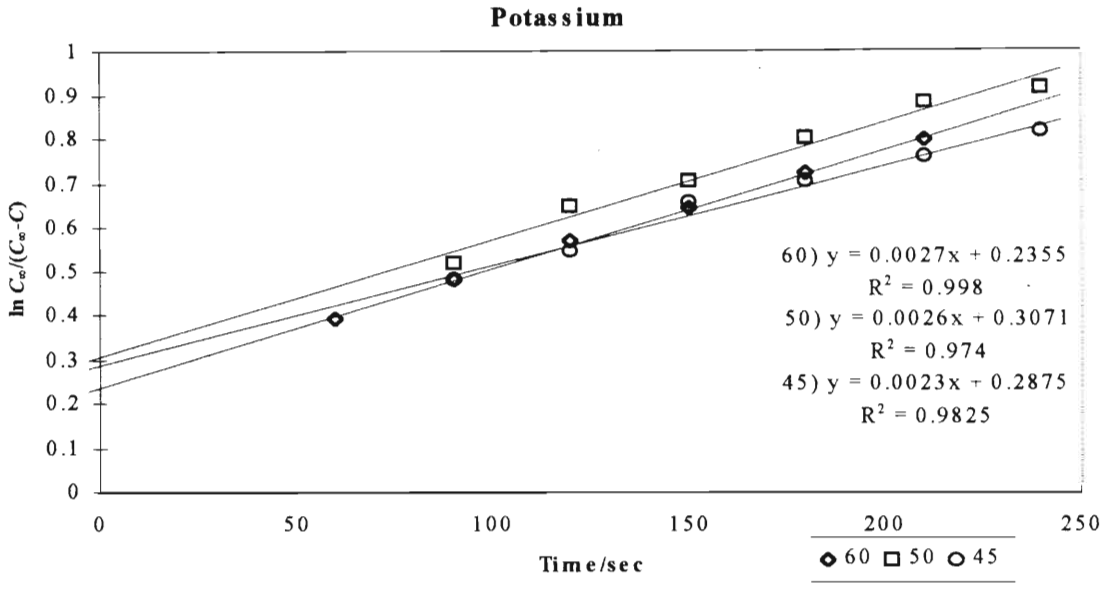

Figure 4.39 Typical kinetic plots for the potassium ion at 45°, 50° and 60°C.

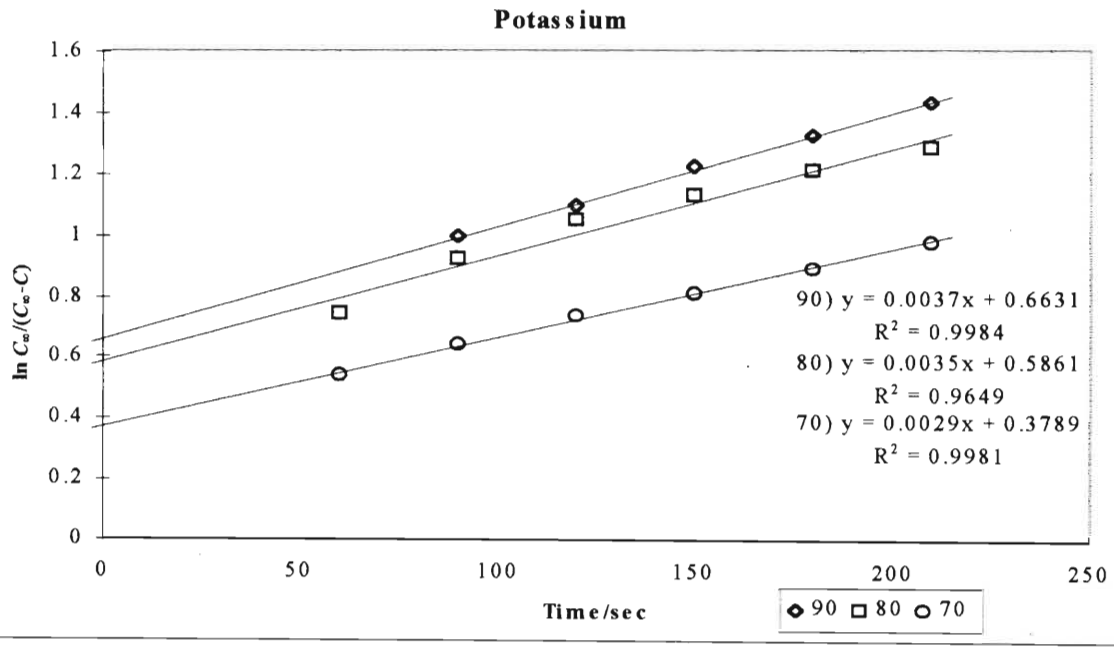

Figure 4.38 Typical kinetic plots for the potassium ion at 70°, 80° and 90°C.

Table 4.27 Observed and corrected concentrations and rate constants for the magnesium ion at various temperatures.

Temp/°C	45	50	60	70	80	90
Time/s	Observed and corrected concentrations / ppm					
0	0.00 (0.00)	0.00 (0.00)	0.00 (0.00)	0.00 (0.00)	0.00 (0.00)	0.00 (0.00)
30	0.23 (0.23)	0.54 (0.53)	0.80 (0.80)	1.02 (1.02)	1.56 (1.56)	0.98 (0.98)
60	1.01 (1.00)	1.14 (1.12)	1.51 (1.50)	1.89 (1.88)	2.40 (2.39)	2.46 (2.45)
90	1.53 (1.52)	1.64 (1.61)	2.07 (2.06)	2.66 (2.65)	2.81 (2.80)	3.52 (3.49)
120	1.92 (1.90)	2.13 (2.09)	2.47 (2.45)	3.02 (3.00)	3.51 (3.49)	4.03 (4.00)
150	2.30 (2.27)	2.55 (2.49)	2.81 (2.78)	3.34 (3.31)	4.08 (4.04)	4.46 (4.41)
180	2.53 (2.50)	2.86 (2.79)	2.99 (2.95)	3.77 (3.73)	4.32 (4.27)	4.82 (4.76)
210	2.70 (2.66)	3.07 (2.99)	3.21 (3.16)	3.92 (3.86)	4.68 (4.61)	4.99 (4.93)
240	2.88 (2.83)	3.35 (3.25)	3.50 (3.44)	3.94 (3.88)	4.84 (4.77)	5.28 (5.20)
300			3.81 (3.73)	4.76 (4.66)	5.35 (5.25)	5.55 (5.45)
3600	7.52 (7.25)	7.77 (7.42)	6.73 (6.48)	9.29 (8.92)	10.79 (10.31)	10.38 (9.98)
5400	7.62 (7.35)	8.28 (7.89)	10.06 (9.59)	10.06 (9.65)	10.83 (10.34)	10.46 (10.05)
Mean values of C_∞, a and k_{obs}. Calculated values of $t_{1/2}$ and k_{eqn}.						
C_∞ / ppm	7.35 ± 0.00	7.15 ± 0.51	8.15 ± 1.05	9.68 ± 0.04	9.61 ± 0.71	10.60 ± 0.80
a	0.07 ± 0.01	0.07 ± 0.04	0.18 ± 0.08	0.05 ± 0.02	0.12 ± 0.03	0.13 ± 0.03
$k_{obs}/10^{-4}s^{-1}$	18.5 ± 0.1	20.3 ± 0.6	22.7 ± 1.1	23.4 ± 0.7	25.3 ± 1.7	27.4 ± 2.6
$t_{1/2}$ /s	336.9	305.7	228.0	273.8	226.4	206.4
$k_{eqn}/10^{-4}s^{-1}$	20.58	22.67	30.4	0.002531	30.62	33.59

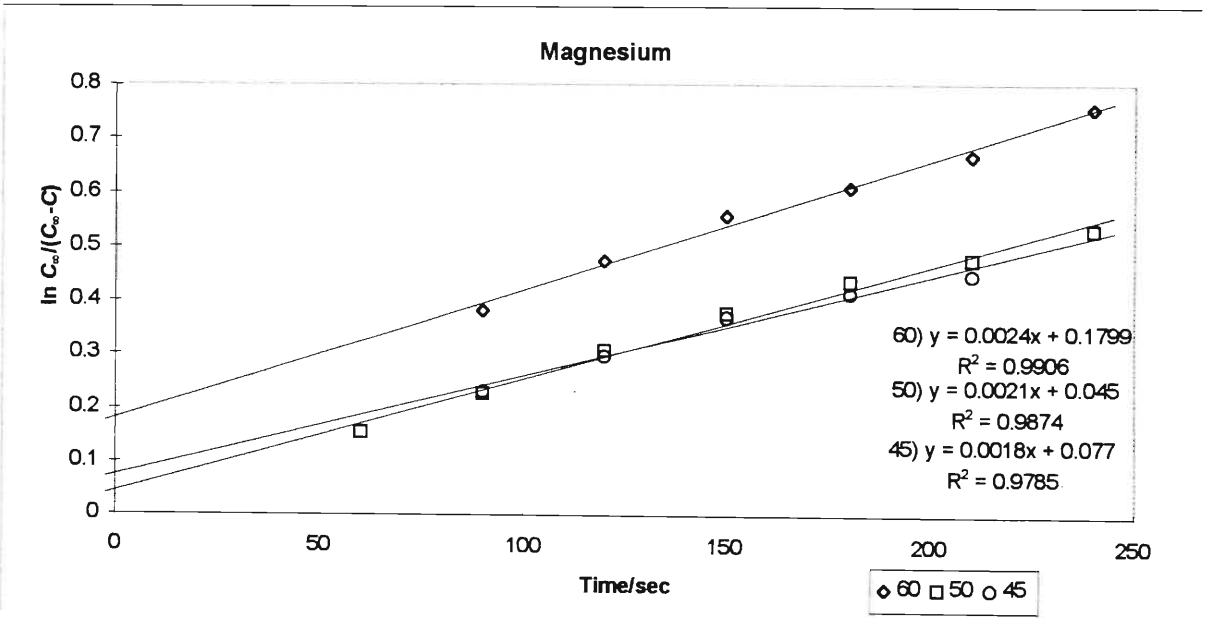

Figure 4.30 Typical kinetic plots for the magnesium ion at 45°, 50° and 60°C.

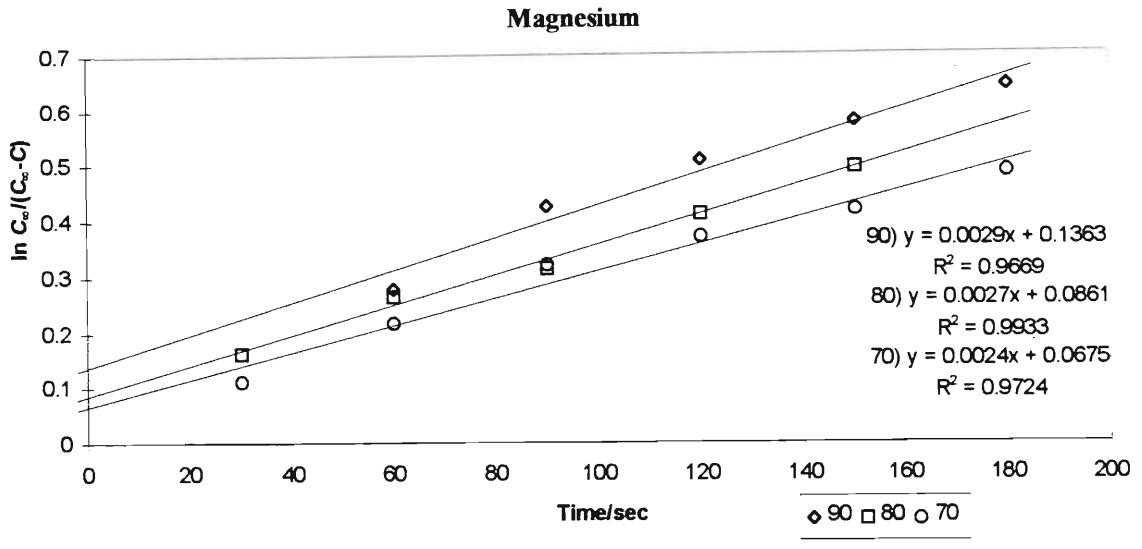

Figure 4.31 Typical kinetic plots for the magnesium ion at 70°, 80° and 90°C.

Table 4.28 Observed and corrected concentrations and rate constants for protocatechuic acid at various temperatures.

Temp/°C	45	50	60	70	80	90
Time/s	Observed and corrected concentrations / ppm					
0	0.00 (0.00)	0.00 (0.00)	0.00 (0.00)	0.00 (0.00)	0.00 (0.00)	0.00 (0.00)
30	0.44 (0.44)	0.64 (0.64)	0.85 (0.85)	0.98 (0.98)	1.14 (1.14)	1.22 (1.22)
60	0.85 (0.84)	1.04 (1.03)	1.13 (1.13)	1.48 (1.48)	1.61 (1.61)	1.81 (1.81)
90	1.08 (1.08)	1.22 (1.22)	1.32 (1.31)	1.77 (1.76)	1.83 (1.83)	2.14 (2.13)
120	1.24 (1.23)	1.42 (1.41)	1.50 (1.50)	1.88 (1.87)	2.04 (2.03)	2.38 (2.37)
150	1.32 (1.31)	1.54 (1.54)	1.70 (1.68)	2.01 (2.00)	2.18 (2.17)	2.56 (2.54)
180	1.47 (1.46)	1.65 (1.64)	1.88 (1.86)	2.22 (2.20)	2.40 (2.38)	2.72 (2.69)
210	1.58 (1.57)	1.78 (1.76)	1.97 (1.95)	2.29 (2.27)	2.53 (2.51)	2.86 (2.83)
240	1.75 (1.72)	1.89 (1.86)	2.09 (2.06)	2.51 (2.48)	2.65 (2.61)	2.95 (2.92)
300			2.22 (2.19)	2.60 (2.56)	2.82 (2.77)	3.11 (3.07)
3600	3.27 (3.18)	3.71 (3.60)	3.84 (3.71)	3.96 (3.84)	4.00 (3.88)	4.19 (4.08)
5400	3.38 (3.28)	3.84 (3.72)	3.91 (3.77)	4.12 (3.99)	4.09 (3.97)	4.38 (4.25)
Mean values of C_∞, a and k_{obs}. Calculated values of $t_{1/2}$ and k_{eqn}.						
C_∞ / ppm	3.33 ± 0.05	3.65 ± 0.07	3.62 ± 0.17	3.92 ± 0.15	3.92 ± 0.03	4.26 ± 0.04
a	0.21 ± 0.01	0.24 ± 0.02	0.26 ± 0.04	0.30 ± 0.02	0.35 ± 0.01	0.42 ± 0.05
$k_{obs}/10^{-4}s^{-1}$	19.8 ± 0.7	20.8 ± 0.6	24.5 ± 0.9	26.2 ± 0.6	30.4 ± 1.5	32.4 ± 1.4
$t_{1/2}$ /s	246.4	219.1	176.7	14 9.3	112.9	83.0
$k_{eqn}/10^{-4}s^{-1}$	28.13	31.64	39.22	46.42	61.38	83.53

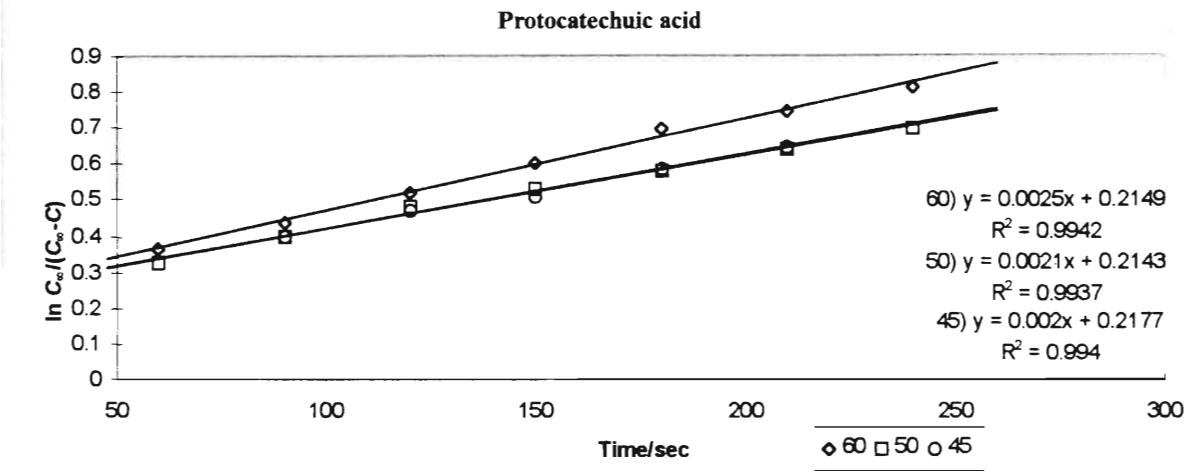

Figure 4.31 Typical kinetic plots for protocatechuic acid 45°, 50° and 60°C.

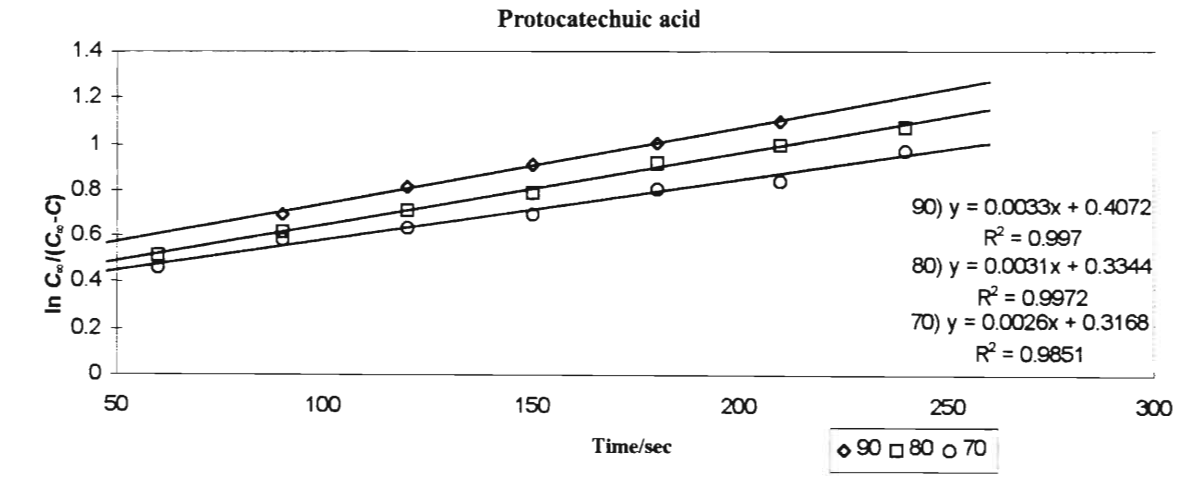

Figure 4.32 Typical kinetic plots for protocatechuic acid 70°, 80° and 90°C.

Table 4.29 Observed and corrected concentrations and rate constants for aspalathin at various temperatures.

Temp/°C	45	50	60	70	80	90
Time/s	Observed and corrected concentrations / ppm					
0	0.00 (0.00)	0.00 (0.00)	0.00 (0.00)	0.00 (0.00)	0.00 (0.00)	0.00 (0.00)
30	0.83 (0.83)	1.55 (1.55)	1.77 (1.77)	2.24 (2.24)	2.54 (2.54)	2.84 (2.84)
60	1.57 (1.56)	1.79 (1.79)	2.76 (2.75)	3.23 (3.22)	3.77 (3.76)	4.36 (4.35)
90	2.08 (2.06)	2.46 (2.44)	3.43 (3.41)	4.11 (4.09)	4.44 (4.42)	5.29 (5.27)
120	2.55 (2.53)	2.98 (2.96)	4.13 (4.10)	4.66 (4.63)	5.07 (5.04)	6.13 (6.09)
150	2.79 (2.76)	3.31 (3.28)	4.50 (4.46)	5.04 (5.00)	5.57 (5.53)	6.72 (6.66)
180	3.20 (3.16)	3.70 (3.66)	5.00 (4.95)	5.46 (5.40)	6.08 (6.02)	7.26 (7.18)
210	3.56 (3.50)	4.07 (4.02)	5.25 (5.18)	5.88 (5.81)	6.48 (6.40)	7.50 (7.42)
240	3.92 (3.86)	4.30 (4.24)	5.59 (5.50)	6.25 (6.16)	6.98 (6.88)	8.04 (7.93)
300			6.20 (6.09)	6.80 (6.68)	7.63 (7.49)	8.84 (8.68)
3600	10.40 (10.03)	10.71 (10.32)	10.96 (10.56)	13.74 (13.22)	13.47 (13.00)	15.31 (14.75)
5400	10.61 (10.24)	11.71 (11.27)	12.22 (11.74)	14.06 (13.51)	12.53 (12.12)	16.04 (15.43)
Mean values of C_∞, a and k_{obs}. Calculated values of $t_{1/2}$ and k_{eqn}.						
C_∞ / ppm	10.06 ± 0.18	11.41 ± 0.14	11.62 ± 0.29	12.78 ± 0.58	12.97 ± 0.07	16.20 ± 0.73
a	0.07 ± 0.01	0.11 ± 0.00	0.17 ± 0.02	0.20 ± 0.01	0.20 ± 0.05	0.21 ± 0.04
$k_{obs}/10^{-4}s^{-1}$	16.4 ± 0.2	16.3 ± 0.3	18.3 ± 0.9	18.5± 1.5	22.0 ± 0.4	25.9 ± 1.9
$t_{1/2}$ /s	382.4	359.1	286.6	265.9	224.3	187.9
$k_{eqn}/10^{-4}s^{-1}$	18.12	19.3	24.19	26.07	30.9	36.88

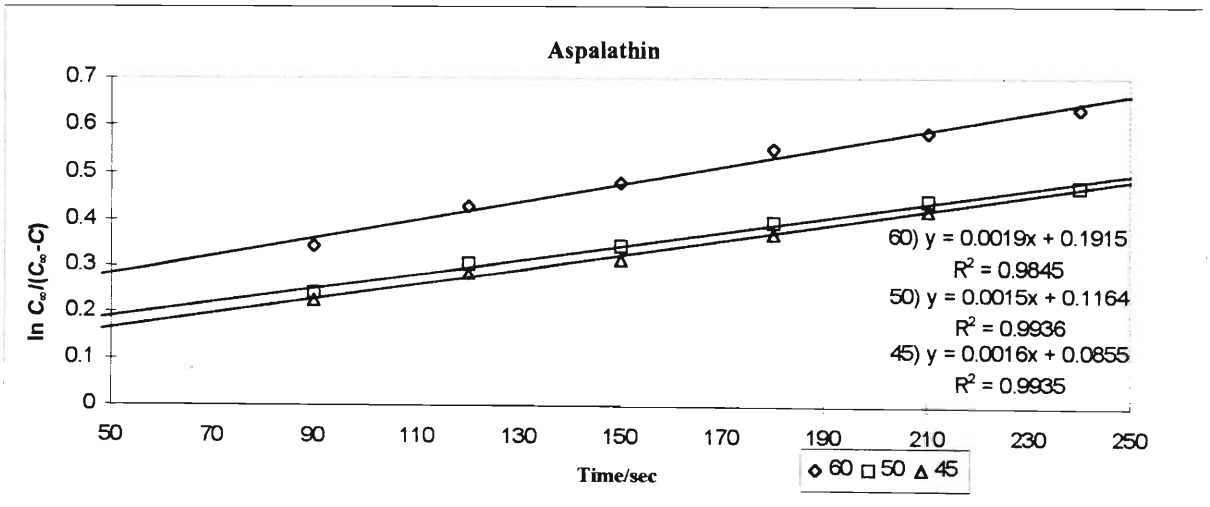

Figure 4.33 Typical kinetic plots for aspalathin at 45°, 50° and 60°C.

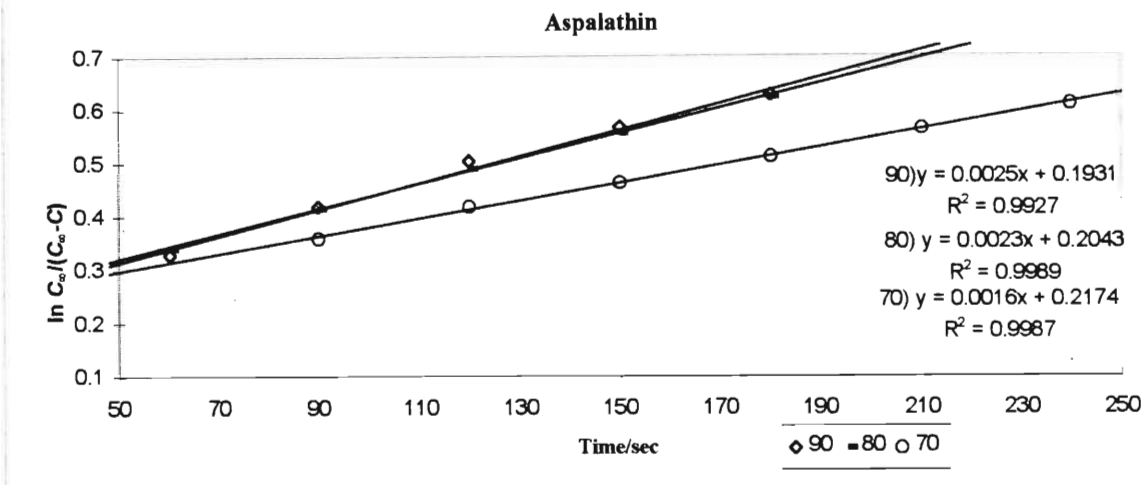

Figure 4.34 Typical kinetic plots for aspalathin at 70°, 80° and 90°C.

Table 4.30 Observed and corrected concentrations and rate constants for rutin at various temperatures.

Temp/°C	**45**	**50**	**60**	**70**	**80**	**90**
Time/s	Observed and corrected concentrations / ppm					
0	0.00 (0.00)	0.00 (0.00)	0.00 (0.00)	0.00 (0.00)	0.00 (0.00)	0.00 (0.00)
30	1.59 (1.59)	2.05 (2.05)	3.16 (3.16)	4.12 (4.12)	5.31 (5.31)	4.87 (4.87)
60	2.98 (2.97)	3.59 (3.57)	4.57 (4.56)	6.64 (6.63)	7.85 (7.83)	9.11 (9.08)
90	4.38 (4.35)	4.75 (4.72)	5.92 (5.89)	8.34 (8.30)	9.69 (9.65)	10.70 (10.64)
120	5.34 (5.29)	5.77 (5.73)	7.04 (6.99)	9.24 (9.18)	10.58 (10.52)	11.75 (11.67)
150	5.80 (5.74)	6.91 (6.83)	8.04 (7.96)	9.94 (9.86)	12.06 (11.96)	12.95 (12.84)
180	6.80 (6.71)	7.38 (7.30)	8.96 (8.85)	11.53 (11.40)	12.69 (12.57)	13.53 (13.40)
210	7.56 (7.44)	8.40 (8.27)	9.90 (9.75)	12.35 (12.19)	13.14 (13.00)	15.28 (15.08)
240	8.17 (8.03)	9.16 (9.01)	10.91 (10.72)	12.94 (12.75)	14.42 (14.22)	15.28 (15.08)
300			11.33 (11.12)	12.81 (12.62)	15.86 (15.59)	16.17 (15.92)
3600	23.03 (22.21)	23.78 (22.92)	24.32 (23.33)	27.11 (26.07)	27.96 (26.99)	26.31 (25.43)
5400	25.69 (24.73)	24.61 (23.71)	27.24 (26.06)	30.00 (28.77)	28.11 (27.13)	27.25 (26.30)
Mean values of C_∞, a and k_{obs}. Calculated values of $t_{1/2}$ and k_{eqn}.						
C_∞ / ppm	24.70 ± 0.03	24.17 ± 0.46	25.44 ± 0.77	29.71 ± 1.75	28.56 ± 1.08	28.52 ± 2.01
a	0.07 ± 0.02	0.07 ± 0.01	0.14 ± 0.04	0.18 ± 0.01	0.20 ± 0.03	0.30 ± 0.06
$k_{obs}/10^{-4}s^{-1}$	15.7 ± 0.2	17.2 ± 0.2	18.4 ± 1.6	17.6 ± 0.5	19.9 ± 1.4	22.5 ± 0.6
$t_{1/2}$ /s	400.8	360.3	297.5	289.3	246.2	173.8
$k_{eqn}/10^{-4}s^{-1}$	17.3	19.24	23.3	23.96	28.16	39.88

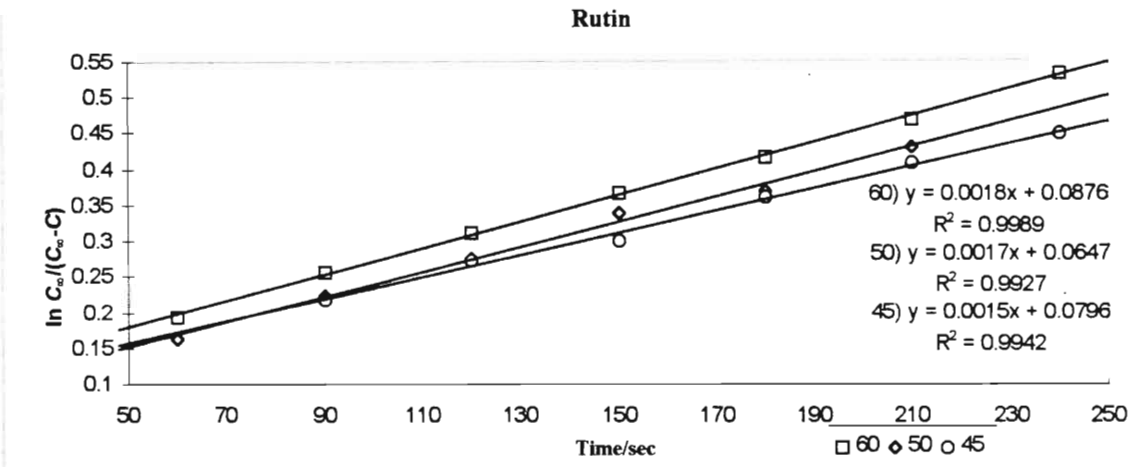

Figure 4.35 Typical kinetic plots for rutin at 45°, 50° and 60°C.

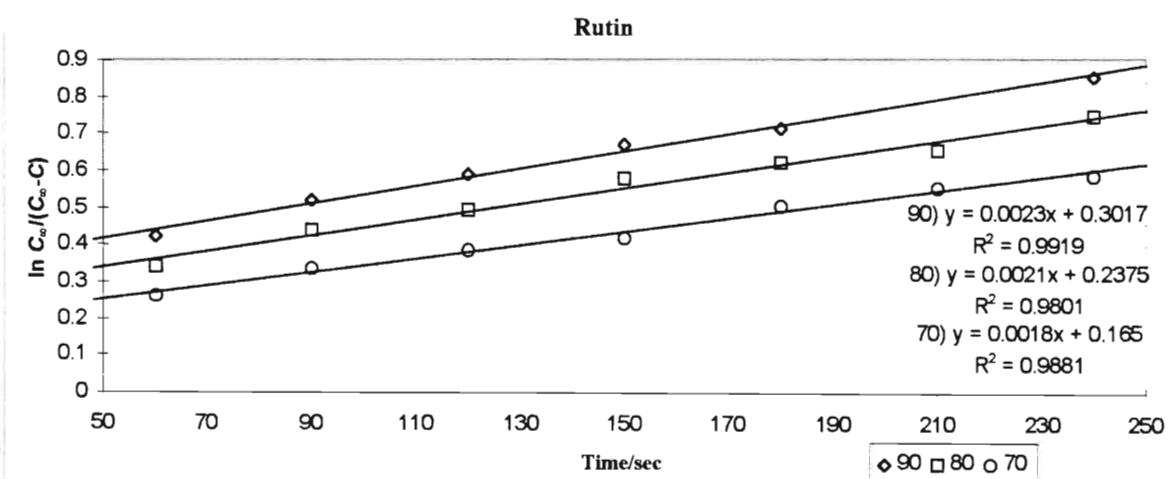

Figure 4.36 Typical kinetic plots for rutin at 70°, 80° and 90°C.

Table 4.31 Observed and corrected concentrations and rate constants for the orthophosphate ion at various temperatures.

Temp/°C	45	50	60	70	80	90
Time/s	Observed and corrected concentrations / ppm					
0	0.00 (0.00)	0.00 (0.00)	0.00 (0.00)	0.00 (0.00)	0.00 (0.00)	0.00 (0.00)
30	0.64 (0.64)	0.62 (0.62)	0.92 (0.92)	1.10 (1.10)	1.02 (1.02)	1.13 (1.13)
60	1.09 (1.08)	0.96 (0.96)	1.17 (1.17)	1.38 (1.38)	1.40 (1.40)	1.58 (1.57)
90	1.28 (1.28)	1.13 (1.12)	1.36 (1.36)	1.60 (1.59)	1.63 (1.63)	1.90 (1.89)
120	1.42 (1.41)	1.27 (1.26)	1.55 (1.54)	1.75 (1.74)	1.79 (1.78)	2.03 (2.02)
150	1.55 (1.54)	1.37 (1.36)	1.65 (1.64)	1.81 (1.80)	1.89 (1.88)	2.15 (2.13)
180	1.67 (1.65)	1.49 (1.48)	1.72 (1.71)	1.96 (1.95)	2.01 (2.00)	2.30 (2.28)
210	1.74 (1.72)	1.57 (1.55)	1.80 (1.79)	2.14 (2.12)	2.11 (2.09)	2.37 (2.35)
240	1.81 (1.79)	1.67 (1.65)	1.92 (1.89)	2.33 (2.30)	2.11 (2.09)	2.41 (2.38)
300			2.15 (2.12)	2.43 (2.39)	2.23 (2.20)	2.53 (2.50)
3600	3.05 (2.98)	2.63 (2.57)	2.89 (2.81)	3.64 (3.54)	2.84 (2.78)	3.61 (3.51)
5400	2.69 (2.63)	2.78 (2.71)	3.84 (3.70)	3.90 (3.77)	3.24 (3.15)	3.55 (3.45)
Mean values of C_∞, a and k_{obs}. Calculated values of $t_{1/2}$ and k_{eqn}.						
C_∞ / ppm	2.62 ± 0.00	2.67 ± 0.04	3.42 ± 0.38	3.58 ± 0.28	3.17 ± 0.25	3.30 ± 0.22
a	0.37 ± 0.02	0.28 ± 0.09	0.23 ± 0.04	0.30 ± 0.03	0.44 ± 0.02	0.50 ± 0.05
$k_{obs}/10^{-4}s^{-1}$	22.8 ± 1.5	24.6 ± 1.5	25.4 ± 0.8	28.1 ± 2.4	31.2 ± 1.7	33.6 ± 0.6
$t_{1/2}$ /s	142.0	168.8	181.2	139.3	82.7	57.9
$k_{eqn}/10^{-4}s^{-1}$	48.82	41.06	38.25	49.75	83.81	119.72

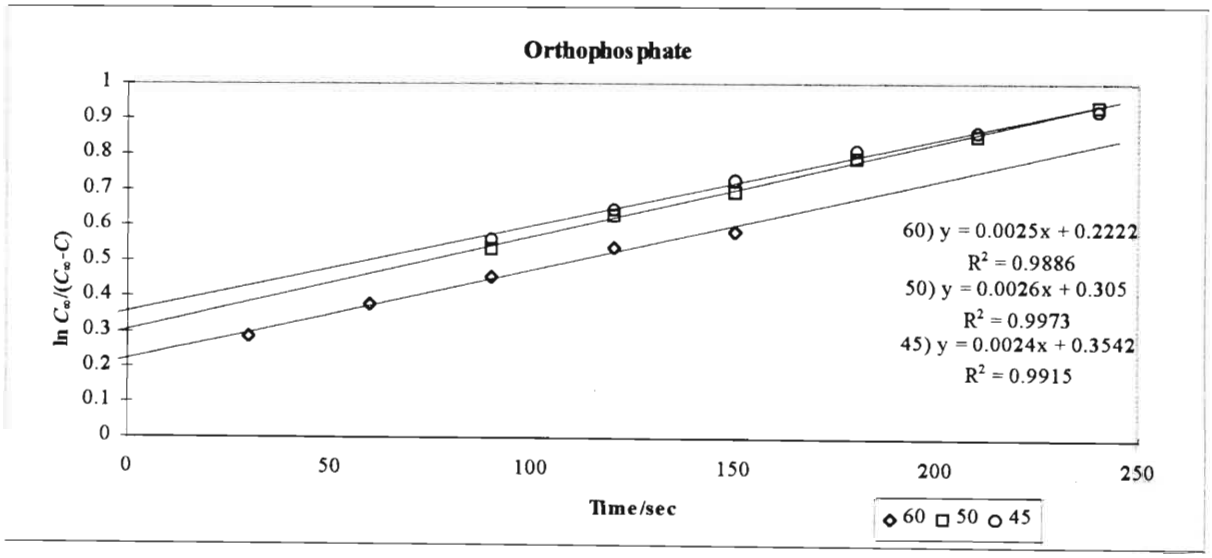

Figure 4.37 Typical kinetic plots for the orthophosphate ion at 45°, 50° and 60°C.

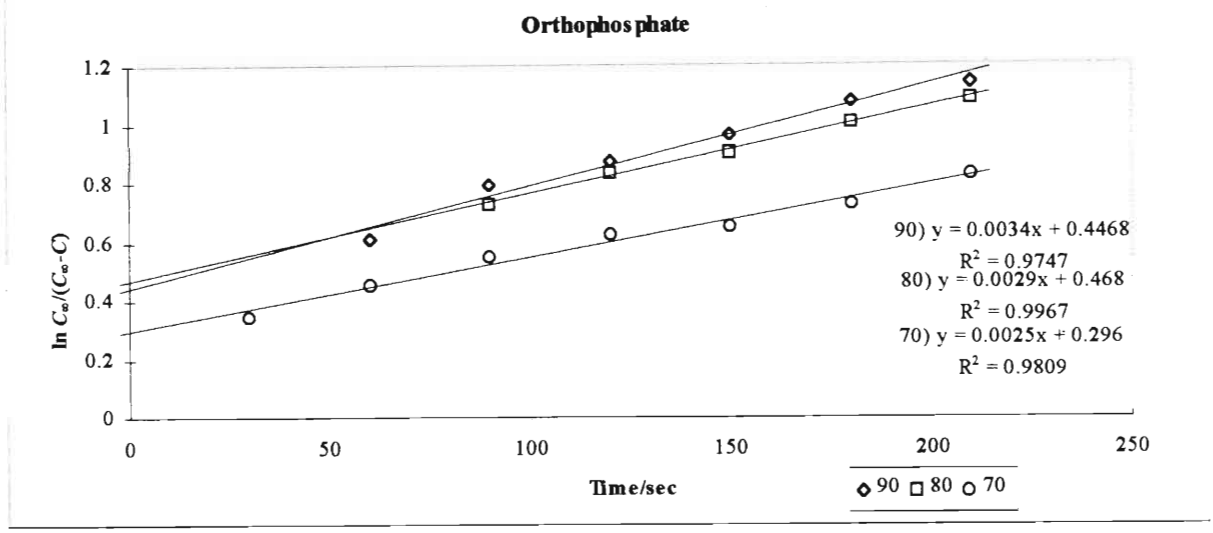

Figure 4.38 Typical kinetic plots for the orthophosphate ion at 70°, 80° and 90°C.

Table 4.32 Observed and corrected concentrations and rate constants for the chloride ion at various temperatures.

Temp/°C	**50**	**60**	**70**	**80**	**90**
Time/s	**Observed and corrected concentrations / ppm**				
0	0.00 (0.00)	0.00 (0.00)	0.00 (0.00)	0.00 (0.00)	0.00 (0.00)
30	15.76 (15.32)	23.79 (23.79)	15.33 (15.33)	27.70 (27.70)	25.34 (25.34)
60	17.56 (17.04)	31.39 (31.32)	17.63 (17.60)	20.30 (20.33)	38.64 (38.54)
90	21.81 (21.12)	42.29 (42.08)	19.68 (19.62)	22.25 (22.26)	42.14 (42.00)
120	20.86 (20.21)	23.39 (23.53)	23.48 (23.35)	33.85 (33.63)	47.94 (47.68)
150	22.11 (21.39)	24.94 (25.04)	22.93 (22.82)	26.80 (26.76)	45.74 (45.54)
180	23.26 (22.48)	26.09 (26.16)	24.78 (24.61)	28.20 (28.12)	51.09 (50.71)
210	29.16 (28.00)	31.29 (31.17)	28.83 (28.51)	29.55 (29.42)	52.59 (52.15)
240	28.46 (27.35)	28.04 (28.06)	29.08 (28.75)	46.50 (45.61)	52.09 (51.67)
5400	41.06 (39.00)	37.79 (37.33)	30.58 (30.17)	32.45 (32.28)	52.59 (52.14)
Mean values of C_∞, a and k_{obs}. Calculated values of $t_{1/2}$ and k_{eqn}.					
C_∞ / ppm	36.93 ± 2.07	37.33	30.17	50.21	51.45 ± 0.70
a	0.46 ± 0.03	0.612	0.494	0.308	-0.19 ± 0.26
$k_{obs}/10^{-4}s^{-1}$	27.5 ± 3.3	32.7	64.0	112.4	197.8 ± 3.6
$t_{1/2}$ /s	86.0	24.9	31.1	34.3	44.6
$k_{eqn}/10^{-4}s^{-1}$	80.62	278.19	223.17	202.35	155.51

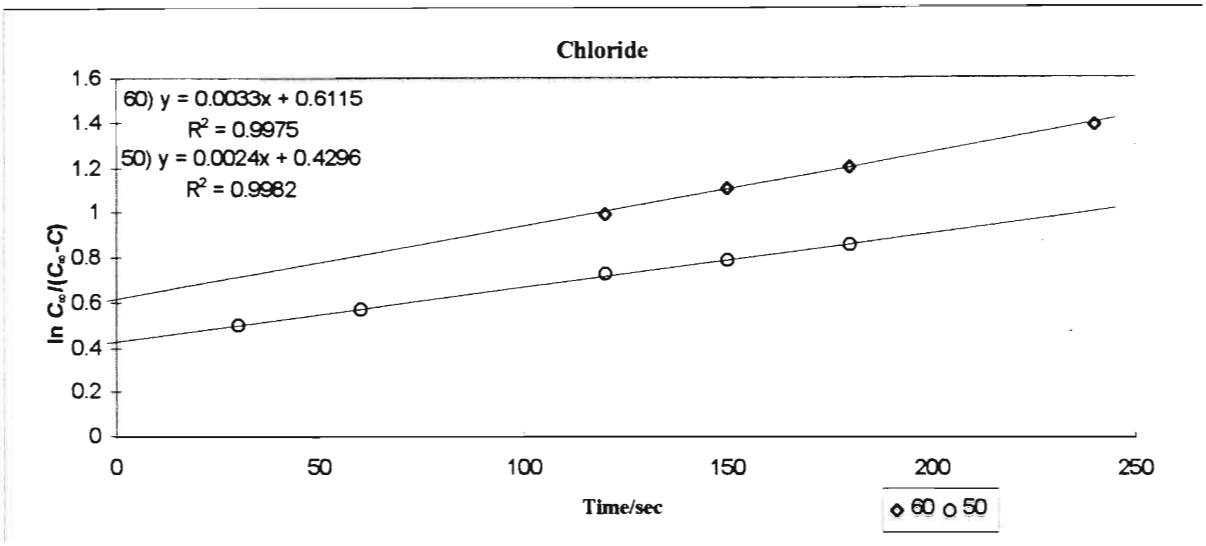

Figure 4.39 Typical kinetic plots for the chloride ion at 50° and 60° C.

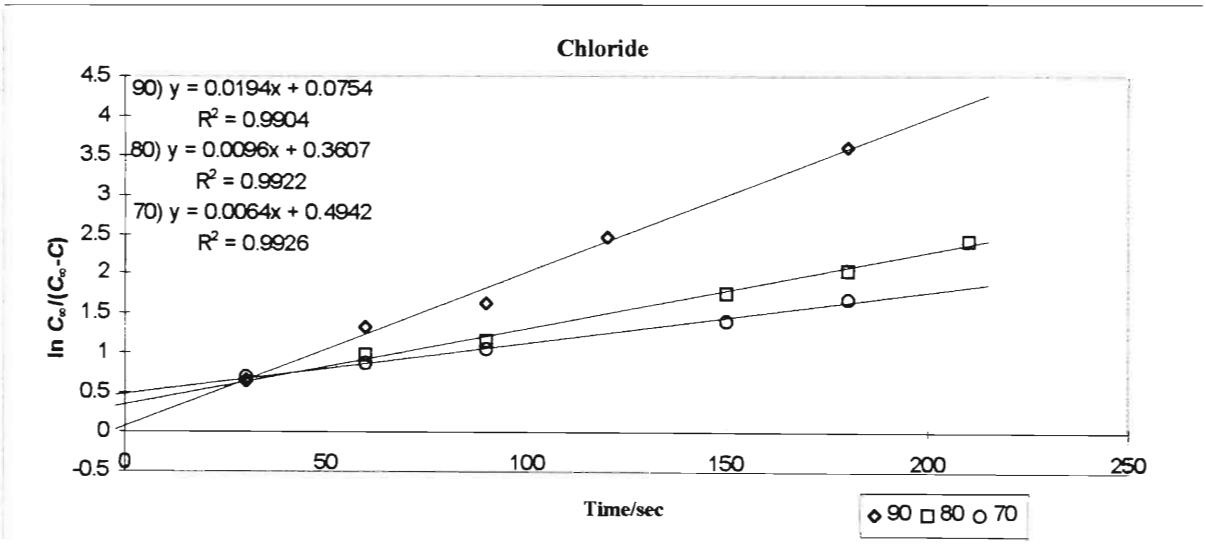

Figure 4.40 Typical kinetic plots for the chloride ion at 70°, 80° and 90°C.

Table 4.33 Observed and corrected concentrations and rate constants for the sulfate ion at various temperatures.

Temp/°C	50	60	70	80	90
Time/s	**Observed and corrected concentrations / ppm**				
0	0.00 (0.00)	0.00 (0.00)	0.00 (0.00)	0.00 (0.00)	0.00 (0.00)
30	0.75 (0.75)	0.61 (0.61)	1.60 (1.61)	2.75 (2.76)	3.41 (3.42)
60	2.65 (2.64)	2.86 (2.85)	2.60 (2.60)	3.15 (3.16)	2.66 (2.67)
90	4.50 (4.46)	3.41 (3.40)	3.80 (3.79)	4.10 (4.10)	2.91 (2.92)
120	4.85 (4.81)	3.51 (3.50)	3.85 (3.84)	3.75 (3.75)	3.86 (3.85)
150	5.65 (5.59)	3.96 (3.94)	4.20 (4.18)	5.00 (4.97)	6.51 (6.44)
180	5.20 (5.15)	3.96 (3.94)	4.35 (4.33)	5.55 (5.51)	6.61 (6.54)
210	7.65 (7.51)	4.96 (4.90)	4.65 (4.62)	5.80 (5.75)	7.51 (7.40)
240	7.50 (7.37)	4.81 (4.76)	5.10 (5.05)	5.35 (5.32)	4.86 (4.87)
5400	10.35 (10.08)	9.16 (8.91)	8.35 (8.15)	9.30 (9.08)	9.56 (9.33)
Mean values of C_∞, a and k_{obs}. Calculated values of $t_{1/2}$ and k_{eqn}.					
C_∞ / ppm	9.46 ± 0.61	8.26 ± 0.65	8.11 ± 0.04	8.93 ± 0.14	9.63 ± 0.30
a	0.39 ± 0.05	0.25 ± 0.03	0.23 ± 0.00	0.19 ± 0.02	0.02 ± 0.10
$k_{obs}/10^{-4}s^{-1}$	30.9 ±2.5	29.5 ± 2.9	32.5 ± 2.5	38.0 ± 0.7	45.3 ± 12.7
$t_{1/2}$ /s	98.4	150.6	142.0	131.5	149.1
$k_{eqn}/10^{-4}s^{-1}$	70.46	46.02	48.81	52.73	46.49

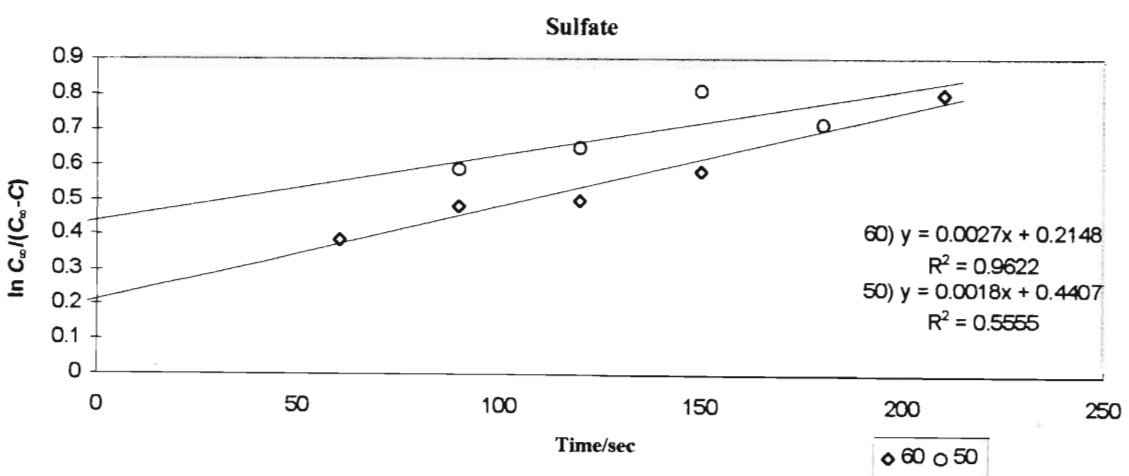

Figure 4.41 Typical kinetic plots for the sulfate ion at 50° and 60°C.

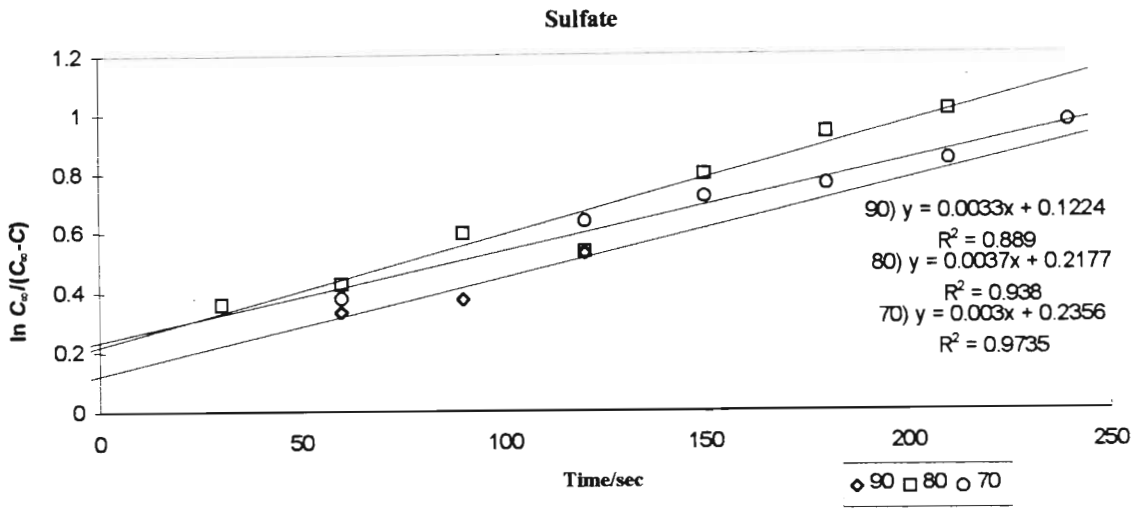

Figure 4.42 Typical kinetic plots for sulfate at 70°, 80° and 90°C.

4.4.7 Diffusion Coefficients and Hindrance Factors

It has been shown that the rate determining factor in the black tea infusion is the diffusion of soluble constituents through the swollen leaf[60]. Assuming that this is true for Rooibos Tea as well, Equation 20 can be shortened to

$$D_{leaf} = k_{obs} d^2 / 2 \qquad (22)$$

from where the effective internal diffusion coefficients can be obtained. In this equation $2d$ represents the thickness of the water-swollen leaf that is regarded as a lamina. This was found to be 0.15 ± 0.02 mm from 10 individual measurements of swollen leaves using a micrometer. In this exercise the leaf chosen for measurement was free of stalk and veins, and care was taken not to compress the leaf. Substituting the experimentally determined d value and k_{obs} values listed in Tables 4.25 - 4.33 into Equation 22, the experimental diffusion coefficient D_{leaf} was obtained for the respective species at each of the investigated temperatures. The values obtained are given in Tables 4.34 - 4.36. For the D_{leaf} values to have any meaning, they must be compared with diffusion coefficients in aqueous media, D_{aq}, calculated at the same temperature. This was possible for the ionic species only, due to the lack of relevant data for the organic compounds.

The limiting tracer diffusion coefficients, D_{aq}, for the various ionic constituents shown in Tables 4.34 – 4.36 were calculated using the Nernst-Einstein equation:

$$D_{aq} = \frac{RT\lambda^{\circ}}{|z|F^2}$$

In this equation R is the gas constant, T is the absolute temperature, and z is the ionic charge number, F is Faraday's constant and λ° is the limiting equivalent conductance of the ion at a specific temperature. The values of λ° (equiv.$^{-1}$) at the required temperature were obtained by fitting literature values[99] to quadratic equations in temperature by plotting λ° versus T (°C) using Microsoft Excel software. The equations generated are shown below in equations 43-47

$$\lambda^{\circ}(Na^{+}) = 2.540 \times 10^{-3} + 9.607 \times 10^{-5} T + 2.388 \times 10^{-7} T^2 \quad (43)$$

$$\lambda^{\circ}(K^{+}) = 4.022 \times 10^{-3} + 1.280 \times 10^{-4} T + 2.691 \times 10^{-7} T^2 \quad (44)$$

$$\lambda^{\circ}(Mg^{2+}) = 2.880 \times 10^{-3} + 8.211 \times 10^{-5} T + 5.410 \times 10^{-7} T^2 \quad (45)$$

$$\lambda^{\circ}(Cl^{-}) = 4.063 \times 10^{-3} + 1.351 \times 10^{-4} T + 3.642 \times 10^{-7} T^2 \quad (46)$$

$$\lambda^{\circ}(SO_4^{2-}) = 4.105 \times 10^{-3} + 1.358 \times 10^{-4} T + 8.318 \times 10^{-7} T^2 \quad (47)$$

The limiting conductance for $H_2PO_4^{-}$ was only available at 25°C [100], subsequently the λ° value for this ion at the required temperature was estimated from the Walden rule[99] that states

$$\eta \lambda^{\circ} = \text{constant} \quad (48)$$

where η is the viscosity of water at the required temperature. To be able to compare how different species are hindered during the infusion process, the hindrance factors (HF) for each species were determined using Equation (48).

$$HF = D_{aq} / D_{leaf} \quad (49)$$

The values for the cationic, organic and anionic species are given in Table 4.34, 4.35 and 4.36 respectively.

Table 4.34 shows that D_{leaf} values for the cations that were investigated increase in the order of $Mg^{2+} < K^{+} < Na^{+}$ between 45° and 60 °C, pass through a transitional stage at 70 °C where D_{leaf} for $Mg^{2+} < Na^{+} \approx K^{+}$, after which (80 ° and 90 °C) the trend becomes $Mg^{2+} < Na^{+} < K^{+}$. These values are much smaller than the corresponding D_{aq} values, indicating that their diffusion through the leaf matrix is a hindered process. The doubly charged Mg^{2+} ion displayed a smaller diffusion coefficeint than the other two ions, this could be due to the

larger effective hydrodynamic radius of the ion. Included in Table 4.34 are the hindrance factors (HF), these were calculated from the various diffusion coefficients before rounding them off to two significant figures. The observed trend is that the Mg^{2+} ion is least hindered followed by the Na^{+} ion and the K^{+} ion is the most hindered. A similar trend has been reported for Rose-hip tea[101], black Assam Bukial and green Chun Mee teas[98].

Table 4.34 Calculated diffusion coefficients and hindrance factors for the cations over temperature range.

Temperature °C	Species	D_{leaf} ($10^{-12} m^2 s^{-1}$)	D_{aq} ($10^{-9} m^2 s^{-1}$)	HF
45	Na^{+}	7.7	2.1	271
	K^{+}	6.6	2.9	433
	Mg^{2+}	5.2	1.1	209
50	Na^{+}	8.3	2.3	277
	K^{+}	7.1	3.2	452
	Mg^{2+}	5.7	1.2	211
60	Na^{+}	8.4	2.7	324
	K^{+}	7.8	3.8	483
	Mg^{2+}	6.4	1.5	227
70	Na^{+}	8.5	3.2	376
	K^{+}	8.5	4.4	517
	Mg^{2+}	6.6	1.7	262
80	Na^{+}	9.5	3.7	389
	K^{+}	9.8	5.0	514
	Mg^{2+}	7.1	2.0	286
90	Na^{+}	9.7	4.3	439
	K^{+}	10.0	5.7	550
	Mg^{2+}	7.7	2.4	308

All three of the investigated cations show an increase in hindrance factor with increase in temperature, as shown in Figure 4.43. This observation is contrary to what would be expected. With an increase in temperature, one would expect the binding forces between the species in question and the other compounds and or the leaf matrix to weaken allowing faster diffusion. The result of which would be the lowering of the hindrance factor values as has been reported by Jaganyi and co-workers in the case of coffee[102].

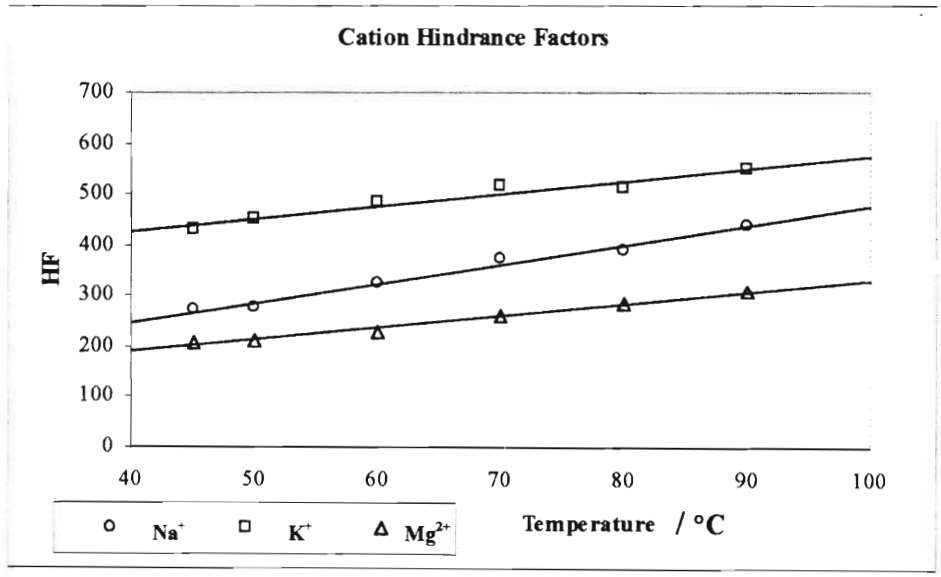

Figure 4.43 Linear increase in HF with increase in temperature for the cations.

A possible explanation of the increase in hindrance factor with temperature is that the increase in D_{leaf} is much smaller in comparison to the increase of D_{aq} with temperature. Using the Mg^{2+} ion as an example, the value for D_{leaf} increases b 48 % while the the D_{aq} value increases by 209 % over the same temperature range.

The hindrance factors of 514 and 286 for the K^+ and Mg^{2+} ions respectively in Rooibos Tea at 80 °C are much larger than those documented for other teas at the same temperature. In the case of black Assam Bukial tea the values were reported to be 255 and 202, while for the green Chun Mee tea the values were reported to be 248 and 165 respectively[98]. Much lower hindrance factors of 82 and 64 for K^+ and Mg^{2+} ions respectively were found for Rose-hip tea[101].

It was not possible to calculate the hindrance factors for the organic compounds due to the

lack of D_{aq} values. D_{leaf} values for these compounds were calculated using Equation (22) at various temperatures, and are listed in Table 4.35 At all the temperatures protocatechuic acid had the largest diffusion coefficient. At lower temperatures between 45 ° and 60 °C the D_{leaf} values for aspalathin and rutin were found to be comparable. The differences were more apparent at temperatures above 60 °C, where the value for aspalathin was 6 % larger at 70 °C increasing to16 % at 90 °C. It can be concluded that the diffusion of the organic compounds is directly related to their molecular masses. The larger the molecular mass the slower the movement of the compound through the leaf matrix.

Table 4.35 Diffusion coefficients calculated for the organic compounds for temperatures ranging from 45 ° to 90 °C.

Temperature °C	Species	D_{leaf} ($10^{-12} m^2 s^{-1}$)
45	Protocatechuic acid	5.6
	Aspalathin	4.6
	Rutin	4.4
50	Protocatechuic acid	5.8
	Aspalathin	4.6
	Rutin	4.8
60	Protocatechuic acid	6.9
	Aspalathin	5.1
	Rutin	5.2
70	Protocatechuic acid	7.4
	Aspalathin	5.2
	Rutin	4.9
80	Protocatechuic acid	8.6
	Aspalathin	6.2
	Rutin	5.6
90	Protocatechuic acid	9.1
	Aspalathin	7.3
	Rutin	6.3

Values for D_{aq}, D_{leaf} and the hindrance factors were calculated for the three anions investigated, these results are shown in Table 4.36 The D_{leaf} values are much smaller than the D_{aq} value, indicating that their diffusion out of the leaf matrix is a greatly hindered process.

Table 4.36 D_{leaf}, D_{aq} and hindrance factor values for the three anionic species investigated for temperatures ranging from 45 ° to 90 °C.

Temperature °C	Species	D_{leaf} ($10^{-12} m^2 s^{-1}$)	D_{aq} ($10^{-9} m^2 s^{-1}$)	HF
45	$H_2PO_4^-$	6.4	1.4	219
50	$H_2PO_4^-$	6.9	1.6	224
	Cl^-	7.7	3.4	437
	SO_4^{2-}	8.7	1.9	216
60	$H_2PO_4^-$	7.2	1.9	262
	Cl^-	9.2	4.0	435
	SO_4^{2-}	8.3	2.3	274
70	$H_2PO_4^-$	7.9	2.2	281
	Cl^-	18.0	4.7	260
	SO_4^{2-}	9.1	2.7	296
80	$H_2PO_4^-$	8.8	2.6	297
	Cl^-	31.6	5.4	172
	SO_4^{2-}	11.0	3.2	300
90	$H_2PO_4^-$	9.5	3.0	319
	Cl^-	55.6	6.2	112
	SO_4^{2-}	12.7	3.7	294

The order of the D_{leaf} values at 50 °C is $H_2PO_4^- < Cl^- < SO_4^{2-}$. At temperatures of 60 °C and above the order changes to $H_2PO_4^- < SO_4^{2-} < Cl^-$. It is also observed that the increase in the D_{leaf} value for $H_2PO_4^-$ and SO_4^{2-} over the temperature range is only 38 % and 46 % respectively when compared to 622 % by the Cl^- ion. The outcome of this is that the

hindrance factors calculated for the $H_2PO_4^-$ and SO_4^{2-} ions show an increase with temperature. Hindrance factors for the Cl^- ion however decrease linearly with temperature. The hindrance factor versus temperature relationship is indicated in Figure 4.44 From results obtained at 80 °C, it is observed that the hindrance factors for the $H_2PO_4^-$ and SO_4^{2-} ions are of the same magnitude and are almost twice the value for the Cl^- ion. This indicates that the Cl^- ion is less hindered when compared to the other two ions.

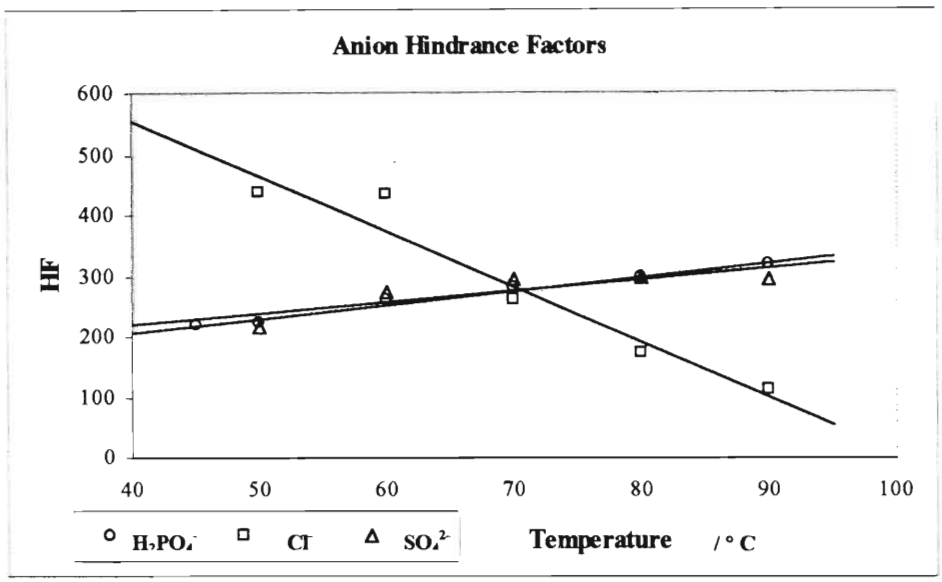

Figure 4.44 Hindrance factor trends for the three anionic species investigated for temperatures ranging from 45 ° to 90 °C. The Cl^- ion alone shows a decrease in hindrance factor with an increase in temperature.

The hindrance factors for the anions investigated were found to range between 3 and 10 times the size of those for the $H_2PO_4^-$ and SO_4^{2-} ions, when compared with the values for Rose-hip, black Assam Bukial and green Chun Mee teas. In the case of the Cl^- ion, the value for Rooibos Tea was 1.5 times that for the black tea and almost twice as big as that for the green tea. This shows that the diffusion of these three anionic species is slower and significantly more hindered in Rooibos Tea than in the Rose-hip, black Assam Bukial and green Chun Mee teas.

Generally all the constituents monitored, except for Cl^-, showed very similar diffusion coefficients. The results show that for the constituents with charge numbers ranging from –2

to +2 there was no significant difference in their rate of migration through the leaf matrix. It is striking that even the much larger bulky organic compounds, from polar to non-polar, infused at very similar rates to the smaller anions and cations. This could mean that the cations and anions are complexed to organic molecules. On the whole it appears that the anions diffuse fastest through the tea leaf, followed by the cations and then by the organic components of Rooibos Tea.

The hindrance factors range from 112 to 550 across all the anions and cations. It is interesting that the smallest and greatest HFs are derived from Cl^- and K^+ ions respectively, both having very similar D_{aq} values and hence similar hydrated radii. This suggests that the K^+ ion is possibly held back by attraction to negative charges within the leaf matrix. It is difficult to distinguish between anionic and cationic hindrance factors with the cationic hindrance factors being only marginally larger than those of the anions for any given temperature. Similarly at 80 °C the average hindrance factor for the cations has been found to be greater than that for the anions in Rose-hip[98], black Assam Bukial and Green Chun Mee teas[98]. This infers a more torturous passage for cations than for anions within the leaves, which can possibly be attributed to the matrix of the leaf itself being more entrapping to positively charged species than to negatively charged ones.

4.4.8 Determination of Activation Energy

The Arrhenius equation

$$\frac{-d\ln(k)}{d\left(\frac{1}{T}\right)} = \frac{E_a}{R} \qquad (50)$$

was used to determine the activation energy by plotting – ln k against $1/T$ (K) where k represents the rate constant and T the temperature. Both the observed rate constant k_{obs} and the rate constant calculated by setting the intercept equal to zero $k_{eqn,}$ were substituted into this equation and plotted. The slopes of the lines were obtained using Microsoft Excel software, these were multiplied by R (8.314 $JK^{-1}mol^{-1}$) the gas constant to give the required activation energy Ea values. Two Arrhenius plots were done for each species, one denoted

(obs) and the other (eqn), making use of k_{obs} and k_{eqn} respectively to produce Ea_{obs} and Ea_{eqn} values in each case. Assuming that the rate-limiting factor in the infusion process is the diffusion through the swollen leaf, expected activation energies can be calculated using diffusion coefficients for each species in aqueous media D_{aq}. To obtain the theoretical activation energies (Ea_{cal}) for ionic species, plots of – ln (D_{aq}) against $1/T$ (K) were drawn and the slope used to determine the activation energy. A typical graph for sodium is illustrated in Figure 4.45 The plots for the cations are illustrated in Figures 4.46 to 4.48, and the calculated activation energies are summarised in Table 4.37

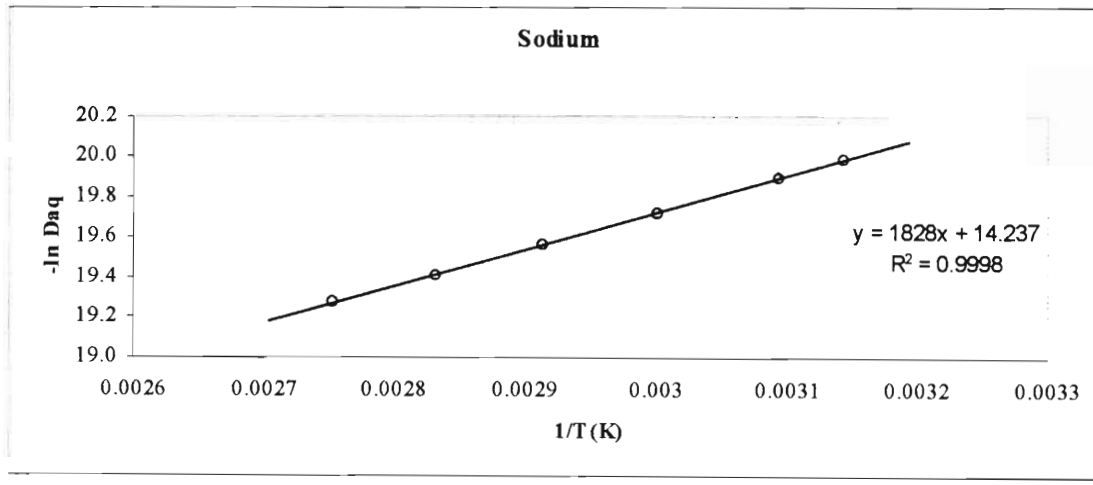

Figure 4.45 A plot of – ln D_{aq} versus $1/T$ for the determination of the theoretically expected activation energy for sodium.

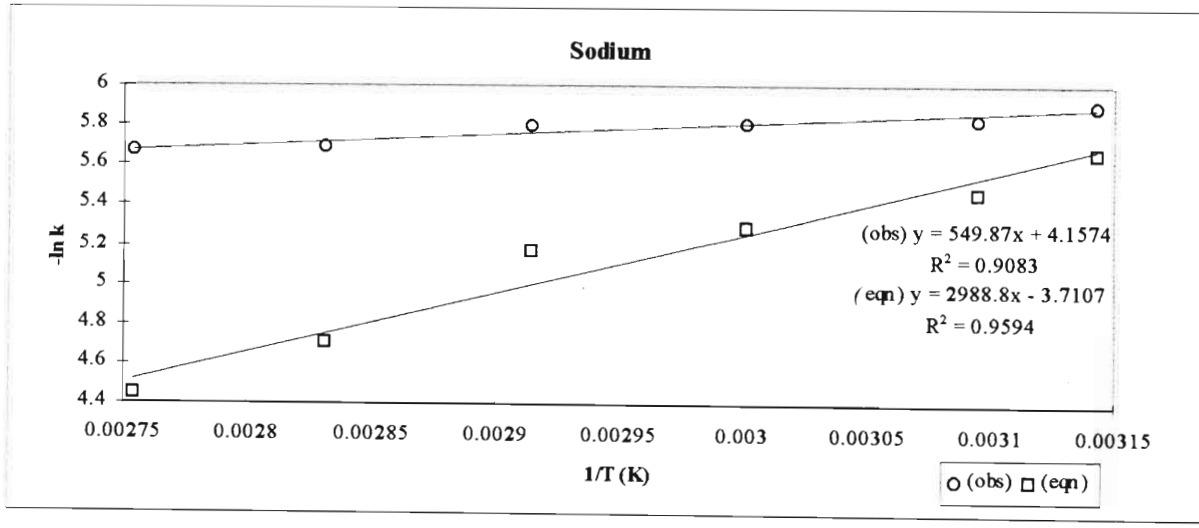

Figure 4.46 The Arrhenius plot of –ln k versus $1/T$ for sodium using both k_{obs} (denoted (obs) in the graph) and k_{eqn} (denoted (eqn) in the graph), to give values for Ea_{obs} and Ea_{eqn} respectively.

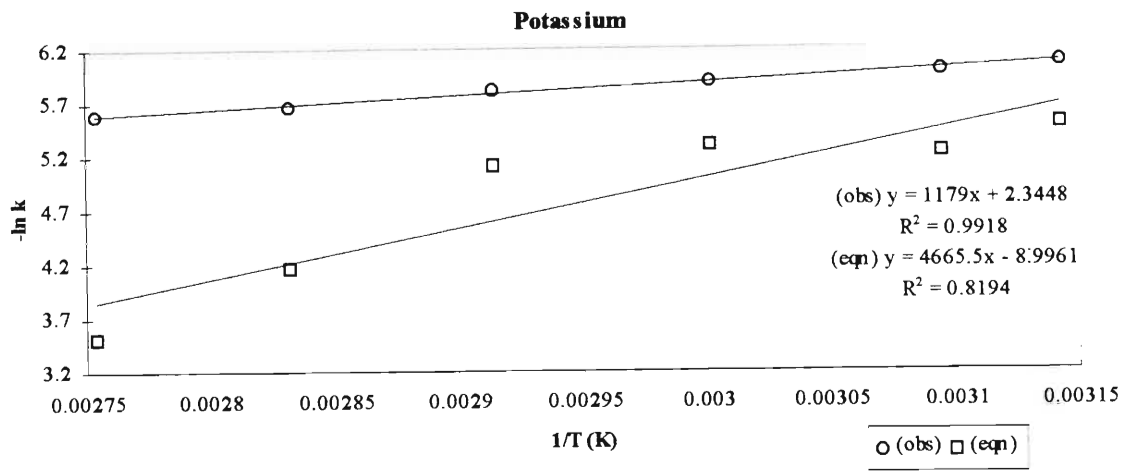

Figure 4.47 The Arrhenius plot of $-\ln k$ versus $1/T$ for potassium using both k_{obs} and k_{eqn} to give the values for Ea_{obs} and Ea_{eqn} respectively.

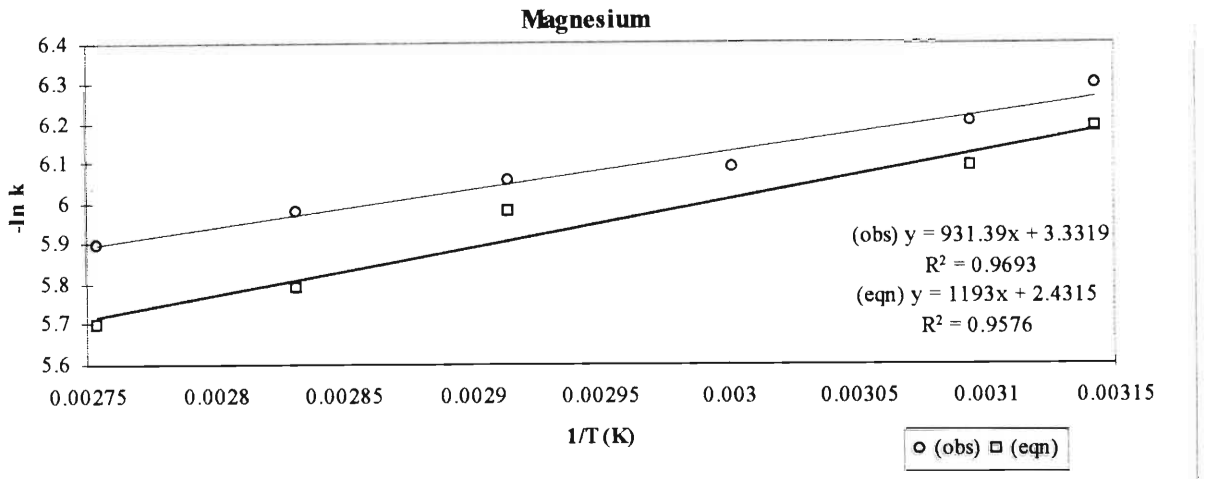

Figure 4.48 The Arrhenius plot of $-\ln k$ versus $1/T$ for magnesium using both k_{obs} and k_{eqn} to give the values for Ea_{obs} and Ea_{eqn} respectively.

Table 4.37 Three different activation energies are presented for the investigated cationic species within Rooibos Tea. Values calculated from k_{obs} (Ea_{obs}), those calculated setting the rate constant (a) equal to zero *i.e.* from k_{eqn} (Ea_{eqn}) and the theoretical values (Ea_{cal}) obtained from diffusion data representing the activation energies required for diffusion in aqueous media.

Cations			
Species	**Ea_{obs} / kJ mol^{-1}**	**Ea_{eqn} / kJ mol^{-1}**	**Ea_{cal} / kJ mol^{-1}**
Na^+	4.6 ± 0.7	24.8 ± 2.6	15.2 ± 0.1
K^+	9.8 ± 0.4	38.8 ± 9.1	14.3 ± 0.1
Mg^{2+}	7.7 ± 0.7	9.9 ± 1.2	16.6 ± 0.0

To determine the theoretical expected activation energy for the organic components it was assumed that the rate constants k_{obs} and k_{eqn} were directly proportional to the diffusion coefficient (D) of the species. This allowed for the use of the Stokes-Einstein equation:

$$D = \frac{kT}{6\pi\eta r} \qquad (51)$$

In this equation k represents the Boltzmann constant, T the absolute temperature, r the effective radius of the solute and η the viscosity of water at the temperature of infusion assuming that the liquor is very dilute. If r is independent of temperature, the rate constant becomes proportional to T/η. This gives rise to an expression relating rate constants, diffusion coefficients, absolute temperature and viscosity. The relationship is described below with subscripts denoting the temperatures in °C. The viscosity data were obtained from literature[99].

$$\frac{k_{90}}{k_{50}} = \frac{D_{90}}{D_{50}} = \left(\frac{T_{90}}{T_{50}} \times \frac{\eta_{50}}{\eta_{90}}\right)$$

$$= \frac{363.15}{323.15} \times \frac{0.5467}{0.3156}$$

$$= 1.9467$$

The ratio obtained was then substituted into an Arrhenius equation

$$\ln 1.9467 = \frac{Ea}{8.314}\left(\frac{1}{323.15} - \frac{1}{363.15}\right)$$

to give $Ea = 16.2$ kJ mol^{-1}

The Arrhenius plots for the three organic compounds investigated are shown in Figures 4. 49 to 4.51. The experimental activation energies Ea_{obs} and Ea_{eqn} obtained from k_{obs} and k_{eqn} including the theoretical values are given in Table 4.38.

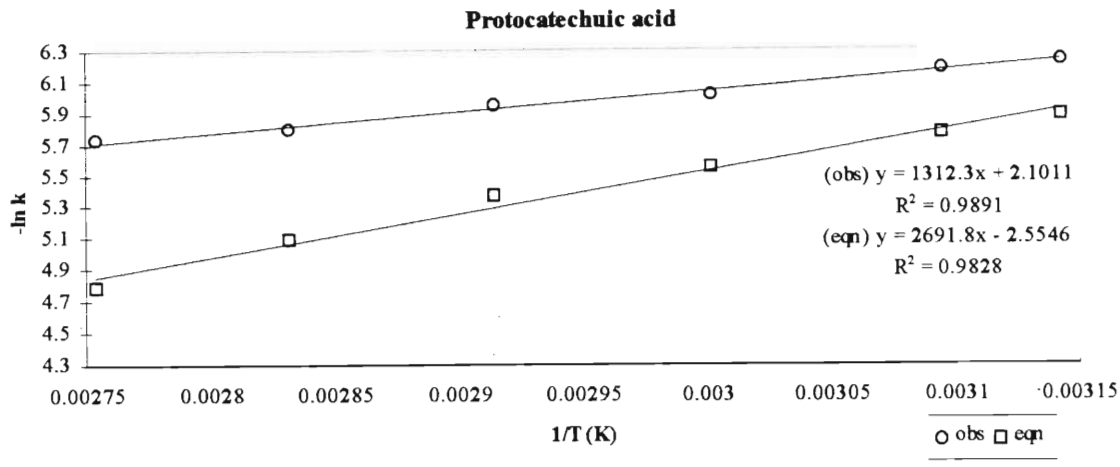

Figure 4.49 The Arrhenius plot of $-\ln k$ versus $1/T$ for protocatechuic acid using both k_{obs} and k_{eqn} to give the values for Ea_{obs} and Ea_{eqn} respectively.

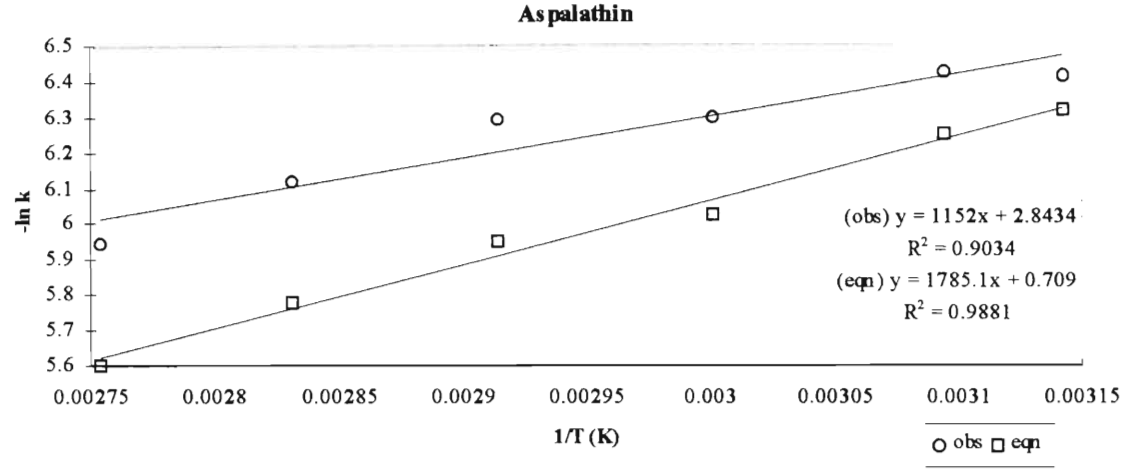

Figure 4.50 The Arrhenius plot of $-\ln k$ versus $1/T$ for aspalathin using both k_{obs} and k_{eqn} to give the values for Ea_{obs} and Ea_{eqn} respectively.

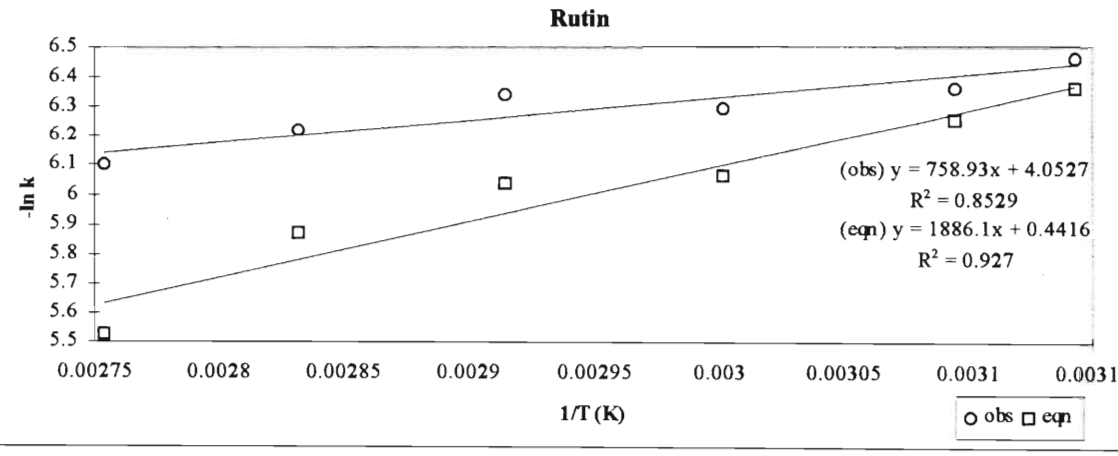

Figure 4.51 The Arrhenius plot of $-\ln k$ versus $1/T$ for rutin using both k_{obs} and k_{eqn} to give the values for Ea_{obs} and Ea_{eqn} respectively.

Table 4.38 Three different activation energies are presented for the investigated organic species within Rooibos Tea. Values calculated from k_{obs} (Ea_{obs}), those calculated setting the rate constant (a) equal to zero *i.e.* from k_{eqn} (Ea_{eqn}) and the theoretical values (Ea_{cal}) obtained from diffusion data representing the activation energies required for diffusion in aqueous media.

Organics			
Species	Ea_{obs} / kJ mol^{-1}	Ea_{eqn} / kJ mol^{-1}	Ea_{cal} / kJ mol^{-1}
Protocatechuic acid	10.8 ± 0.5	22.4 ± 1.5	16.2
Aspalathin	11.3 ± 0.9	14.8 ± 0.8	16.2
Rutin	6.3 ± 1.3	15.7 ± 2.2	16.2

The experimental as well as the theoretical activation energies for the studied anionic species within Rooibos Tea were determined in the same way as for the cationic species. The respective Arrhenius plots for the $H_2PO_4^-$ (as P), Cl^- and SO_4^{2-} ions are shown in Figures 4.52 to 4.54. Table 4.39 summarises the activation energies obtained.

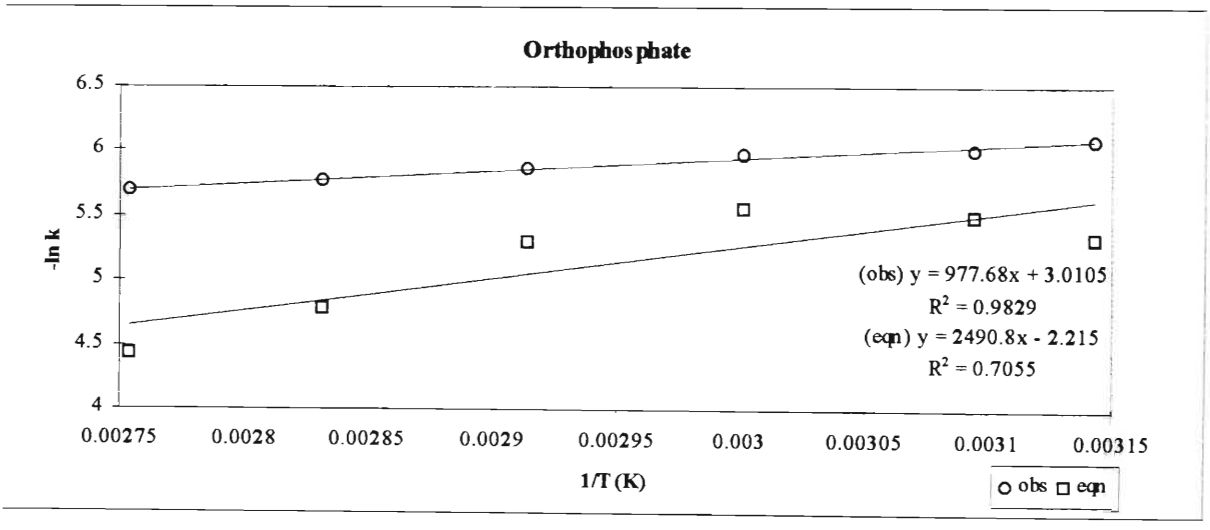

Figure 4.52 The Arrhenius plot of –ln k versus $1/T$ for the orthophosphate ion using both k_{obs} and k_{eqn} to give the values for Ea_{obs} and Ea_{eqn} respectively.

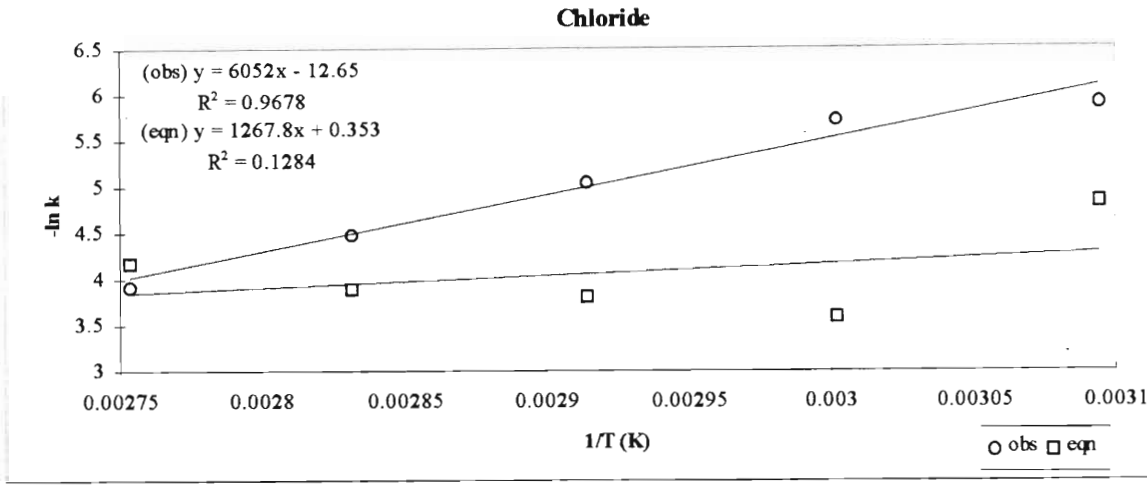

Figure 4.53 The Arrhenius plot of $-\ln k$ versus $1/T$ for the chloride ion using both k_{obs} and k_{eqn} to give the values for Ea_{obs} and Ea_{eqn} respectively.

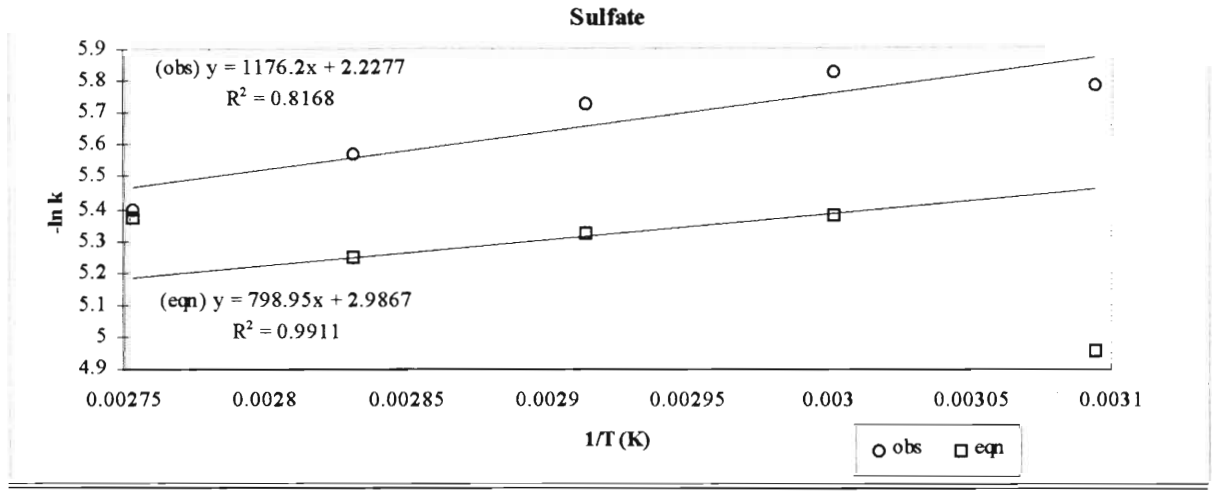

Figure 4.54 The Arrhenius plot of $-\ln k$ versus $1/T$ for the sulfate ion using both k_{obs} and k_{eqn} to give the values for Ea_{obs} and Ea_{eqn} respectively.

Table 4.39 Three different activation energies are presented for the investigated anions in Rooibos Tea. Values calculated from k_{obs} (Ea_{obs}), those calculated setting the rate constant (a) equal to zero *i.e.* from k_{eqn} (Ea_{eqn}) and the theoretical values (Ea_{cal}) obtained from diffusion data representing the activation energies required for diffusion in aqueous media.

Anions			
Species	**Ea_{obs} / kJ mol^{-1}**	**Ea_{eqn} / kJ mol^{-1}**	**Ea_{cal} / kJ mol^{-1}**
$H_2PO_4^-$	8.1 ± 0.5	20.7 ± 6.7	16.3 ± 0.1
Cl^-	50.3 ± 5.3	10.5 ± 15.9	14.8 ± 0.1
SO_4^{2-}	9.8 ± 2.7	6.6 ± 0.6	16.9 ± 0.1

From Table 4.37 it is evident that the Ea_{obs} values for the cations are lower than the values predicted by the Stokes-Einstein relationship (Ea_{cal}). The same phenomenon is found with the organics and the anionic species, except for the Cl^- ion. The values obtained using the intercept-corrected method (Ea_{eqn}) are slightly larger than the theoretical values in most cases, as can be seen in Tables 4.37 –4.39. One would expect the activation energies for the diffusion of the various species to be larger than the theoretical values since $D_{aq} >> D_{leaf}$. This discrepancy could be attributed to the large intercept values encountered while calculating the rate constants as indicated by Price and Spitzer[95].

Activation energies for the cations range from approximately 5 to 10 kJ mol^{-1} as indicated in Table 4.37. The K^+ ion has an activation energy value twice that of the Na^+ ion, with Mg^{2+} about mid-way between them.

Activation energies for the organic compounds range between approximately 6 to 11 kJ mol^{-1} as indicated in Table 4.38 If the activation energies were related to molecular weight, one would expect protocatechuic acid to have the smallest activation energy, followed by aspalathin and then by rutin. No such trend is observed. It is therefore clear that the activation energies of these compounds are influenced by the respective polarities, as was found with the determination of the D_{leaf} values. The polarity of protocatechuic acid and aspalathin are similar, while that of rutin is much lower. This is supported by the different retention times as found on the HPLC in conjunction with the gradient elution profile as described in Figure 3.9. Activation energies for these organics show a similar trend with aspalathin and protocatechuic acid having similar activation energies while that of rutin is much lower, indicating that protocatechuic acid and aspalathin experience stronger forces of attraction within the leaf matrix in comparison to rutin. Using these results it can be concluded that the hindrance factors for protocatechuic acid and aspalathin will be very similar, and larger than that for rutin.

Activation energies for the anions range from approximately 8 to 50 kJ mol^{-1}, with the Cl^- ion value almost 5 times that of the $H_2PO_4^-$ and SO_4^{2-} ions.

In general, the activation energies for the cations and anions were independent of charge. Similar findings have been observed by Spiro and Lam[98]. Excluding the Cl^- ion, activation energies for the cationic, organic and anionic species are all very similar.

4.4.9 Conclusion

Rooibos Tea was ashed and analysed for mineral content making use of Inductively Coupled Plasma-Optical Emission Spectroscopy. The following mineral ions were detected in Rooibos Tea in order of decreasing concentration: Na, K, Mg, Ca, P, Al, Fe, Mn, Sr, Zn, Ba, Cu and Pb. The only cations that displayed first order behaviour during tea infusion, as interpreted using steady state theory, were the Na^+, K^+, and Mg^{2+} ions. Rooibos Tea infusions were also analysed using High Pressure Liquid Chromatography. A unique gradient elution profile was developed for the tea analyses. Three of the many peaks were identified to be protocatechuic acid, aspalathin and rutin and these also displayed first order kinetics during infusion. Ion Chromatography was employed to monitor chloride and sulfate ion levels during infusion, and these also behaved in a first order manner.

Partition coefficients for all the mineral ions and the organic compounds were determined using various methods for infusions at 80 °C. The graphical, successive extraction and total mineral content methods were used for the cations and anions excluding the Cl^- and SO_4^{2-} ions, whilst only the former two could be used for the organic compounds. The graphical method proved unreliable due to the large irreproducible and sometimes negative intercepts that were encountered as found with Rose-hips tea[91]. Values for the total mineral ion concentrations within the tea leaf obtained using the graphical method, differed by 10 – 34 % from those obtained after ashing the leaf and using the ICP-OES directly. The successive extraction method produced reproducible and realistic partition coefficients for all the components investigated, excluding the Cl^- ion that showed significant variations. Values ranged from 1.47 in the case of K^+ to 0.079 for Cl^-. Partition coefficients determined using the total mineral content method compared favourably with those determined using the

former method, all being slightly higher except for in the case of the Mg^{2+} ion, ranging from 0.390 to 1.960 for Ca^{2+} and K^{+} respectively.

Investigations performed at 80 °C allowed the determination of the infusion rate constants for the components of Rooibos Tea displaying first order behaviour. There is no marked difference between values for the cations, organics or anions. Rate constant values for all the species ranged from 2.2 x 10^{-3} s^{-1} to 3.8 x 10^{-3} s^{-1}, except in the case of the Cl^{-} ion which gave a value of 11.2 x 10^{-3} s^{-1}. Rate constants increased in the order of rutin, aspalathin, Mg^{2+}, protocatechuic acid, $H_2PO_4^{-}$, K^{+}, Na^{+}, SO_4^{2-} and Cl^{-}. The effect of the partition coefficients on the rate constants was evaluated, and it was found that differences between the observed and corrected rate constants ranged from 1.2 to 10.6 %. All rate constants were subsequently given as the uncorrected k_{obs} values. Equilibrium concentrations within the tea liquor during these infusion experiments ranged from 3.17 to 50.21 ppm increasing in the order of $H_2PO_4^{-}$, protocatechuic acid, SO_4^{2-}, Mg^{2+}, aspalathin, K^{+}, Na^{+}, rutin and Cl^{-}.

Also investigated at 80 °C was the particle size effect on the infusion rate constants. This was done by determining the rate constants for the various components from tea infusions made from varying tea leaf sieving sizes. Particle sizes investigated were from 0.250 – 0.425, 0.425 – 0.60, 0.60 – 0.85, 0.85 – 1.00 and 1.00 – 1.40 mm sieved fractions. The rate constants for the cations and $H_2PO_4^{-}$ increased with decreasing particle size. No real trend was evident for the protocatechuic acid and aspalathin, while rate constants for rutin were independent of particle size. Significant uptake of calcium by the leaf matrix was found, which was accentuated with the smaller particle sizes.

Large irreproducible intercepts were often encountered during the determination of the rate constants, these intercepts showed no apparent trend. The intercepts are related to the rate of uptake of water by the leaf, the leaf structure and the rapid loss of solubles that coat the surfaces during the manufacturing process. These intercepts are considered by Price and Spitzer[95] to be indicative of the quality of the data obtained, and to highlight deviations from the model employed by the theory.

The temperature dependence of the infusion rate constants of the nine mentioned species was then investigated across a temperature range of 45 – 90 °C. In each case rate constants increased with an increase in temperature. Diffusion coefficients, hindrance factors and activation energies were calculated for the respective components from this data. The diffusion coefficients (D_{leaf}) were calculated once the thickness of the swollen tea leaf was obtained (0.15 ± 0.02 mm). There are no major differences between the values of D_{leaf} for the cations, organics and anions, with values ranging from 5.6 x 10^{-12} m^2s^{-1} to 31.6 x 10^{-12} m^2s^{-1} at 80 °C. Diffusion coefficients in aqueous media (D_{aq}) were also calculated and used with the D_{leaf} values to calculate the hindrance factors for the cations and anions. No hindrance factors could be obtained for the organic compounds, since D_{aq} values for the various organic compounds could not be determined. Hindrance factors for the cations and anions ranged from 172 to 514 increasing in the order of Cl^-, Mg^{2+}, $H_2PO_4^-$, SO_4^{2-}, Na^+ and K^+ for the ions at 80 °C. Both D_{leaf} and D_{aq} values increased with increasing temperature, as well as hindrance factors for all the components except for the Cl^- ion. The increase in hindrance factor with temperature could be attributed to a smaller increase in D_{leaf} with temperature than that calculated for D_{aq} with temperature. On comparison of Rooibos Tea hindrance factors obtained at 80 °C with literature values for the various ions, those obtained for Rooibos Tea are about twice those of black Assam Bukial tea and those for Green Chun Mee[98] teas, and about 7 times larger than for Rose-hip tea[101]. In other words the passage for the same ions within Rooibos Tea is significantly more hindered than in other teas, this may be linked to the different tea leaf matrices and or the manufacturing processes. The generally high hindrance factors found for Rooibos Tea indicate that the diffusion of the various species through the leaf is a greatly hindered process. The origin of this is principally the torturous passage of the soluble species through the internal structure of the leaf as discussed by Spiro, Kandiah and Toumi[103].

Substituting the infusion rate constant values obtained at the various temperatures into the Arrhenius equation, the activation energies of infusion (Ea_{obs}) were calculated for the nine species. These were lower than the theoretically expected activation energies (Ea_{cal}). Using

intercept corrected rate constants in the Arrhenius plots gave Ea_{eqn} values that were higher than the Ea_{cal} values in some instances. It was found that activation energies for the cations and anions were independent of charge, and showed no real trend. Generally the Ea_{obs} values were very similar, except for the Cl^- ion which was about five times the next largest value. The activation energies for the organic compounds were similar to those of the cations and anions. It was apparent that the activation energy of infusion for the organic compounds was related to their respective polarities, with protocatechuic acid and aspalathin having similar polarities and activation energies, while rutin showed much lower values in each case. The observed activation energy values ranged from 4.6 to 50.3 kJ mol^{-1} increasing in the order of Na^+, rutin, Mg^{2+}, $H_2PO_4^-$, K^+, SO_4^{2-}, protocatechuic acid, aspalathin and Cl^-.

The significance of the work done in this research is manifested mainly in the commercial application of the results found. The difference in temperature dependence of the infusion of various constituents as seen with the different activation energy values, although small, could be used in isolation of these constituents. Isolation could possibly be achieved using a flow counter-current technique as described by Price and Spitzer[95] for preferential extraction of flavanols from Japanese green teas. This would be useful especially for aspalathin due to its much sought after antioxidative properties as described in Chapter 1, as well as the other antioxidants within Rooibos Tea.

REFERENCES

1. Rooibos Tea Information Brochure as supplied by Rooibos Ltd., 64 Rooibos Ave, Clanwilliam, South Africa, 8135.
2. R. Dahlgren, *Bot. Notiser*, 1968, **121**, 165.
3. J.F. Morton, *Econ. Bot.*, 1983, **37**, 164
4. M.E. Komaitis, "Off-flavours in Foods and Beverages", ed. G. Charalambous, Elsevier Science Publishers, Amsterdam, 1992, 417.
5. E. Joubert, *Food Chemistry*, 1996, **55**, 403.
6. B.H. Koeppen and D.G. Roux, *Biochem. J.*, 1966, **99**, 604.
7. M. Berg, Private communication, Rooibos Tea Board, 64 Rooibos Ave., Clanwilliam, South Africa, 8135.
8. D. Ferreira, E. Joubert, C. Marais and J.A. Steenkamp, "Rooibos Tea as a Likely Health Food Supplement", *Recent Developments of Technologies on Fundemental Foods for Health (Congress Proceedings 30-06-1995, Seoul). Under auspices of Korean Society of Food Science and Technology.*
9. A. von Gadow, E. Joubert and C.F. Hansmann, *Food Chemistry*, **60**, 1997, 73.
10. T. Yoshikawa, Y. Naito, H. Oyamada, S. Ueda, S. Tanigawa, T. Takemura, S. Sugino and M. Kondo, "Antioxidants in Therapy and Preventative Medicine", Edn 1. Emeril, Plenum Press, New York, 1990, 171.
11. A. Ito, K. Shinohara and K. Kator, "Proceedings of the International Symposium on Tea Science", The Organizing Committee of ISTS, Shizuoka, 1991, 381.
12. M. Khono, M. Yamada, K. Mitsuta, Y. Mizuta and T.Yoshikawa, *Bull. Chem. Soc., Jpn.*, 1991, **64**, 1447.
13. R.A. Larson, *Phytochemistry*, 1988, **27**, 969.
14. C.W.W. Beecher, .R. Farnsworth and C Gyllenhaal, "Natural Products of Woody Plants II", ed. J.W. Rowe, Springer-Verlag, Berlin, 1989, 1070.
15. S.N. Onyeneho and N.S. Hettiarachy, *J. Agric. Food Chem.*, 1992, **40**, 1496.
16. T. Eklund *Int. J. Food Microbiol.* 1985, **2**, 159
17. L.V. Bui and C. Cooper, *J. Assoc. Off. Analyt. Chem.*, 1987, **70**, 892.

18. C. Rabe, J.A. Steenkamp, E. Joubert, J.F.W. Burger and D. Ferreira, *Phytochemistry*, 1994, **35**, 1559.

19. S. Shibata, M. Harada and W. Budidarmu, *Yakugaku Zasshi*, 1960, **80**, 620.

20. F.O. Snyckers and G. Salemi, *J. South African Chem. Inst.*, 1974, **27**, 5.

21. K. Herrman, *J. Food Tech.*, 1976, **11** , 433.

22. S.D. Varma, "Plant Flavonoids in Biology and Medicine", eds. V. Cody, E. Middleton, J.B. Harborne, Alan R. Liss Inc., New York, 1986 ,343.

23. B.H. Koeppen and D.G. Roux, *Biochem. J.*, 1965, **97**, 444.

24. M. Jay, "The Flavonoids- Advances in Research since 1986", ed. J.B. Harborne, Chapman and Hall, London, 1994, 57.

25. A. Arnoldi, A. Bassoli, L. Merlini and E. Ragg, *J. Chem. Perkin Trans.II*, 1991, 1399.

26. W.E. Hillis and T. Inous, *Phytochemistry*, 1967, **6**, 59.

27. S.S. Marais, C. Marais, J.A. Steenkamp, E. Malan and D. Ferreira, "Frank Warren Conference of Organic Chemistry 1997", Poster Session A : Progress in the Investigation of Rooibos Tea Extractives.

28. T. Habu, R.A. Flath, T.R. Mod and J.F. Morton, *J. Agric. Food Chem.*, 1985, **33**,249.

29. L.J. Porter and R.W. Hemingway, "Natural Products of Woody Plants II", ed. J.W. Rowe, Springer-Verlag, Berlin, 1989, 988.

30. L. Chalker-Scott and R.L. Krahmer, "Chemistry and Significance of Condensed Tannins", eds. R.W. Hemingway, J.J. Karchesy, Plenum Press, New York, 1989, 345.

31. F. Petereit, H. Koloziej and A. Nahrstedt, *Phytochemistry*, 1991, **30**, 981.

32. M. J. Berridge, *Nature*, 1993, 315.

33. B. Halliwell and J.M.C. Gutteridge, C.E. Cross, *J. Lab. Clin. Med.*, 1992, 598.

34. B.M.O. Becroft, *New Engl. J. Med.*, 1984, **310**, 133.

35. D.G. Roux and D. Ferreira, *Phytochemistry*, 1974, **13**, 2039.

36. R. Montgomery, T. W. Conway and A.A. Spector, "Biochemistry: A Case-Oriented Approach.", 5th Edn, The C.V. Mosby Company, 1990, 26.

37. L.K. Mahan and S. Escott-Stump "Krause's Food Nutrition and Diet Therapy", 9th Edn, W.B. Saunders Company, 1996, 129.

38. L. Cohen and R. Kitzes, *Isr. J. Med. Sci.*, 1981, **17**, 1123.

39. R. Medalle, C. Waterhouse and T.J. Hahn, *Am. J. Clin. Nutr.*,1971, **29**, 854.

40. A.R. Gaby and J. V. Wright, *J. Nutr. Med.*, 1990, **1**, 63.

41. M. J. Thomas, *Crit. Rev. Food Sci. Nutr.*, 1995, **35**, 21.

42. M. Namiki, *Crit. Rev. Food Sci. Nutr.*, 1990, **29**, 273.

43. B. Halliwell, *FASEB J.*, 1987, **1**, 358.

44. B. Halliwell, M.A. Murcia, S. Chirico and O.O. Aruoma, *Crit. Rev. Food Sci. Nutr.*, 1995, **35**, 7.

45. R.S. Sohal, L. Arnold and W.C. Orr, *Drosophila melanogaster. Mech. Ageing Dev.*, 1990, **56**, 223.

46. M.N.H. Golden and D. Ramdath, *Pro. Nutr. Soc.*, 1987, **46**, 53.

47. W.L. Porter, "Autooxidation in Food and Biological Systems", eds, M.G. Simic, M. Karel, Plenum Press, London, 1990, 295.

48. P. Bermond," Food Antioxidants", ed. B.J.F. Hudson, Elsevier Applied Science, London, 1990, 193.

49. L.R. Dugan, "Autooxidation in Food and Biological Systems", eds, M.G. Simic, M. Karel, Plenum Press, London, 1990, 293.

50. E.A.H. Roberts and R.F. Smith, *J. Sci. Food Agric.*, 1963, **14**, 689.

51. D.D. Pratt and B.J.F. Hudson, "Food Antioxidants", ed. B.J.F. Hudson, Elsevier Applied Science, London, 1990, 171.

52. H. Ogawaram, T. Akiyama, S. Watanable, N. Ito, M. Kobori and Y. Seoda. *J. Antibiot.*, XLII, 1989, 340.

53. S.R. Husain, J. Cillard and P.Cillard, *Phytochemistry*, 1987, **26**, 2489.

54. J. Torel, J. Cillard and P.Cillard, *Phytochemistry*, 1986, **25**, 383.

55. B.J.F. Hudson and J.I. Lewis, *Food Chem.* 1983, **10**, 47.

56. Y. Sorata, U. Takahama and M. Kimura, *Biochim. Biophys. Acta*, 1984, 313.

57. M.G. L. Hertog, P.C.H. Hollman, M.B. Katan, E.J.M. Feskens and D. Kormhout, *Voeding*, 1994, **55**, 23.

58. C. Tournaire, M. Hocquaux, I. Beck, E. Oliveros and M-T. Mauretta, *Tetrahedron*, 1994, **50**, 9303.

59. A. Vongadow, E. Joubert and C.F. Hansmann, *J. Agric. Food Chem.*, 1997, **45**, 632.

60. M Spiro and D.S. Jago, *J. Chem. Soc. Faraday Trans. I*, 1982, **78**, 25.

61. V.D. Long, *J. Food Tecnol.*, 1978, **13**, 195.

62. M. Spiro and S. Siddique, *J. Sci. Food Agric.*, 1981, **32**, 1135.

63. W.J. Albery, A.M. Couper, J. Hardgraft and C.Ryan, *J. Chem. Soc. Faraday Trans. I*, 1974, **70**, 1124.

64. J.H. Petropoulos and P.P. Roussis, *J. Chem. Phys.*, 1967, **47**, 1491.

65. W.E. Price, Ph.D. Thesis, University of London, 1985, 125.

66. M. Spiro and R.Selwood, *J. Sci. Food Agric.*, 1984, **35**, 915.

67. A. Mincher and S. Minkev, *Farmatsilia (Sofia)*, 1982, **32**, 28.

68. M. Spiro and S. Siddique, *J. Sci. Food Agric.*, 1981, **32**, 1027.

69. R. Bock (Translated by I. L. Marr),"A Handbook of Decomposition Methods in Analytical Chemistry", International Textbook Company, 1979.

70.T.Takeo, *JARQ*, 1985, **19**, 34.

71. H.H. Willard, L.L. Merrit Jr, J.A. Dean and F.A. Settle Jr. "Instrumental Methods of Analysis.", Edn 7, Wadsworth Publishing Company, 1988, 284.

72. H.H. Willard, L.L. Merrit Jr, J.A. Dean and F.A. Settle Jr. "Instrumental Methods of Analysis.", Edn 7, Wadsworth Publishing Company, 1988, 228.

73. The U-5000AT+ Ultrasonic Nebulizer Operator's Manual, 1994.

74. D.A. Skoog, D.M. West and F.J.Holler, "Fundamentals of Analytical Chemistry.", Edn 6, Saunders Publishing Company, 1992, 635.

75. D.A. Skoog, D.M. West and F.J.Holler, "Fundamentals of Analytical Chemistry.", Edn 5, Saunders College Publishing, 1988, 473.

76. The Liberty spectrometer system (Liberty 150AX Turbo, Varian) Operation manual, Publication No. 85 10124400 , 1995.

77. K.R. Koch, M.A. Bruno Pougnet and S. De Villiers, *Analyst*, 1989, **114**, 911.

78. D.A. Skoog, D.M. West and F.J.Holler, "Fundamentals of Analytical Chemistry.", Edn 6, Saunders Publishing Company, 1992, 688.

79. D.A. Skoog, D.M. West and F.J.Holler, "Fundamentals of Analytical Chemistry.", Edn 6, Saunders Publishing Company, 1992, 679.

80. H.H. Willard, L.L. Merrit Jr, J.A. Dean and F.A. Settle Jr. "Instrumental Methods of Analysis.", Edn 7, Wadsworth Publishing Company, 1988, 516.

81. H.H. Willard, L.L. Merrit Jr, J.A. Dean and F.A. Settle Jr. "Instrumental Methods of Analysis.", Edn 7, Wadsworth Publishing Company, 1988, 524.

82. K. vande Casteele, H. Geiger and C.F. van Sumere, *J. Chromatogr.*, 1982, **240**, 81.

83. P.G. Pietta, P.L. Mauri, E. Manera, P.L. Ceva and A. Rava, *Chromatographia*, 1989, **27**, 509.

84. Macherey Nagel Technical Reference : HPLC, M.N. 1995, e1/10/05/95 PD.

85. K.R. Markham, "Techniques of Flavonoid Identification.", Academic Press, 1982, 46.

86. B.H. Koeppen and D.G. Roux, *Tetrahedron Letters*, 1965, **39**, 3497.

87. J.B. Harborne, "Phytochemical Methods, a guide to modern techniques of plant analysis.", Edn 2, Chapman and Hall, 1984, 42.

88. H.H. Willard, L.L. Merrit Jr, J.A. Dean and F.A. Settle Jr. "Instrumental Methods of Analysis.", Edn 7, Wadsworth Publishing Company, 1988, 643.

89. D.A. Skoog, D.M. West and F.J.Holler, "Fundamentals of Analytical Chemistry.", Edn 6, Saunders Publishing Company, 1992, 721.

90. E. Joubert, *Int. J. Food Sci. Tech.*, 1990, **25**, 339.

91. M. Spiro and S. S. Chen, *Food Chem.*, 1993, **48**, 39.

92. S. Natesan and V. Ranganathan, *J. Sci. Food Agric.*, 1990, **51**, 125.

93. W.E. Price and M. Spiro, *J. Sci. Food Agric.*, 1985, **36**, 1309.

94. M. Spiro and Y.Y. Chong, *J. Sci. Food Agric.*, 1997, **74**, 416.

95. W.E. Price and J.C. Spitzer, *Food Chem.*, 1994, **50**, 19.

96. S. Chapman and T.G. Cowling, "The Mathematical Theory of Non-uniform Gases."1960, Cambridge University Press, Cambridge, UK.

97. J.D. Lee, "Concise Inorganic Chemistry", Edn 4, 1991, Chapman and Hall, 298.

98. M. Spiro and P-L. L. Lam, *Food Chem.*, 1995, **54**, 393.

99. R.A. Robinson and R.H. Stokes, "Electrolyte Solutions", 2nd Edn, Butterworths, London, 1959, pp 12, 130, 289, 317, 457,463-465

100. D.R. Lide (Editor-in-Chief), "CRC Handbook of Chemistry and Physics", 72nd Edn (Special Student Edition), 1991-1992, CRC Press, 5-97.

101. M. Spiro and S. S. Chen, *Food Chem.*, 1993, **48**, 47.

102. D. Jaganyi, J. Vanmare and T. Clarke, *S. Afr. J. Chem.*, 1997, **50 (4)**, 203.

103. M. Spiro, R. Toumi and M. Kandiah, *J. Sci. Food Agric.*, 1989, **46**, 349.